PHDG

Professor Heinemanns
Doktorandengruppe
Verein zur Förderung
von wissenschaftlichen Arbeiten
in Reservoircharakterisierung und -simulation

TEXTBOOK SERIES

VOLUME 5

Natural Fractured Reservoir Engineering

by

Zoltán E. HEINEMANN
Professor for Reservoir Engineering
and
Dr. Georg Mittermeir

Tehran
February 2014

For kind Attention

The Textbook series of the PHDG is an aid for PhD students accepted by the Association or those applying for support from it. These scripts have the objective to stabilize and homogenize the knowledge of the candidates, not necessarily studied petroleum engineering and originating from different countries and universities.

The textbooks are subject to continuous update and improvement. PHDG suggests to download them in yearly sequence. In some cases they are provided on different levels of knowledge making it easier to enter the subjects. Therefore there is also some overlapping between the volumes. It is expected that the users will suggest improvements for both, the contents and the formulations.

PHDG's Textbooks available at 1.1.2015:

1. Fluid Flow in Porous Medium
2. Well Testing
3. Systematic of the Reservoir Flow Equations
4. Introduction to Reservoir Simulation
5. Natural Fractured Reservoir Engineering

***PHDG Textbooks in preparation, intended to be issued during 2015*:**

1. Discretization and Gridding in Reservoir Simulation
2. Advanced Reservoir Simulation
3. Reservoir Fluid Characterisation

***Supplementary scripts** used at the Montanuniversität up to the retirement of Professor Zoltán E. Heinemann in July 2006.*

1. Reservoir Fluids
2. Petroleum Recovery

Table of Contents

Chapter 1

Chapter 2

Chapter 3

Chapter 4

Chapter 5

Chapter 6

Chapter 7

List of Figures

Chapter 1

Fractured Reservoirs and Their Properties

1.1. Introduction

1.1.1 Importance and Limitations

Fractured reservoirs are becoming a major issue throughout the entire world for both old and new fields. Many newly discovered oil and gas fields happen to be fractured and their development constitutes a real challenge for the E&P industry. Naturally Fractured Reservoirs often abbreviated as NFRs - have been the subject of extensive studies during the past decades.

The goal of a reservoir engineer should be estimating the reserves, forecasting the production and understanding how fractures could be used to positively affect production and, last but not least, estimating the range of uncertainty. In dealing with conventional reservoirs, engineers can generally provide a reasonable assessment of the reservoir performance by combining information on the reservoir's geologic framework, the rock and fluid properties, and results from well logs, rock mechanic tests and formation evaluation tests. Furthermore, in the recent past, reservoir-scale seismic information has greatly aided reservoir characterization. However, for fractured reservoirs, obtaining the right data and forecasting the reservoir performance is much more difficult than for conventional reservoirs. To design an appropriate plan of development, one needs a credible reservoir description that *includes fracture maps in terms of size, orientation, connectivity, conductivity, and frequency distribution* and then turning this information into a reliable fracture network characterization. Due to the complexity of NFR, it may appear to be rather hopeless to get a unique answer. But instead the question should be "can we estimate the range of uncertainty?"

Natural fractures exist practically in all reservoirs, dividing the reservoir rock in pieces, called matrix blocks. In this case one must distinguish between matrix and fracture porosity and permeabilities. The reservoir is a single porosity one which does not need special consideration and the reservoir rock can be regarded as a single continuum if:

- No fractures exist or they are isolated. The fractures contribute merely to the local pore volume and the local conductivity.
- The matrix is tight, containing no hydrocarbon or the stored hydrocarbon is not accessible, due to lack of matrix permeability. The matrix do not contribute to the hydrocarbon production.

If the matrix has reservoir quality and the fractures are interconnected, building more or less extended networks, then the reservoir can not be modeled as a single continuum anymore. This led to the multiple continua concept where typically two continua, matrix and fracture, overlap each other. The main problem is then to find the right description of the fluid exchange between them while modeling a recovery process. Mathematically, this leads to the extension of the material balance equation by the so-called *transfer term*. It can consider some or all acting forces as the force of compression, chemical potential (diffusion), gravitational force, capillary forces and viscous forces with or without hysteresis or alteration of the properties (e.g.: wettability). The relative importances of these forces (mechanisms) strongly depend on the geometry of the fracture-matrix system and its petrophysical properties. All formulations have their own advantages, but also show deficiencies in describing specific issues of fractured reservoirs and in the computational efficiency.

In most cases not the entire reservoir must be described by dual (or multiple) continua, it is enough to apply them for limited areas were (1) a fracture network exists, (2) the matrix contains hydrocarbons and is permeable, (3) the interaction between fracture and matrix is not instantaneous. No dual continuum description is necessary for a one phase area, e.g.: in the aquifer or in a gas bubble (gas reservoir or gas cap) before water intrudes or until condensate drops out. On the other hand the mechanisms of the mass transfer can be quite different in some parts of the reservoir and can change in time. In favor of the most appropriate but also economic handling of fractured reservoir Bremaier, Fink and Heinemann[15] promoted the general purpose and mixed model concept, in which black oil and compositional formulation, single and dual continuum solutions and the transfer term were applied on a block by block bases. The first simulation software based on this adaptive or mixed model concept was SURE Version 3.1[41].

The reservoir characterization part is mostly based on the publication of Ahmed Ouenes, Feng Shen[63] and Abdel M. Zellou[99]. The general numerical model for the simulation of three-dimensional, multi phase flow in naturally fractured reservoirs presented in this chapter is based on a compositional approach. The formulation is taken, with small modifications from the work of Bremeier, Fink and Heinemann[15]. Most of the discussion of practical aspects originate from Jim Gilman's work[33].

1.1.2 Reservoir Modeling Approaches

When facing a problem of modeling a fractured reservoir, oil and gas companies have three available approaches:

The first one is the *geomechanical approach* where an attempt is made to reconstruct the tectonic history of the fractured reservoir. Unfortunately, all the existing tools based on this approach use overly simplistic models where the complex geology of the reservoir is ignored and homogenous and isotropic rock properties are assumed in the calculations. Furthermore, the end result of this approach is a strain map which is most of the time very similar to a simple curvature map easily derived from the current structural surfaces. In addition to the inability of this approach to account for the complex and heterogeneous geology of all fractured reservoirs, there is no room to incorporate any 3D seismic attribute in the geomechanical process.

The second approach commonly used to model fractured reservoirs is the *Discrete Fracture Network (DFN*) where the reservoir volume is filled with fractures represented by planes or disks. For many years the DFN models lacked geologic realism since they were randomly distributed in the reservoir, ignoring the fact that fracture density at any point is affected by the thickness of the reservoir at that point, its lithology and porosity, its proximity to faults and numerous other geologic drivers. Since the introduction of DFN models, there was a need for constraining the realizations to some geologic input. Attempts have been made to control the fracture generation with some indicator. However, these attempts used a single geologic driver and ignored the others, and most importantly did not account for the complex interplay of the drivers. Ouenes and Hartley[64] introduced the concept of conditioned DFN whereas a large effort is spent in integrating all the geologic drivers in a continuous fracture model which is then used to constrain the DFN models. A recent field example illustrating this approach is given by Zellou *et al.*[100].

Finally, the third approach uses a *continuous framework* where many geologic drivers could be incorporated in creating an integrated fracture model. These continuous fracture models stem from the simple observation that fracture intensity depends on many geologic drivers (the most commonly known being structural setting, proximity to a fault, lithology, porosity and thickness). Because all these drivers and their complex interaction must be accounted for during the modeling process, Ouenes *et al.*[65] use a regular 3D grid model similar to the one used in geologic modeling or in seismic cubes along with a collection of artificial intelligence tools to create truly integrated fractured reservoirs. The approach described in detail by Ouenes *et al.*[64] was successfully used in various fields and basins and one of its most striking advantage is its ability to integrate seismic data in the modeling process.

1.1.3 Classification of Naturally Fractured Reservoirs

Naturally fractured reservoirs can be classified in different types, depending on the storage capacities or porosity and permeability of the matrix and the fractures. Different definitions for these types can be found in literature. Aguilera[5] classified the naturally fractured reservoirs in types A, B and C (see Figure 1.1). In reservoirs of type A most fluid is stored in the matrix; the fractures provide only a very small storage capacity. Typically the matrix rock tends to have a low permeability, whereas the fractures exhibit a much larger permeability. In type B reservoirs approximately half of the hydrocarbon storage is in the matrix and half in the fractures. The fractures provide the storage capacity of type C reservoirs, without contribution of the matrix.

.

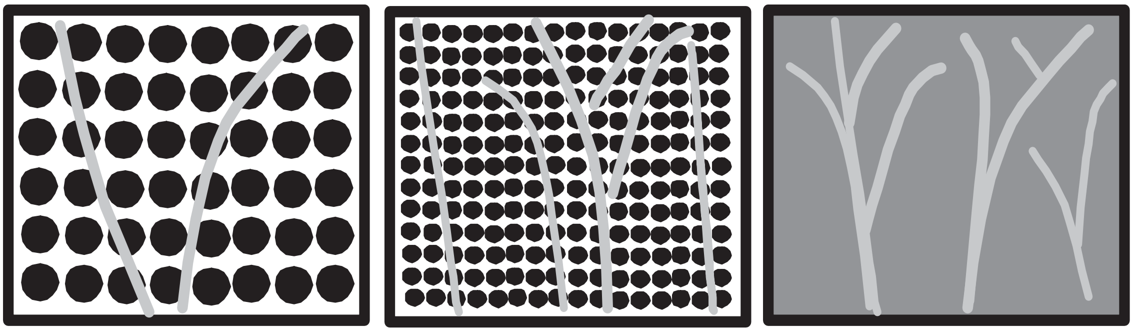

Type A: High storage capacity in the matrix, low storage capacity in the fractures.

Type B: Approx.equal storage capacity in the fractures and in the matrix

Type C: All storage capacity in the fractures, thight matrix

Figure 1.1: Porosity distribution in fractured rocks (after McNaughton and Garb[56])

Another classification of fractured reservoirs is given by Nelson[61], which is based on percent of total porosity and permeability (Figure 1.2). The parameters range in percent due to matrix versus percent due to fracture. In reservoirs of type I fractures dominate porosity and permeability. In type II reservoirs the fractures control essential permeability, and in a type III reservoir, fractures assist permeability. In reservoirs of type IV the fractures provide no additional porosity or permeability, but can create anisotropic barriers.

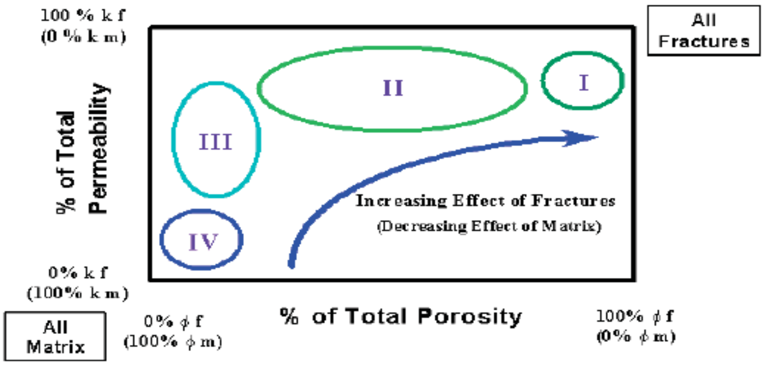

Figure 1.2: Classification of fractured reservoirs after Nelson[61]

1.2. Fractured Rocks Properties

Different fracture properties affect the reservoir performance of a naturally fractured reservoir. The fluid flow properties of the fractures include fracture porosity, fracture permeability, or the fluid saturation within the fracture system. Another important factor is the wettability of the rock and possible wettability changes during the production time of the reservoir.

1.2.1 Porosity

Porosity can be classified as primary or secondary. Primary porosity forms during deposition of sediments and includes interparticle and intraparticle porosities. Secondary porosity forms after deposition and develops during diagenesis by dissolution, dolomitization and through production of fractures in the rock. The matrix porosity, also often called fabric porosity, can be both primary and secondary. The fracture porosity is always a secondary one and generally refers to porosity that occurs along breaks in a sediment or rock body where there has been little mutual displacement along the fracture.

Figure 1.3: Fractured rock outcrop in Mali by courtesy of John Scott

Fracture porosity grades into breccia porosity with increasing dislocation. The fractures enable fluid movement and as a consequence solution of minerals. Depending on the extent of solution, the resulting pores are classified as molds, solution enlarged molds or vugs. Vuggy porosity is a non-fabric selective porosity caused by selective removal (solution) of grains in a rock. If vugs and molds are connected by fractures then their volume become part of the fracture porosity. In carbonate rocks, fracture porosity may originate from collapse related to solution, slumping, or tectonic deformation. Fractures can be observed on cores, and can be characterized as filled, semi-filled and open fractures. Filled fractures do not contribute to the porosity. The fractures are described by their orientation as horizontal, vertical or oblique fractures.

The significance of the fracture porosity depends on the type of the fractured reservoir. In reservoirs where the fractures provide the essential porosity and permeability to the reservoir it is important to have a knowledge on the storage volume of the fracture network as early as possible, to evaluate the reservoir and to design a proper development plan. In fractured reservoirs where the fractures have little storage volume and where the fractures provide basically permeability, the knowledge of the fracture porosity is not that important, if not negligible. In such systems the matrix porosity is usually several magnitudes of order greater than the fracture porosity, which makes an early estimation of the fracture porosity unimportant. Because of the great difference concerning the importance of the fracture porosity, the type of the reservoir should be estimated as early as possible.

Let ϕ_f be the fracture porosity and ϕ_m the matrix porosity, then the storativity dimensionless parameter

$$\omega = \frac{\phi_f c_f}{\phi_f c_f + \phi_m c_m}, \tag{1.1}$$

expresses the ratio between the storage capacity of the fracture network and the total storage capacity.

1.2.2 Permeability

The permeability of a porous rock is a measure of the ability to transmit fluids. A reservoir can have primary and secondary permeability. The primary permeability is referred to as matrix permeability, the secondary permeability can be either called fracture permeability or solution vugs permeability. Matrix- and fracture permeability are other important parameters that have to be known for an estimate of the influence of the fractures on the overall reservoir performance. Solution vug permeability refers to an increased permeability in matrix rocks (especially in carbonate reservoirs) where the natural permeability of the matrix is increased by percolation of acid waters that dissolve the matrix rock. The permeability in these flow channels can be calculated by combining Darcy’s law for fluid flow and Poiseuille’s law for capillary flow[61]. Open fractures in Naturally Fractured Reservoirs generally have a higher permeability than the matrix, building the flow channels of the system. The flow rate through a narrow cleavage can be calculated by Lamb’s law:

$$q = -\left(\frac{W^2}{12}\right)\frac{A}{\mu}\frac{dp}{dx}, \tag{1.2}$$

where W is the effective fracture aperture (fracture width). The fracture cross section A is the product of the fracture width W and the breadth b:

$$A = W \cdot b,. \tag{1.3}$$

μ is the viscosity, and dp/dx is the pressure gradient. The flow rate can also be expressed by the Darcy equations:

$$q = -k\frac{A}{\mu}\frac{dp}{dx}, \tag{1.4}$$

Both Equation 1.2 and Equation 1.4 are valid for laminar flow. So it is evident that the permeability of a single fracture is:

$$k = \frac{W^2}{12}. \tag{1.5}$$

According to Aziz[7], a fracture with 10^{-5} m width (i.e.: *0.1* mm) has a permeability of *844* Darcy. As a consequence of Equation 1.2 and Equation 1.3, between two flat plates, the flow rate is proportional to the cube of the aperture *W*. This is naturally not valid for natural fractures because they are rough as shown in Figure 1.5

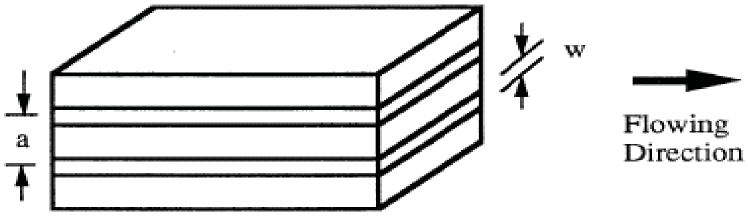

Figure 1.4: Parallel fractures in flow direction

The effective permeability in a fractured solid cube, shown in Figure 1.4 is:

$$k_{ef} = k_f\frac{W}{a}, \tag{1.6}$$

where

$$\frac{W}{a} = \phi \tag{1.7}$$

is the fracture porosity. Inserting Equation 1.7 in Equation 1.6 results in

$$k_{ef} = \phi_f k_f. \tag{1.8}$$

Note that as a consequence of the Equation 1.5 and Equation 1.6 the effective permeability is proportional to the cube of the aperture *W*:

$$k_{ef} \propto W^3. \tag{1.9}$$

If the matrix is also permeable, then the overall effective permeability is:

$$k_e = k_{ef} + (1 - \phi_f)k_m \approx k_{ef} + k_m. \tag{1.10}$$

The approximation is valid if $\phi_f \ll 1$.

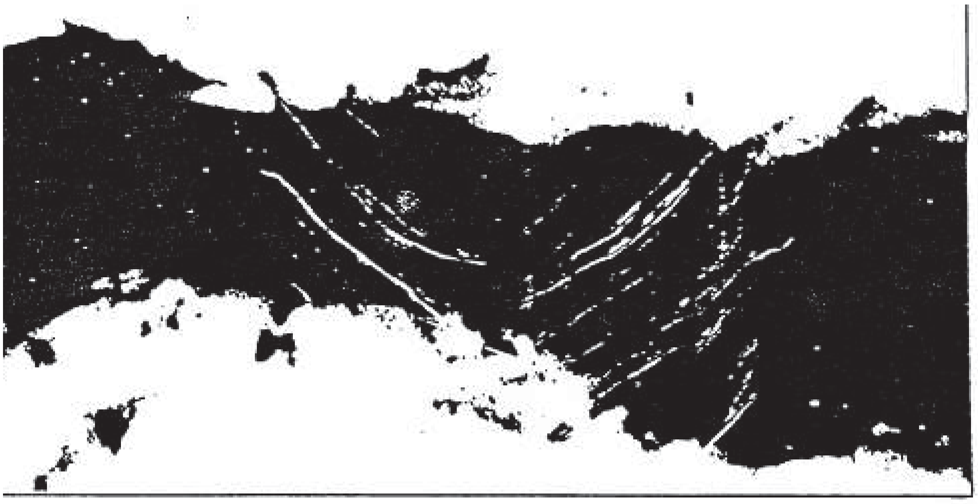

Figure 1.5: Sandstone fracture (average aperture 0.4 mm) (from Jones[44])

Note, that Equation 1.5 and Equation 1.6 cannot be used for real fractures in porous rocks, because it is derived for steady state, isothermal, laminar flow between parallel glass plates. Fracture permeability is, similarly to the fracture porosity, highly scale-dependent[5]. A fracture of width *W* expressed in inches has a permeability of:

$$k_f = 54 \cdot 10^6 \cdot W^2 [Darcys] \tag{1.11}$$

The resultant intrinsic permeability of a fracture of *0.01* in. would be *5400* darcys. The intrinsic permeability of Equation 1.11 is valid for a single point. The formulation can be extended for the bulk properties of the system for one set of parallel fractures[5]:

$$k_2 = \frac{k_f \cdot w_o}{D} \tag{1.12}$$

where *D* is the distance between the fractures.

1.2.3 Compressibility

The stress on the reservoir rock is determined by the confining and the pore pressures. The confining (or overburden) pressure, caused by the weight of overlying rock is partially compensated by the pressure of the fluids in the pores. The net confining pressure, p_e, is the difference of the two pressures:

$$p_e = \bar{\sigma} - p . \tag{1.13}$$

A number of investigations indicate that the effect of varying the confining and pore pressure on porosity and permeability is mainly governed by the net confining pressure and is not greatly dependent on the absolute values of either total confining pressure or pore fluid pressure.

Figure 1.6 shows a typical stress-strain curve manifesting three regions. The linear region of elastic deformation exists up to a stress called yield stress. Beyond that, the material shows plastic behavior. Increase in stress causes a non-linear increase of strain and if the strain is relaxed, the response curve does not retrace the original load path but rather follows an elastic path typical of a more consolidated rock. Ultimately, if enough stress is applied, the rock becomes fully compacted and the stress/strain relation regains linearity. For consolidated sandstone the yield point may exceed *1380* bara (*20,000* psia), while for soft chalk it can be as low as *60-70* bara (*800* to *1,000* psia).

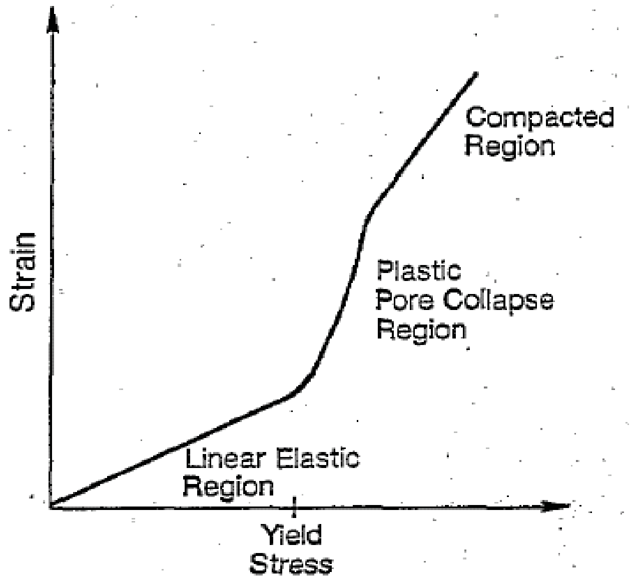

Figure 1.6: Typical rock stress/strain curve showing three regions of behavior: elastic, plastic pore collapse, and compacted work-hardening (after Ruddy *et al.*[81])

Note, that also if often pore collapse and compaction will be modelled by increased compressibility factor, the following discussion is valid only for the elastic state of the reservoir rocks. Dealing with deep carbonate reservoirs, the first step must always be to estimate or better yet, to measure the yield point.

The isothermal compressibility factor, in general, is defined as the specific volume change caused by change of pressure:

$$c = -\frac{1}{V}\left(\frac{\partial V}{\partial p}\right)_T . \tag{1.14}$$

The volume V may refer to the bulk volume (V_b), the solid volume (V_s) or the fluid, e.g. the oil volume (V_o).

The pore volume and therefore, the porosity have no compressibility; they change because the solid phase is compressible. Excluding a possible compaction (i.e.: below the yield point), the solid phase of an intergranular porous medium can be expanded towards the voids (pores) only, therefore, the apparent pore compressibility factor has to be defined as:

$$c_\phi = \frac{1}{\phi}\frac{d\phi}{dp} = \frac{1-\phi}{\phi}c_s, \tag{1.15}$$

where c_s is the compressibility factor of the solid phase. The matrix block, tight or porous, surrounded by fractures will expand towards the fractures, therefore the compressibility of the fracture porosity is determined by the compressibility of the matrix bulk volume:

$$c_{\phi f} = \frac{1-\phi_f}{\phi_f}c_b. \tag{1.16}$$

If the matrix is tight, then

$$c_b = c_s \tag{1.17}$$

Based on Equation 1.9 a simple relation exists between fracture porosity and permeability, given by:

$$\frac{\phi}{\phi_i} = \left(\frac{k}{k_i}\right)^{1/3}. \tag{1.18}$$

Equation 1.18 is rigorously valid only for a tight matrix, where the subscript *i* denotes the value of the variable at the initial condition. The normalization in Equation 1.18 generalizes the expression deduced from the planar model. Since the geometry of the fractured medium should remain relatively constant during compression, it is reasonable to assume that Equation 1.18 might apply to the real, general case where fractures are non-uniform, tortuous, and intersect.

The fracture porosity has a considerably greater compressibility than the intergranular one. Moreover, the fracture compressibility factor cannot be regarded as a constant over the entire range of the reservoir pressure decline. Jones[44] suggested to use the following relation:

$$\frac{\phi}{\phi_i} = \frac{\log(p_e/p_h)}{\log(p_{ei}/p_h)}, \tag{1.19}$$

where p_e is the net confining (overburden) pressure and p_h is the apparent healing pressure. The last one is the pressure at which the fractures would be closed. The behavior of fractures in limestone, dolomite and marble is sufficient similar to be represented by the same expression, all having an apparent healing pressure of approximately *40,000* psia (*2700* bara).

The fracture compressibility in a *20,000* ft deep dense carbonate reservoir is estimated by Jones[44] for 96.10^{-6} psi^{-1} at initial pressure, that decreases to about 72.10^{-6} psi^{-1} at depletion. Intergranular porosity compressibility factors usually range between 2.10^{-6} and 15.10^{-6} psi^{-1}.

1.2.4 Compaction - Example on the Valhall Field

The Valhall field[73],[81] is an overpressured, undersaturated Upper Cretaceous chalk reservoir located approximately *180* miles (~*290* km) offshore of southern Norway. The reservoir has *2.0* billion barrels of OOIP in approximate depth interval of *7870-8530* ft (~*2400-2600* m) The reservoir rock is a relatively pure high porosity (*30-50%*) chalk with high initial oil saturation (> *90%*). Original matrix permeability ranges from *1* to *10* mD, while fracture permeability goes up to *350* mD. At discovery, the reservoir pressure was only *500* psi less than the *7000* psia overburden weight indicating only minor formation compaction during burial. Rock compressibility is the major primary drive mechanism in Valhall. Figure 1.7 gives the compressibility factor curves versus reservoir pressure for different initial porosities. Here, *15%* pore volume reduction occurs in *50%* porosity rock if the pressure is reduced from *6500* to *3500* psia.

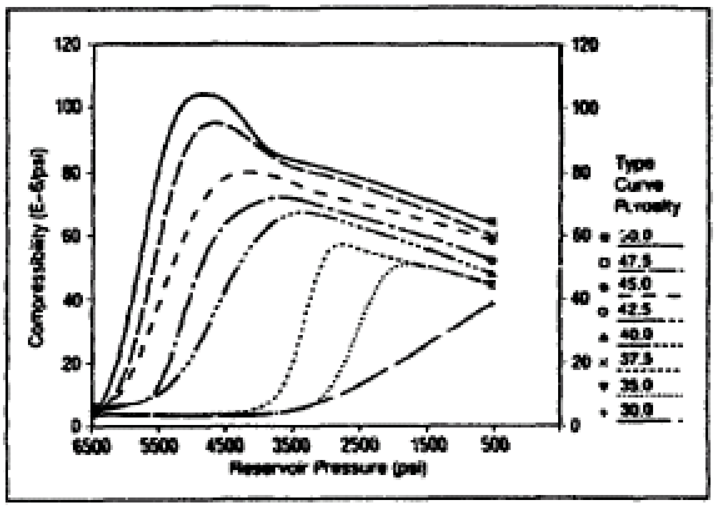

Figure 1.7: Type curves for compressibility factor for Valhall field (after Powley *et al.*[73])

The matrix permeability was correlated based on the porosity determined by density log and corrected to the actual pressure across the field. In this way it was possible to estimate the fracture permeability values as the difference between pressure transient (PTA) total permeabilities at the time of the PTA test. The result is shown in Figure 1.8. It should be emphasized that this is valid for the Valhall field and can not be applied to other cases.

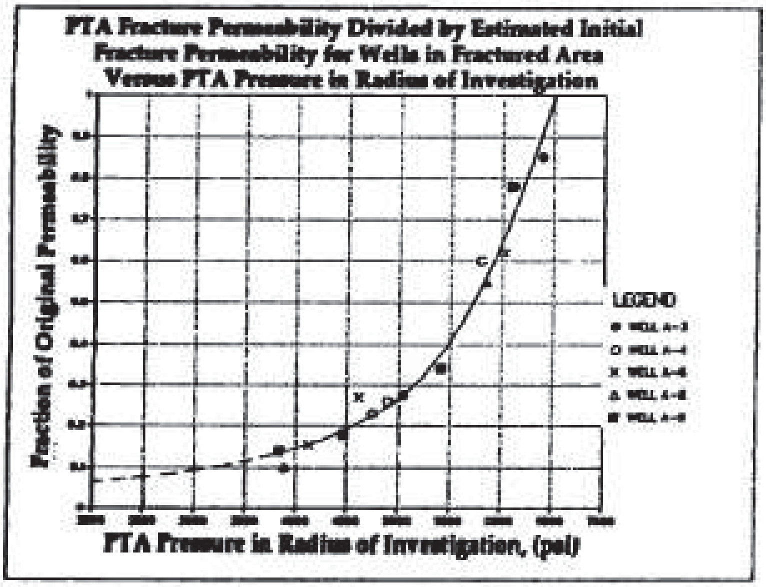

Figure 1.8: Fracture permeability, determined by transient pressure analysis (PTA) versus reservoir pressure in Valhall field (after Powley *et al.*[73])

1.3. Rock and Fluid Interaction

1.3.1 Wettability

Dealing with dual-porosity fractured reservoirs, the wettability is one of the most decisive factors. Wettability plays an important role in the production of oil and gas as it not only determines the initial fluid distributions, but also is a major factor in the flow processes taking place within the reservoir rock. It has a fundamental influence on the fracture-matrix interaction and therefore the ultimate recovery factor.

Wettability of a reservoir-rock fluid system is the ability of one fluid in the presence of another to spread on the surface of the rock. The degree of wetting of solids by liquids is usually measured by the contact angle that a liquid-liquid interface makes with a solid.

A fluid drop on a plane, solid surface can take various shapes. The respective shape (either flat or shaped like a pearl) depends on the wettability of the considered solid. Figure 1.9 illustrates that property. In case of air and water, the water is the wetting fluid, for air and mercury, the air is the wetting fluid.

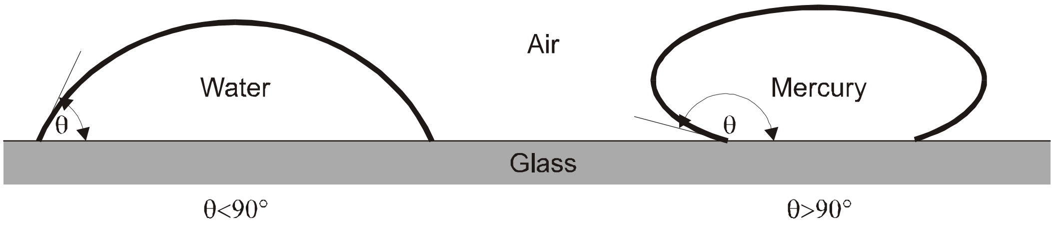

Figure 1.9: Comparison of wetting and non-wetting fluid

The contact angle, θ, is used as a measure of wettability. In case of a wetting fluid, the contact angle is smaller than $90°$. If the contact angle is larger than $90°$, then the fluid is referred to as non-wetting.

Interfacial tensions $\sigma_{pp'}$ between the fluids p and p', and thus the contact angle, θ, are temperature-dependent. At room temperature, the interfacial tension between water and air is 0.073 N/m and between oil and water about 0.03 N/m.

The wettability of a reservoir rock system depends on many factors:

- reservoir rock material
- pore geometry
- geological mechanisms
- composition and amount of oil and brine
- pressure and temperature
- changes in saturation, pressure and composition during production.

When regarding oil reservoirs it is necessary to consider the specific rock and fluid properties in order to determine whether the reservoir rock is *water-* or *oil-wet*. Rocks which are neither water- nor oil-wet are called *intermediate- or neutral-wet*. The data published by Treiber *et al.*[91] (Table 1.1) show that most of the carbonate reservoirs are oil-wet, while the sandstone reservoirs can be equally water- or oil-wet.

Table 1.1: Reservoir wettability based on contact angle measurements (Treiber *et al.*[91])

Wettability	Contact Angle [°]	Number of Reservoir Investigated		
		Sand	Carbonate	Total
water wet	0-75	13	2	15
intermediate wet	75-105	2	1	3
oil wet	105-180	15	22	37

The internal surface of a reservoir rock is composed of many minerals with different surface chemistry and adsorption properties, which may lead to variations in wettability. The concept of *fractional wettability,* also called heterogeneous or *spotted wettability*, was proposed by many authors. Note that the fractional wettability conceptually differs from the *intermediate wettability*, which assumes that all portions of the rock surface have a slight but equal preference to being wetted by water or oil.

Mixed wettability is a special type of fractional wettability where the oil-wet surface forms continuous paths through the larger pores. The smaller pores remain water-wet and contain no oil. Salathiel[84] explained the situation when oil invades an originally water-wet reservoir it displaces water from the larger pores, while the smaller pores remain water-filled. A mixed-wettability condition occurs if in the oil deposits a film of oil-wet organic material only on those solid surfaces that are in direct contact with the oil but not on the surfaces covered by water.

1.3.2 Capillary Pressure

Figure 1.10 shows regular capillary functions for primary drainage, imbibition and secondary drainage. They are applicable to the inter- and intra-granular matrix. Two of these functions are used to determine the wettability by the USBM (U.S. Bureau of Mines) method developed by Donaldson[26].

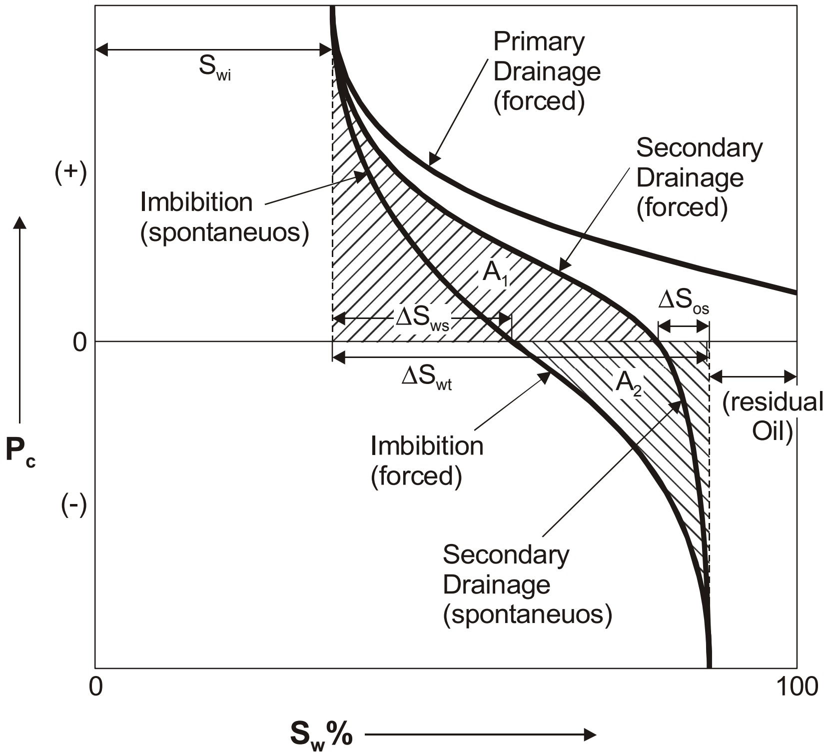

Figure 1.10: Typical capillary pressure curves and the relationships of wettability measurements by Amott and USBM tests to P_c (see Torsaeter[90])

The imbibition curve: Displacement of the oil by brine, starting at the irreducible water saturation and end up with the residual oil saturation.

The secondary drainage curve: Displacement of oil in the reverse direction.

The USBM test compares the work necessary for one fluid to displace the other. The work required for the wetting fluid to displace the non-wetting fluid from the core is less than the work required in the opposite direction. The work required is proportional to the area under the capillary pressure curve. In other words, when a core is water-wet, the area under the brine-drive capillary pressure curve (when the water displaces the oil) is smaller than the area under the capillary pressure curve for the reverse displacement.

Before the test is run, the plug is prepared by centrifugation at high speed and submersed in oil to achieve irreducible water saturation, respectively maximum oil saturation. In the first step of the measurement the core is placed in brine and centrifuged at incrementally increasing speeds until a capillary pressure of *-10* psi. This step is called the brine drive because brine displaces oil from the core. At each incremental capillary pressure the average saturation of the plug is calculated from the volume of expelled oil.

In the second step the core is placed in oil and centrifuged. During this oil drive step, oil displaces brine from the core. The capillary pressures and average saturations are measured until a capillary pressure of *10* psi is reached.

The USBM method uses the ratio of areas under the two capillary pressure curves to calculate a wettability index:

$$W = \log\left(\frac{A_1}{A_2}\right) \tag{1.20}$$

where A_1 and A_2 are the areas under the oil- and brine-drive curves, respectively.

Regarding the multiphase flow the matrix and fracture behave fundamentally different. It is commonly accepted that fracture capillary pressure is zero or negligible for the fractures. These are assumed physically correct fracture properties.

There is no doubt above it that capillary forces can act also in the fracture. Between two plates the meniscus of the wetting fluid rises similar as in a capillary tube. The capillary pressure can be calculated from the Laplace equation in which one of the main curvature radii is infinite:

$$P_{cow} = \sigma_{ow}\left(\frac{1}{r_1} + \frac{1}{r_2}\right) = \frac{\sigma_{ow}\cos\theta}{d} = p_{nw} - p_w,\ r_1\cos\theta = d;\ \ r_2 = \infty \tag{1.21}$$

where d is the fracture width, and θ the wetting angel. In such an ideal case, a fracture aperture (distance between the two plates) of *0.1* mm (10^{-4} m) would produce a water oil capillary pressure ($\sigma = 0.03$ N/m and $\theta = 0°$) not more than

$$Pc = 0.03/10^{-4} = 300\ Pa = 0.003\ bara. \tag{1.22}$$

A fissure with *0.1* mm cannot be continuos and if it exists then manifests solely a contribution to the intergranular pore space of the matrix. Discontinuities in the rock, characterized as fractures, have greater apertures and also smaller capillary pressures, without any relevance for practical application. It should also be mentioned that the fracture capillary pressure cannot be measured on a natural rock sample. The fracture cannot be extracted from a sample for the sake of measurements and from broken cores the in-situ fracture cannot be restored.

The question whether the fracture capillary pressure has an influence on the fluid exchange between matrix and fracture is therefore solely a theoretical question without any practical importance. Commercial simulation software normally offers possibilities to define capillary pressures for the fracture domain too. However, it is not recommend to apply it. The fracture capillary pressure should be regarded as zero.

1.3.3 Fracture Relative Permeabilities

It is commonly believed that the immobile saturations (S_{wc}, S_{or}, S_{gc}) are zero in the fracture and the relative permeability are linear functions as is shown in Figure 1.11. This is certainly true for a single fracture, but questionable in the case of a fracture network. In this respect the fracture orientation will also play a decisive role. This is demonstrated on the Figure 1.12. Also the history matching practices suggest that relative permeability in the fractures is not a linear function of phase saturations. This may be because the relative permeability for a fracture network is not the same as for an individual fracture.

In high-permeability fractures the segregation of the phases is a possible assumption. Under this condition in lateral fracture-fracture and in fracture-matrix connection, the relative permeability could be equal with the phase saturation. This is certainly not valid in the vertical direction where in the multiphase case on the top, the lighter phase's relative permeability becomes *1* and the heavier *0*. On the bottom, the opposite is true.

It should be understood that there is no real chance to predict the fracture's relative permeability for an actual field. The practical approach could be using the well-established model for the water and oil relative permeability function: Nonlinear fracture relative permeability will affect the interblock flow as well as the matrix-fracture transfer (upstream values). Therefore, the water-oil capillary pressure will favor the imbibition of water into the matrix blocks while the gas-oil capillary pressure will prevent gas from entering the matrix block. Without proper treatment for the transfer, gas is not able to displace the oil from matrix blocks (see Section 4.1.2 for more details).

The Corey-exponent representation is a well-established model for the water and oil relative permeability functions:

$$k_{rw}(S_w) = k_{rw@S_{or}} \left(\frac{S_w - S_{wi}}{1 - S_{wi} - S_{or}} \right)^{N_w} \tag{1.23}$$

$$k_{ro}(S_w) = k_{ro@S_{wi}} \left(\frac{1 - S_w - S_{or}}{1 - S_{wi} - S_{or}} \right)^{N_o} \tag{1.24}$$

Where:

$k_{rw@Sor}$ and $k_{ro@Swi}$…end-point relative permeabilities, usually both are *1*.
N_w and N_o …Corey exponents for water and oil,
S_w…water saturation,
S_{wi}…connate water saturation, usually *0*.
S_{or}…residual oil saturation, usually *0*.

Typical Corey exponents for intergranular porosity are summarized in Table 1.1. The exponents $N_w = N_o = 1$ result in straight line functions. Until now, no serious suggestions were published which values would have to be used for fracture networks.

PRS applies the exponents $N_w = 1$ and $N_o = 2$ as default values. Analogously an exponent of $N_g = 2$ is used for the gas relative permeability. Moreover, the immobile phase saturations (S_{wir}, S_{gc}, S_{or}) are not *0* but *0.01*. Figure 1.11 displays such functions.

Table 1-1: Typical values for Corey exponents N_o and N_w

Wettability	No	Nw
water-wet	2-4	5-8
intermediate-wet	4-6	3-5
oil-wet	6-8	2-3

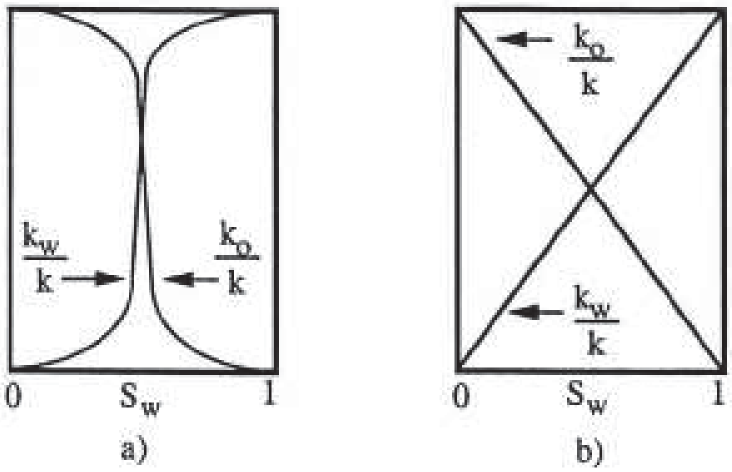

Figure 1.11: Relative permeabilities for: a) cores with fractures non parallel to the flow, b) cores with fractures parallel to the flow.

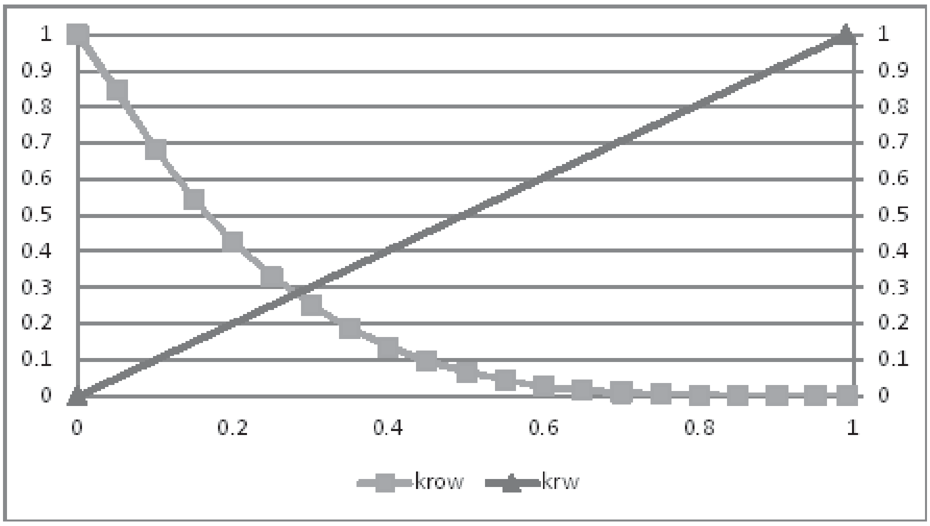

Figure 1.12: PRS default fracture relative permeability functions (calculated from Corey equation $N_w = 1$ and $N_o = 2$).

1.4. Characterization of Fractured Reservoirs

1.4.1 Definitions

In the Textbook *"Fluid Flow in Porous Media"*, Section 1.1 [38]the porous rocks were already categorized as intergranular, fractured and dual porous ones. Following the single continuum approach the medium can be decomposed to Representative Elementary Volumes (REV), which serve for the definition of relevant properties. The size of the REV depends on the rock type, the defined property, the method of measurement and the application of the quantity. Typical for the continuum approach is that for a REV only one value (or function) exists for each property. Under certain conditions, all mentioned rock types can be handled as a single continuum, therefore no differences were made so far in this respect. The basic properties were porosity, rock compressibility, permeability tensor, capillary and relative permeability functions. The state variables, describing the actual state of REV were pressure, temperature, fluid saturations and fluid composition.

Diagenesis can alter the permeability and porosity of open fractures to the extent that they would not behave like fractures, and fully mineralized fractures could, potentially, even become baffles or barriers to flow. Thus, the mere presence of fractures does not require dual-porosity/dual-permeability modeling. Also, a reservoir needs not to be modeled entirely as a dual-porosity or single-porosity system; different parts of the reservoir may be characterized differently.

However, for fractured reservoirs, obtaining the right data and forecasting the reservoir performance is much more difficult than for single continuum type reservoirs. Figure 1.13 shows some naturally fractured rock. Intuitively, one can distinguish between two continua, namely between the (1) fracture network and (2) the blocks of rock separated and connected by the fractures. The second is called the matrix. It is evident that many different fracture-matrix patterns could exist and it will be difficult to find one single way to describe the geometry and the flow process in such a system. Note, that the matrix can also be tight, without effective porosity and without storing any fluids. In this case the entire pore volume is formed by the fractures. Also if the porosity is very low, such a reservoir can store a considerable amount of hydrocarbons. The main difference between the first continuum (fractures) and the second one (matrix) is the size of the Representative Elementary Volume (REV), or in other words, the bulk volume V_T necessary to define average properties as the porosity ($\phi = V_p / V_T$). This can be of greater magnitudes for the fractures.

Figure 1.13: Fractures and Matrices

To design an appropriate development plan (dynamic reservoir model), one needs a credible reservoir description that includes all fracture related properties as:

- Size of the fractures,
- Number of fractures per length (called fracture count),
- Fracture orientation,
- Fracture aperture,

- Fracture porosity,
- Conductivity,
- Fracture connectivity,
- Fracture relative permeabilities.

Characterization of Naturally Fracture Systems can be made from analysis of cores and logs for the subsurface and from surface outcrops. Harstad *et al.*[37] performed an outcrop study on the Frontier sandstone (Green River Basin, Wyoming, US.). Three of them are presented in Figure 1.14 through Figure 1.16.

Permeability tensor deduced from fracture description. Harstad *et al*[37], references a paper from Oda[62]. This should be understand and referenced.

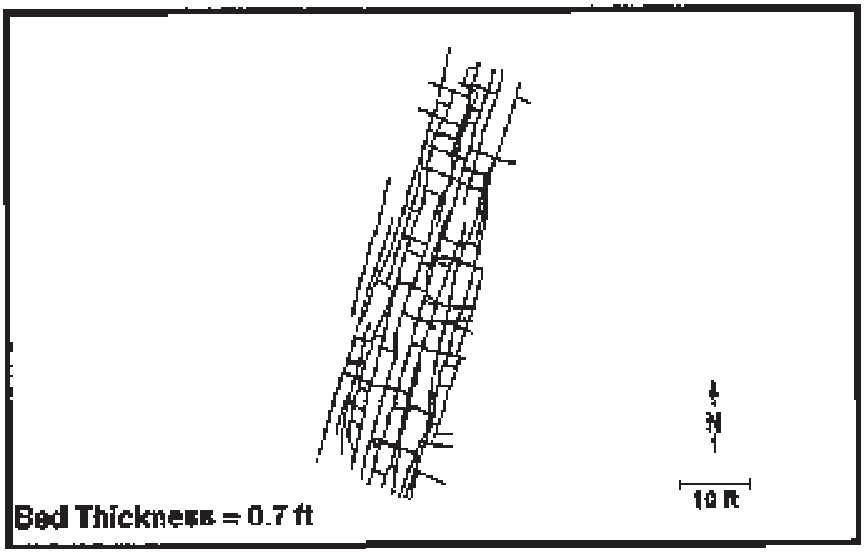

Figure 1.14: Fracture network map at Scullys Gap outcrop, Bed thickness 0.2 m. (after Harstad *et al.*[37])

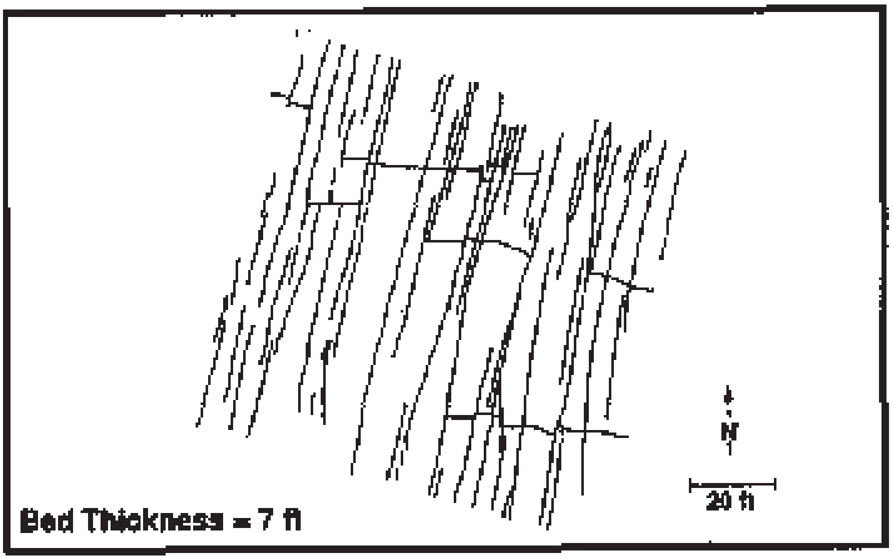

Figure 1.15: Fracture network map at Bridger Gap outcrop, Bed thickness 2 m. (after Harstad *et al.*[37])

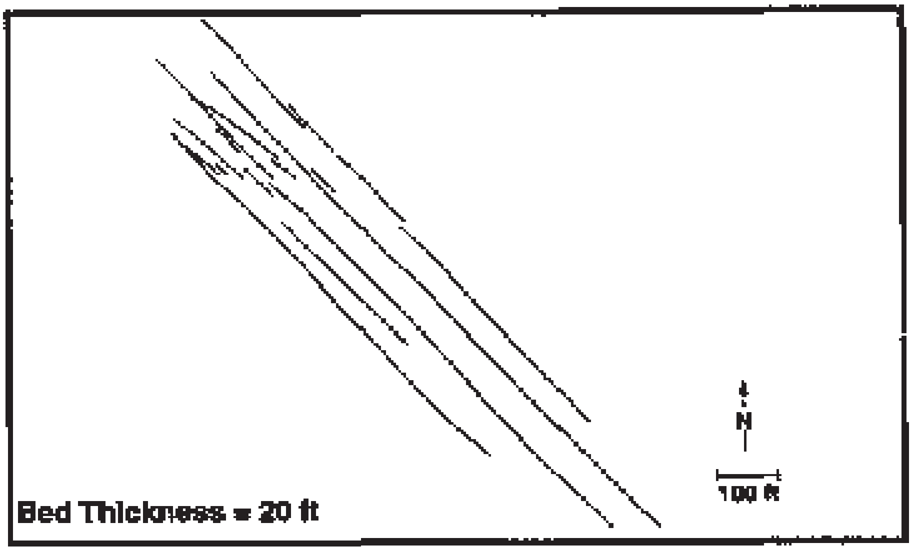

Figure 1.16: Fracture network map for Fronitier Sandstone at Muddy Gap outcrop, Bed thickness 6 m. (after Harstad *et al.*[37])

1.4.2 Characterization Methods

1.4.2.1 Direct sources of information

Direct sources of information include core, outcrop analysis and image logs. *Core analysis* provides valuable information for the fracture characterization process. Figure 1.17 shows a core taken from a fractured reservoir. The relationship between specific fractures and the reservoir rock can be analyzed in cores. Cores provide the material for routine and advanced reservoir engineering analysis as well as information about the geomechanical modification to the fractures, such as timing of the fracture development relative to the digenesis of the reservoir[59]. Important parameters for the development of a fracture model are gained from core analysis, including single- and multi-fracture parameters. Single-fracture parameters such as fracture width, size and orientation are analyzed from thin sections of the core. A fracture description should be done from the whole core before the core is sliced. There is also information about the nature of the fractures. The fracture morphology (open, filled, partially-open fractures) has to be combined with the fracture size and fracture orientation. The fracture orientation gives information about the fracture's induced anisotropy. Measuring the fracture aperture and height is essential to compute the fracture density, fracture porosity and other fracture characteristics. The areal fracture density is a multi-fracture parameter that can be inferred from thin-section analysis of cores[97]:

$$A_{fd} = \frac{\text{number of fractures} \cdot \text{length in thin section}}{\text{area of the thin section}} \tag{1.25}$$

The linear fracture density is obtained from the intersection of fractures along a vertical line.

The main problem with core analysis is that most of the cores are drilled from vertical wells which will seldom intersect the vertical fractures parallel to the well.

Figure 1.17: Fractured core[97]

Outcrop studies involve the collection of various information about the fracture system and can provide an understanding of how the fractures relate to the lithology or stratigraphy of the reservoir rock. Observations are made either on the reservoir rock formation or on a rock chosen on the basis of similarity to the reservoir in lithology, stratigraphic setting, rock properties, age, structure, etc[59]. Figure 1.18 shows an impressive photograph of an outcrop of a fracture network in Zagros Mountains in Iran. The main problem with outcrops is that the same stress history cannot be assumed at the surface and at a depth of thousands of meters subsurface. If a rock is uplifted to the surface, the overburden is removed, it has been eroded and also the tectonic stress is reduced. Furthermore, the temperature at the surface is cooler than subsurface and the pore fluid pressure will change significantly[27],[59]. All these processes are capable of changing the properties of the fractured rock at surface from the down-hole properties.

Figure 1.18: Parallel sets of fractures in steeply dipping marly limestone, Zagros Mountains, Iran[96] (for scale see the pick, on the left in the center).

Another source of direct information about the fracture system are *image logs*, which create images of the interior of the bore-hole. There are two basic measurement methods in use for the fracture characterization: acoustic imaging logs and resistivity based image logs. Figure 1.19 shows an example of the visualization of fractures using a resistivity image log tool. The fractures can be clearly distinguished from the matrix. Resistivity-based image log tools measure the resistivity of minerals and produce high resolution resistivity images of the bore-hole wall. Arrays of electrodes are dragged along the bore-hole wall to generate the image. Acoustic imaging logs use an acoustic pulse to image the shape of the bore-hole wall. The bore-hole wall is scanned with a narrow pulse acoustic beam from rotating transducers while the logging tool is pulled out of the hole. The Amplitude and travel time of the acoustic signals reflected from the bore-hole wall is measured with the same transducer that generates the acoustic beam. The images are oriented using a magnetic sensor. Location, size and orientation of fractures intersecting the bore-hole can be diagnosed from image logs, which provide a *360°* view of the bore-hole wall. Some limitations of these logging tools is that they are not applicable to oil-based mud. In water-based mud it is possible to distinguish open fractures filled with mud filtrate from filled fractures if resistivity tools are used. Fracture aperture, which is an essential parameter in determining the fracture porosity, can be calculated from resistivity image logs.

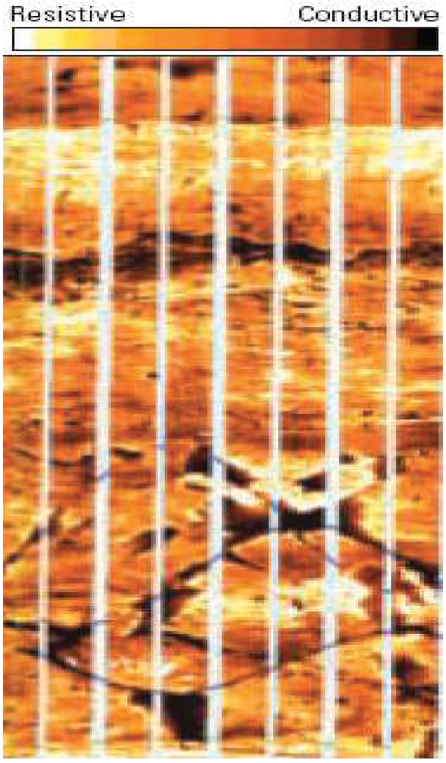

Figure 1.19: Borehole image from a Formation Micro-Imager (Schlumberger)[14]

1.4.2.2 Indirect sources of information

As mentioned before, core and image log analysis provide the most precise data about the presence of fractures and the fracture geometry, but may not indicate the effectiveness of the fractures if used alone. Combining the observed fractures from cores and image logs with the information from other sources increases the knowledge about the fracture system. The indirect sources of information include the drilling and production history, log analysis and well tests. The indirect fracture indicators can provide information about fracture network properties, the transmissivity (connectivity, conductivity or intensity), the fracture storativity (size, aperture and frequency), the anisotropy (stress field) or the areal and vertical heterogeneity.

Lost circulation during *drilling* is an indication of natural fractures, underground caverns, or induced fractures. An increase in the rate of penetration might occur while drilling through a formation with secondary porosity. *Tracer testing* provides an inexpensive, direct indication of fracture connection and directional tendencies. A distinct tracer is injected into a well and surrounding wells are monitored for presence of the tracer. Limitations might be long response times and well interference tendencies.

Different *well logging tools* can provide valuable information in combination with the already discussed image logs. Only a few examples are shortly discussed here. Porosity logs can be used in conjunction with image logs to recognize open fractures. If barite mud is used, a photoelectric effect log (PEF) can be used to recognize open fractures. The mud filled fracture will induce a spike on the PEF log, thereby showing that the fracture is open. The spontaneous-potential log (SP) might show anomalies which can be associated with a fractured zone. Temperature logs measure the temperature gradient in the bore-hole. The circulation of cooler mud reduces the temperature gradient throughout the well depth, with more cooling in permeable zones. The presence of fractures can lead to mus losses to the fractures, which will cause a modification of the temperature gradient in the fractured zone.

Well test analysis can also provide valuable information about the fracture system. Pressure analysis is used to evaluate fracture, matrix and combined permeability and porosity. Basically, the same parameters as for well test interpretation in conventional reservoirs can be gathered, such as *kh*. Two important parameters describing the storativity of the fracture system, ω and λ, can be determined from pressure transient testing:

$$\omega = \frac{(\phi c_t)_f}{(\phi c_t)_f + (\phi c_t)_m}, \qquad \lambda = \frac{\sigma k_m r_w^2}{k_{fe}} \tag{1.26}$$

In Equation 1.26, ω is a dimensionless parameter relating the storage of the secondary porosity to that of the combined system and λ is a dimensionless parameter governing the inter-porosity flow. Furthermore, the effective permeability can be determined with the help of pressure transient testing. Ideal well tests show both, fracture and matrix flow in the transient flow period. This results in two straight lines with a transition zone in between, on the semilog plot of time versus pressure. The earlier time line corresponds to the flow in the fractures and the second to the flow in the matrix. The first straight line is, because of well-bore storage effects, often difficult to detect. Figure 1.20 shows ideal examples of a pressure drawdown and a pressure buildup test. Both plots show the characteristic straight lines and the transition zone in between. The location of the transition relative to the time axis relates to the inter-porosity flow quantified by the inter-porosity flow coefficient λ (Equation 1.26). The separation between the two straight lines represents the storage capacity ω (Equation 1.26).

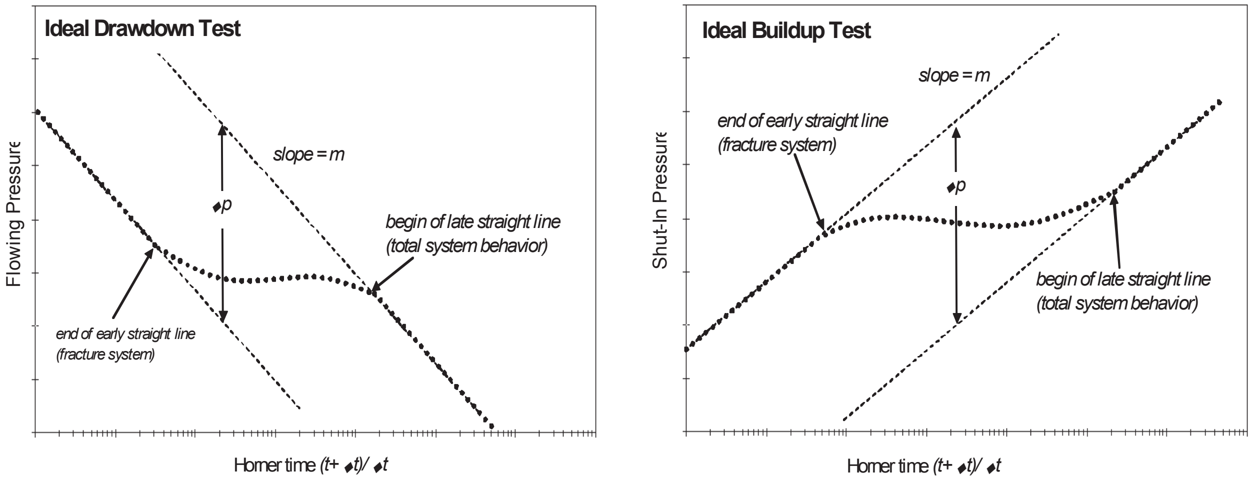

Figure 1.20: Pressure response in a naturally fractured reservoir showing ideal dual porosity behavior

Well test analysis should not be used as a single indicator for a Naturally Fractured Reservoir, since the dual porosity response is limited. Many Naturally Fractured Reservoirs do not show dual porosity behavior in well tests. The transition between the fracture and entire system flow is often reached very quickly, so that it is utterly masked by well-bore storage effects. Interference testing, during which a pressure pulse is created in one well and its response is measured in another, can be used as a direct indication of fracture connection and gives a measure of the permeability anisotropy. These are some important parameters, because fracture systems have a strongly preferred orientation.

Chapter 2

Formulation of the Fluid Flow Equations

2.1. Integral Formulation of the Fluid Flow Equations

This chapter only deals with isothermal flow models, therefore no entalphy balance will be considered. For the sake of generality and future extensibility the temperature will be handled as an independent variable.

2.1.1 Single Continuum Model

The porous material has a porosity ϕ, which is a function of the pressure (and temperature). The pore space is occupied by fluids and separated by phase surfaces. The proportion of one phase in the pore volume is defined as the phase saturation S_p. It is evident that

$$\sum_{p=1}^{P} S_p = 1; \tag{2.1}$$

where P is the number of phases. Equation 2.1 is called “saturation constraint”.

The fluid system is composed of C components. The composition of the p^{th} phase is given by the mole fractions x_{pc}:

$$\sum_{c=1}^{C} x_{pc} = 1; \qquad p \in \{1, \ldots, P\} . \tag{2.2}$$

Equation 2.2 is called “*mole constraint*”.

The continuity equation in a *single continuum space* can be written for component *c* in k-moles:

$$-\nabla\left(\sum_{p=1}^{P}\vec{u}_p D_p x_{pc} M_c\right) - \nabla\left(\sum_{p=1}^{P}\vec{J}_{pc} M_c\right) + q_c M_c = \frac{\partial}{\partial t}\left(\phi \sum_{p=1}^{P} S_p D_p x_{pc} M_c\right) \tag{2.3}$$

The first term on the left-hand side in Equation 2.3 is the *convection term* or *flow term*. It gives the mass of component *c* flowing through the unit surface per unit time (mass velocity). The summation over all phases is necessary, because the particular component may be present in several phases. The second term is the *diffusion term*. It gives the mass of the component *c* moving through the unit of surface per unit time, driven by the concentration gradient. The third term is the *volumetric source/sink term*. It determines how much of component *c* will be taken out, or is supplied to the unit volume per time unit. The right-hand side is the *accumulation term*. It contains $S_p D_p x_{pc}$ moles and $S_p D_p x_{pc} M_c$ mass of the component *c*. The summation over all phases and the integral over the whole control volume gives the accumulation of component *c* within this control volume.

2.1.2 Convection and Diffusion

Equation 2.3 assumes that two transport mechanisms have an influence on the mass flow rate for which the driving forces and parameters have to be specified:

- Convection, described by Darcy’s law and
- Diffusion, defined by Fick’s law.

The total molar flux [kmole.s^{-1}.m^{-2}] for the component *c,* in general*,* is:

$$\vec{U}_c = \sum_{p=1}^{P}\vec{u}_p D_p x_{pc} + \sum_{p=1}^{P}\vec{J}_{pc}\,. \tag{2.4}$$

$\vec{u}_p$ is the filtration velocity of the phase *p*, and is given by Darcy's law (for the multi-phase case):

$$\vec{u}_p = -\lambda_p \bar{\bar{k}} \nabla \Phi_p, \tag{2.5}$$

where the permeability $\bar{\bar{k}}$, in general, is a symmetrical tensor (see Section 2.1.2.1 for more details).

$$\bar{\bar{k}} = \begin{bmatrix} k_{11} & k_{12} & k_{13} \\ k_{21} & k_{22} & k_{23} \\ k_{31} & k_{32} & k_{33} \end{bmatrix}, \text{ where } k_{ij} = k_{ji} . \tag{2.6}$$

$$.\lambda_p = \frac{k_{rp}}{\mu_p}, \text{ is the phase mobility, and} \tag{2.7}$$

$$\nabla\Phi_p = \nabla p_p - \rho_p \vec{g} \text{ , the potential gradient,} \tag{2.8}$$

$$D_p = D_p(p_p, T_p, \bar{x}_{pc}) \text{ , is the specific molar density} \tag{2.9}$$

where x_{pc} is the mole fraction of the component c in phase p. If M_c is the mole mass of the component c, we can also calculate the phase densities, ρ_p as:

$$\rho_p = D_p \sum_{c=1}^{C} M_c x_{pc} . \tag{2.10}$$

The differences between the phase pressures is the capillary pressure:

$$p_p - p_{p'} = P_{cpp'} \qquad p \neq p' \;\; p, p' \in \{1, \ldots, P\} . \tag{2.11}$$

J_{pc} [kmol.m^{-2}.s^{-1}] is the molar flux of the component c in phase p, which can be expressed by Fick's law:

$$\vec{J}_{pc} = -\phi S_p D_p \mathrm{D}_{pc} \nabla x_{pc} , \tag{2.12}$$

where D_{pc} [m²/s] is the diffusion coefficient. The diffusion coefficient is specific for the compound (solute) and depends on the composition of the system (solvent) and on the temperature.

2.1.2.1 The Permeability Tensor

The permeability tensor is symmetrical per definition. Some upscaling methods can produce a non-symmetrical permeability tensor, which would mean that Darcy flow shows shear effects. For such an effect no physical evidence exists. The asymmetric permeability tensor is solely the product of the upscaling method.

The permeability tensor from Equation 2.6 can be split into a normalized tensorial part and an effective scalar permeability k_a. Therefore, the permeability tensor of Equation 2.6 can be rewritten as:

$$\bar{\bar{k}} = \begin{pmatrix} k_{11} & k_{12} & k_{13} \\ k_{12} & k_{22} & k_{23} \\ k_{13} & k_{23} & k_{33} \end{pmatrix} = k_a \bar{\bar{k}}' = k_a \begin{pmatrix} k'_{11} & k'_{12} & k'_{13} \\ k'_{12} & k'_{22} & k'_{23} \\ k'_{13} & k'_{23} & k'_{33} \end{pmatrix} . \tag{2.13}$$

k_a can be any number to calculate the new tensor values as $k'_{ij} = k_{ij}/k_a$. This step is to separate the apparent permeability which is locally more variant, and the anisotropy tensor which tends to be the same in larger scales. However, as shown in Equation 2.37, when calculating the matrix-fracture inter-flow, this value will be multiplied again in the tensor to result in the actual k_{ij} permeability values. Mathematically speaking, this takes effect as a simple factorization of the value k_a from the tensor. It has been tried over the years to give physical definitions for k_a and k'_{ij} tensor values, all suggest that for the matrix apparent permeability k_a the following inequality should be true:[18],[23],[54]:

$$\kappa_b \leq k_a \leq \kappa_a \ , \tag{2.14}$$

where κ_b is the harmonic mean and κ_a is the arithmetic mean of k_{ij}'s in Equation 2.6. But as mentioned previously, this number can be any value greater than zero theoretically. It is suggested to use the maximum principle permeability value k_x or the equivalent isotropic permeability after Muskat[59]:

$$k_a = k_x \quad \text{or} \quad k_a = \sqrt[3]{k_x k_y k_z} \ , \tag{2.15}$$

where k_x, k_y, k_z are the permeability values in x-, y- and z- principle permeability directions respectively.

2.1.3 Dual Continua Model

It will be assumed that two continua exist in the same space, both fill the space completely without gaps and overlaps. One continuum represents the fractures and the other one the matrix. Both porous materials have the same type of properties and their own variables. The matrix properties and variables are signed by the subscript *m* and the fracture by *f*. For example the porosities are ϕ_m, and ϕ_f which are functions of the pressure p_m and p_f, respectively. The pore space is occupied by fluids and separated by phase surfaces. The proportion of one phase in the pore volumes are defined as the phase saturations S_{pm} and S_{pf}. Consequently, Equation 2.1 through Equation 2.3 shall be duplicated once with the subscript *m* and once with the subscript *f*.

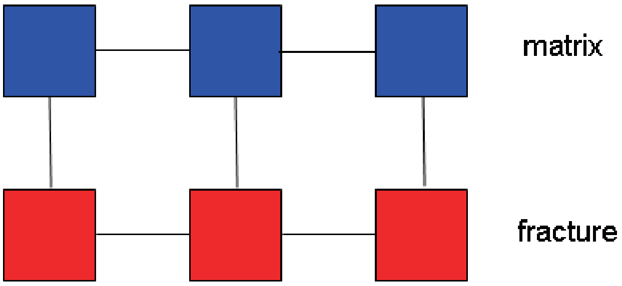

Figure 2.1: Dual porosity - dual permeability dual permeability concept

The balance equation for the fracture continuum:

$$-\nabla\left(\sum_{p=1}^{P}\vec{u}_pD_px_{pc}M_c\right)_f-\nabla\left(\sum_{p=1}^{P}\vec{J}_{pc}M_c\right)_f+q_{cf}M_c-q_{cmf}M_c$$
$$=\frac{\partial}{\partial t}\left(\phi\sum^{P}S_pD_px_{pc}M_c\right) \tag{2.16}$$

The balance equation for the matrix continuum:

$$-\nabla\left(\sum_{p=1}^{P}\vec{u}_pD_px_{pc}M_c\right)_m-\nabla\left(\sum_{p=1}^{P}\vec{J}_{pc}M_c\right)_m+q_{cm}M_c+q_{cmf}M_c$$
$$=\frac{\partial}{\partial t}\left(\phi\sum^{P}S_pD_px_{pc}M_c\right) \tag{2.17}$$

Note, that the third term in the left side of the Equation 2.3 is split into two terms. The source/sink term q_{cm} and q_{cf} represent are the wells, while q_{cmf} is the matrix-fracture transfer term. The Equation 2.16 and Equation 2.17 can be rewritten in terms of mole balance rather than mass balance by using Equation 2.5 and Equation 2.12 in Equation 2.16, to get the fracture mole balance equation,

$$\nabla\left(\sum_{p=1}^{P}\Lambda_{pc}k_a\bar{\bar{k}}'\nabla\Phi_p\right)_f+\nabla\left(\sum_{p=1}^{P}\phi S_pD_p\mathrm{D}_{pc}\nabla x_{pc}\right)_f+q_{cf}-q_{cmf}=\frac{\partial}{\partial t}\left(\phi\sum_{p=1}^{P}S_pD_px_{pc}\right)_f \tag{2.18}$$

and using Equation 2.5 and Equation 2.12 in Equation 2.17, to give the matrix mole balance equation.

$$\nabla\left(\sum_{p=1}^{P}\Lambda_{pc}k_a\bar{\bar{k}}'\nabla\Phi_p\right)_m+\nabla\left(\sum_{p=1}^{P}\phi S_pD_p\mathrm{D}_{pc}\nabla x_{pc}\right)_m+q_{cm}+q_{cmf}=\frac{\partial}{\partial t}\left(\phi\sum_{p=1}^{P}S_pD_px_{pc}\right)_m \tag{2.19}$$

Equation 2.16 and Equation 2.17 describe a dual-porosity-dual-permeability case in which the fluids can flow within both domains as shown in Figure 2.1.

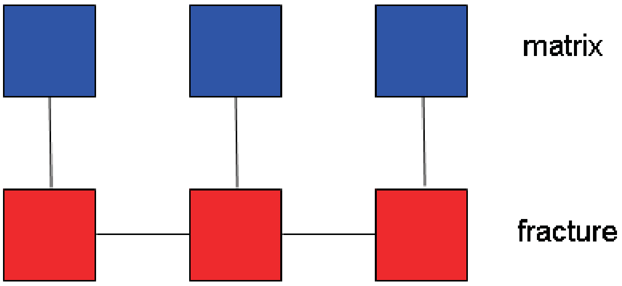

Figure 2.2: Dual porosity (single permeability) concept, only the fractures are continuous

Very often the permeability of the matrix is of less magnitudes than the permeability of the fractures and/or is not continuous (i.e. it is broken into discontinuous chunks). The matrix serves just as volume source or sink for the continuous fracture system, as shown in Figure 2.2. Therefore, production is only possible from the fractures but not from the matrix. In this case Equation 2.17 simplifies to

$$q_{cmf} M_c = \frac{\partial}{\partial t}\left(\phi \sum_{p=1}^{P} S_p D_p x_{pc} M_c \right)_m , \tag{2.20}$$

where the matrix-fracture transfer q_{cmf} term includes convective and diffusive material transport as well. Figure 2.3 shows a schematic of a dual continuum model, including the transfer term.

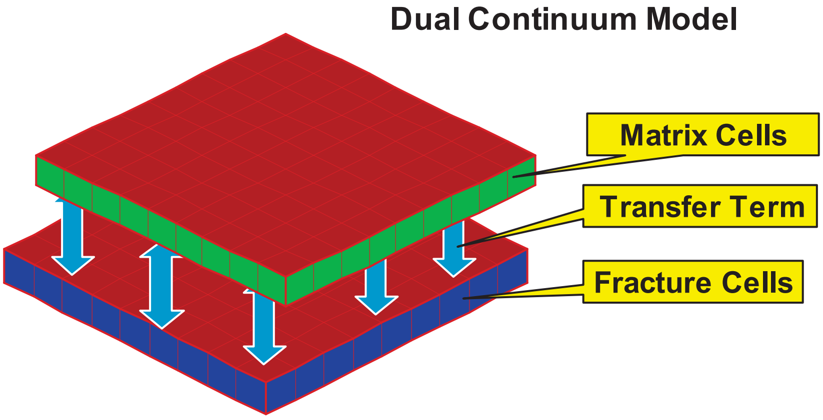

Figure 2.3: Illustration of a dual continuum model.

2.1.4 Application of Green Divergence Theorem

In order to being able to discretize the differential equations on a generalized grid, the control volume finite difference (CVFD) method should be applied. This will be explained here just for one of the domains without using the subscript *m* or *f* but the same equations are valid for both continua. The Equation 2.17 can be integrated over an arbitrary control volume V_i, leading to

$$-\iiint_{V_i}\left[\nabla\left(\sum_{p=1}^{P}\vec{u}_p D_p x_{pc} M_c\right)\right]dV = \iiint_{V_i}\left[\frac{\partial}{\partial t}\left(\phi\sum_{p=1}^{P} S_p D_p x_{pc} M_c\right)\right]dV, \tag{2.21}$$

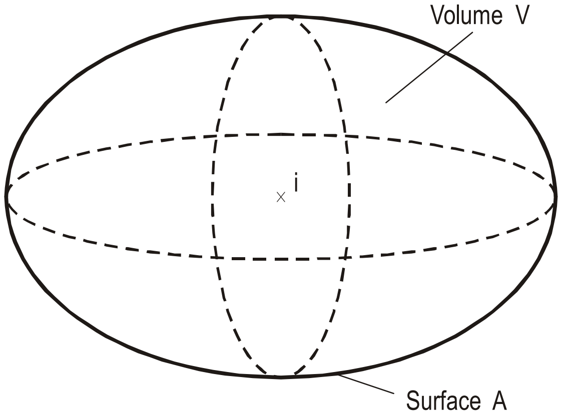

Figure 2.4: Control volume around grid point

where the diffusion and production terms were disregarded for the sake of simplicity. V_i is a finite control volume around the grid point *i*.

The flow term can be rewritten using the GREEN divergence theorem:

$$-\iiint_{V_i}\left[\nabla\left(\sum_{p=1}^{P}\vec{u}_p D_p x_{pc} M_c\right)\right]dV = -\iint_{A_i}\left(\sum_{p=1}^{P}\vec{u}_p D_p x_{pc} M_c\right)\vec{n}\,dA \tag{2.22}$$

where $\iint_{A_i}$ denotes the integration over the total surface A_i of V_i and $\vec{n}$ is normal vector (the outward pointing unit vector) to the surface A_i. The same theorem can be applied to the diffusion term in the same manner. Inserting into Equation 2.21 yields

$$-\iint_{A_i}\left(\sum_{p=1}^{P}\vec{u}_p D_p x_{pc} M_c\right)\vec{n}\,dA = \iiint_{V_i}\left[\frac{\partial}{\partial t}\left(\phi\sum_{p=1}^{P} S_p D_p x_{pc} M_c\right)\right]dV\ . \tag{2.23}$$

Equation 2.23 is a mass balance. But it is obvious that mass and mole balances are equivalent when cancelling the constant mole mass M_c from both sides. This leads to a mole balance equation:

$$-\iint_{A_i}\left(\sum_{p=1}^{P}\vec{u}_p D_p x_{pc}\right)\vec{n}\,dA = \iiint_{V_i}\left[\frac{\partial}{\partial t}\left(\phi\sum_{p=1}^{P} S_p D_p x_{pc}\right)\right]dV. \tag{2.24}$$

Substituting the velocity according to Darcy's law and splitting up the double integral $\iint_{A_i}$ into a sum over all surfaces A_{ij} connecting the block i with its neighbors j, yields for the flow term:

$$-\iint_{A_i}\left(\sum_{p=1}^{P}\vec{u}_p D_p x_{pc}\right)\vec{n}\,dA = \sum_{j=1}^{N}\iint_{A_{ij}}\left(\sum_{p=1}^{P}\Lambda_{pc}k_a\bar{\bar{k}}'\nabla\Phi_p\right)\vec{n}\,dA, \tag{2.25}$$

where already the component mobility and the normalized permeability tensor

$$\Lambda_{pc} = \lambda_p D_p x_{pc} \quad \text{and} \quad \bar{\bar{k}} = k_a\bar{\bar{k}}' \tag{2.26}$$

were substituted. A similar expression can be written for the diffusion term:

$$-\iint_{A_i}\left(\sum_{p=1}^{P}\vec{J}_{pc}M_c\right)\vec{n}\,dA = \sum_{j=1}^{N}\iint_{A_{ij}}(\phi S_p D_p D_{pc}\nabla x_{pc})\vec{n}\,dA. \tag{2.27}$$

Now the fluid flow equation in integral formulation has the following form:

$$\sum_{j=1}^{N}\iint_{A_{ij}}\left(\sum_{p=1}^{P}\Lambda_{pc}k_a\bar{\bar{k}}'\nabla\Phi_p\right)\vec{n}\,dA + \sum_{j=1}^{N}\iint_{A_{ij}}(\phi S_p D_p D_{pc}\nabla x_{pc})\vec{n}\,dA + q_c \pm q_{cmf} = \tag{2.28}$$

$$\iiint_{V_i}\left[\frac{\partial}{\partial t}\left(\phi\sum_{p=1}^{P} S_p D_p x_{pc}\right)\right]dV$$

where q_c is the discrete sink/source term for the component c acting in the volume V_i.

2.1.5 Matrix-fracture transfer term

2.1.5.1 A historical review

In numerical modeling of dual porosity reservoirs the matrix-fracture fluid transfer has ever been and still is an area of extensive research and discussion. Warren and Root[95] gave the first definition of the shape factor when they introduced their idealized sugar cube model (Figure 2.6) of fractured porous rocks. One of the most accepted and widely implemented (e.g. in ECLIPSE[87]) shape factor definitions used in numerical modeling was given by Kazemi *et al.*[47].

$$\sigma = 4\left(\frac{1}{L_x^2} + \frac{1}{L_y^2} + \frac{1}{L_z^2}\right), \tag{2.29}$$

Coats[20] recommended a shape factor that is twice the value of Kazemi *et al.*[47]. All mentioned authors assumed the mass transfer between matrix and fracture to be pseudo-steady state. Numerous other authors proposed shape factors based on numerical and/or laboratory experiments. Vicarious Thomas *et al.*[89] and Ueda *et al.*[92] are mentioned. Gilman[33] claims that the shape factor is a function of fracture spacing (or intensity), and is not inherently a time-dependent parameter.

To the knowledge of the author, Barker[9] presented the most general formulation of the matrix-fracture transport equations so far. In his phraseology the matrix block has an arbitrary shape with a volume to surface ratio of *a*. The boundary value problem leads to a solution containing the time depending non-dimensional Block-Geometry Function (*BGF*). The *BGF* depends on the geometry of the characteristic matrix block but not on its absolute size. The volume to area ratio of the blocks captures the block shape. Assuming pseudo- (quasi-)steady state conditions, the BGF becomes time independent and leads to a definition of the shape factor. The shape factor after Barker[9] is:

$$\sigma = \alpha\left(\frac{V_m}{A_m}\right)^{-2}, \tag{2.30}$$

where V_m is the volume, A_m is the surface of the matrix block and α is a non-dimensional parameter. Consequently, the assumption of pseudo-steady flow between matrix and fracture always leads to a constant parameter called “shape factor”. Otherwise, the time depending Block-Geometry Function must be considered and a *function* should not be titled a *factor*. Nevertheless, some authors (Penuela[67], Rangel-German and Kovscek[77]) published such functions calling them time-dependent shape factors.

The supposition that the exchange term for all possible physical situations will depend on the geometry of the discontinuous element (the matrix) of the model, was postulated from the beginning onwards by Warren and Root[95]. It should be also mentioned that their sugar cube model and the resulting shape factor are already based on discretization and homogenization. The weakness of the concept was that the shape factor was defined for specified geometries. In reality, the matrix blocks are neither cubes nor spheres; therefore, it was necessary to find a general applicable geometrical measure.

Based on water imbibition experiments of Mattax and Kyte[55], Kazemi *et al.*[45] introduced a generalized shape factor given by Equation 2.43. It is easy to show that for idealized cases this equation becomes identical to the Warren and Root[95] expression given in Equation 2.48. Despite of this asymptotic accordance and its widely acceptance, its general validity was shown first by Heinemann and Mittermeir[43]. The derivation of Heinemann and Mittermeir will be elaborated on in the next section.

Also Gerke and van Genuchten[30] tried to find a generalized geometrical factor, and found that such a factor must contain the relation of the surface to the matrix volume as given in Equation 2.30. Their geometry factor still contains, similar to Barker[9], an inaccurate-defined non-dimensional geometry-dependent coefficient. It should be emphasized, that the dual continuum concept is one but not the only method to describe flow in heterogenous porous media. On the other hand, the dual continuum approach is still the most accepted one and a very successful method in describing oil and gas recovery from naturally fractured dual porosity reservoirs. Lewandowska *et al.*[51] claims to have found a more general approach. Their work contains interesting ideas but does not give any experimental evidence or demonstrates its practical applicability.

2.1.5.2 Derivation of the generalized shape factor

Consider a single matrix block surrounded by fractures. The matrix block is a porous permeable piece of rock containing the multi-component multi-phase fluid system. The state of the fluids and its movement is described by the Equation 2.1 through Equation 2.16. Consequently, the Equation 2.28 is applicable for a single matrix block having an arbitrary shape as shown in Figure 2.5.

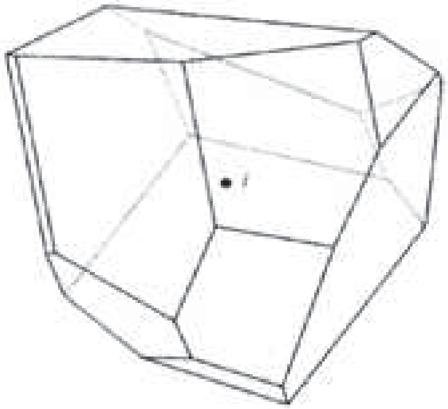

Figure 2.5: General 3D grid block

The dual continua approach handles the matrix-fracture transfer term as a discrete term, expressed as the rate of a volume source. This rate can be derived from Equation 2.28 by discretizing it in time and space of the matrix block. The matrix block is then the control volume on which the flow term is integrated. By neglecting the diffusion term and replacing the right side of the Equation 2.31 by the average values

$$\iiint_{V_m} \frac{\partial}{\partial t}\left(\phi \sum_{p=1}^{P} S_p D_p x_{pc}\right) dV = \frac{V_{mi}}{\Delta t}\Delta_t\left(\phi \sum_{p=1}^{P} S_p D_p x_{pc}\right)_{mi} , \tag{2.31}$$

results in the equation

$$\frac{1}{V_{mi}} \sum_{j=1}^{N} \iint_{A_{ij}} \left(\sum_{p=1}^{P} (\Lambda_{pc} k_a \bar{\bar{k}}' \nabla \Phi_p) \right) \vec{n} \, dA = \frac{1}{\Delta t}\Delta_t\left(\phi \sum_{p=1}^{P} S_p D_p x_{pc}\right)_{mi} . \tag{2.32}$$

The equation was already divided by $V_{mi.}$. The permeability in Equation 2.32 is the effective matrix-fracture permeability which, if the fracture block volume can be neglected, compared to the matrix block volume, is equivalent to the matrix permeability. Δt is the time step and Δ_t the time difference operator

$$\Delta_t x = x^{n+1} - x^{n} . \tag{2.33}$$

Assuming bilinear distribution of pressure, the density and the porosity depend on the average pressure, calculated from the matrix grid point and the fracture. It is evident, that the left side of the Equation 2.32 is the specific matrix fracture flow rate

$$q_{cmf} = \frac{1}{V_{mi}} \sum_{j=1}^{N} \iint_{A_{ij}} \left(\sum_{p=1}^{P} (\Lambda_{pc} k_a \bar{\bar{k}}' \nabla \Phi_p) \right) \vec{n} \, dA , \tag{2.34}$$

To be able to introduce this value in Equation 2.28 the right hand side of Equation 2.34 has to be discretized. This means that the surface integral will be replaced by multiplication with the surface, the mobility will be determined from the average of the block state variables and the potential gradient by its component effective on the block sides. Therefore one has to approximate

- the surface A_{ij} facing the matrix block i to the fracture side j,
- the component mobility $\Lambda_{pc} = \lambda_p D_p x_{pc}$,
- the scalar product $(\bar{\bar{k}}' \nabla \Phi_p)\vec{n}$.

The surfaces A_{ij} and the orientation of the unit normal vector $\vec{n}_{ij}$ are determined by the shape of the matrix block. Once the matrix block is identified, as in Figure 2.4, the area and the orientation can be calculated by means of geometry.

The mass mobility Λ_p, is required on A_{ij}. To get an approximate value for Λ_p, some sort of averaging is necessary. For multi-phase flow, upstream-weighting has shown to converge to the physically correct solution. The simplest way is to take one of the values, which leads to one-point upstream-weighting.

For the approximation of the scalar product $(\bar{\bar{k}}'\nabla\Phi_p)\vec{n}$ imaginary grid points must be set into the surrounding fracture network to every block faces $j = 1, N$. The fracture width is negligeable compared to the matrix block volume, therefore they are situated within the plane of the block sides. The fracture cells, containing a greater number of matrix blocks according the Warren-Root concept (see Figure 2.6) is represented by average pressure and saturation. Consequently all of the neighboring fracture grid points have the same potential and can be set anywhere into the matrix block sides.

The vector $\vec{d}_{ij}$ measuring the distance must be k-orthogonal on the surface A_{ij}. to between grid the point i and its neighbor j, therefore:

$$\bar{\bar{k}}'\vec{n}_{ij} \parallel \vec{d}_{ij} . \tag{2.35}$$

In analogy to the derivation of Equation 2.36,

$$(\nabla\Phi_p \cdot (\bar{\bar{k}}'\vec{n}))_{ij} = \left|\bar{\bar{k}}'\vec{n}\right| \frac{(\Phi_{pj} - \Phi_{pi})}{\left|\vec{d}_{ij}\right|} \tag{2.36}$$

Inserting Equation 2.34 into Equation 2.34 and

$$q_{cmf} = \frac{1}{V_{mi}} \sum_{j=1}^{N} A_{ij} \frac{\left|\bar{\bar{k}}'\vec{n}_j\right|}{\left|\vec{d}_j\right|} \sum_{p=1}^{P} \Lambda_{pc} k_a (\Phi_{pj} - \Phi_{pi}) . \tag{2.37}$$

The first term of Equation 2.37 contains only quantities depending on the geometry of the matrix block and its orientation in the coordinate system built by the principal permeability direction. These terms can be united as one constant called, according to the Warren-Root concept, shape factor:

$$\sigma = \frac{1}{V_{mi}} \sum_{j=1}^{N} A_{ij} \frac{\left|\bar{\bar{k}}'\vec{n}_j\right|}{\left|\vec{d}_j\right|} . \tag{2.38}$$

which has to be seen as a characteristic value of the fractured dual continuum and has a dimension L^{-2}. The shape factor as expected semantically, has to be a factor representing the effects of the shape of the system in the matrix-fracture transfer function and obviously it is expected that as long as the shape of the system (matrix shape, orientation etc.) has not changed, the shape factor should remain constant. The expression ‘time-dependent shape factor’ proposed and used by some authors is self-contradictory.

The resulting matrix-fracture transfer rate for a component is then:

$$q_{cmf} = \sigma k_a \sum_{p=1}^{P} \Lambda_{pc} (\Phi_{pj} - \Phi_{pi}) \tag{2.39}$$

The shape factor σ, defined by Equation 2.38, is a characteristic of the fractured rock, proportional to the specific surface of the matrix block.

The expression given in Equation 2.38, derived by Heinemann and Mittermeir[43] in year 2006, is the most general definition of the shape factor. It is easy to show that this expression contains all other forms of the shape factor introduced earlier.

2.1.5.3 The Kazemi-Gilman-ElSharkawy generalized shape factor.

In an isotropic medium the scaled permeability tensor $\bar{\bar{k}}'$ is a unit tensor and can be discarded. The fracture grid point j should be set in such a way that the connection line to point i is orthogonal to the surface A_{ij}. In this case the following approximation is applicable:

$$(\nabla\Phi_p \cdot \vec{n})_{ij} \approx \frac{(\Phi_j - \Phi_i)_p}{d_{ij}} . \tag{2.40}$$

where d_{ij} is the distance of the point i from the side A_{ij}. Applying Equation 2.40 to Equation 2.37 yields to

$$q_{cmf} = \frac{1}{V_{mi}} \sum_{j=1}^{N} \frac{A_{ij}}{d_{ij}} k_a \sum_{p=1}^{P} \Lambda_{pc}(\Phi_{pj} - \Phi_{pi}) . \tag{2.41}$$

The comparison of Equation 2.39 and Equation 2.41 results in the definition:

$$\sigma = \frac{1}{V_{mi}} \sum_{j=1}^{N} \frac{A_{ij}}{d_{ij}} \tag{2.42}$$

Based on water imbibition experiments Kazemi *et al.*[45] suggested a general definition for the shape factor

$$\sigma = \frac{1}{V_{mi}} \sum_{j=1}^{N} \left(\frac{A}{d}\right)_i , \tag{2.43}$$

where V_{mi} is the volume of the matrix block, A is a surface and d is the orthogonal distance of the point of gravity to this surface. Equation 2.42 is identical to the general definition for the shape factor by Kazemi *et al.*[45]. For this reason both the Kazemi-Gilman-El Sharkawy[45] and the more general Heinemann-Mittermeir[43] definition can be considered as theoretically well funded and experimentally verified.

2.1.5.4 The Warren and Root model

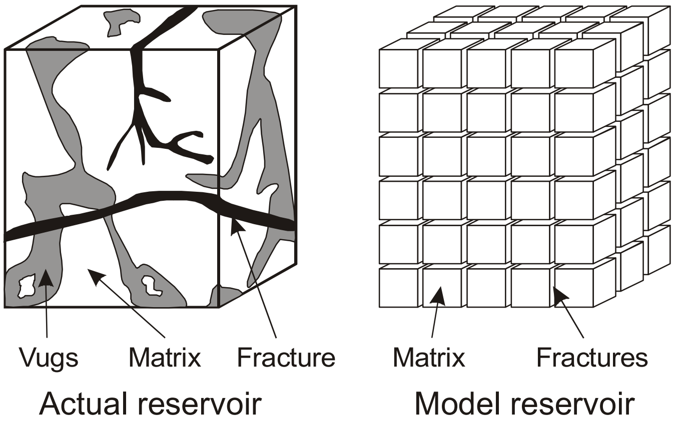

Figure 2.6: Idealization of fractured reservoirs (after Warren and Root[95])

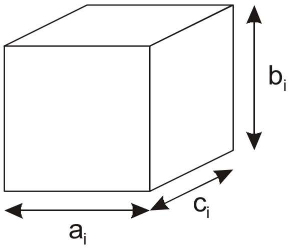

Figure 2.7: Size of an idealized matrix block

Figure 2.6 and Figure 2.7 show the Warren-Root[95] idealized concept of a fractured rock. Let p_m be the pressure in the matrix block and p_f the uniform pressure in the surrounding fracture. The total matrix-fracture exchange flow rate can then be calculated using Darcy law:

$$q = 2q_x + 2q_y + 2q_z = 2\left(\frac{bc}{a/2}k_x + \frac{ab}{c/2}k_y + \frac{ac}{b/2}k_z\right)\frac{1}{\mu}(p_f - p_m) \tag{2.44}$$

or

$$q = 4abc\left(\frac{1}{a^2}k_x + \frac{1}{c^2}k_y + \frac{1}{b^2}k_z\right)\frac{1}{\mu}(p_f - p_m). \tag{2.45}$$

q is negative if the fluid is flowing from the matrix into the fracture.

Assuming isotropic permeability, $k_x = k_y = k_z = k$:

$$q = 4abc\left(\frac{1}{a^2} + \frac{1}{c^2} + \frac{1}{b^2}\right)\frac{k}{\mu}(p_f - p_m). \tag{2.46}$$

The volume of the matrix block is

$$V_m = abc\,, \tag{2.47}$$

therefore, compared with the shape factor is:

$$\sigma = 4\left(\frac{1}{a^2} + \frac{1}{b^2} + \frac{1}{c^2}\right) \tag{2.48}$$

2.1.5.5 Additional Remarks

The shape factor as expected semantically, has to be a factor representing the effects of the shape of the system in the matrix-fracture transfer function and as long as the shape of the system (matrix shape, orientation etc.) has not changed, the shape factor should remain constant. The expression ‘time-dependent shape factor’ proposed and used by some authors is self-contradictory.

Furthermore, it must be recognized that the shape of the matrix block has an influence on the driving forces. Two blocks of different shape can have the same shape factor; but block shape, especially the aspect ratio, can be different. The aspect ratio influences the gravitational and viscous forces and thus has a dominant impact on reservoir performance. These effects must be considered separately from the shape factor. It is also not true that the shape factor looses its validity for anisotropic matrices. The expression, given in Equation 2.38 considers properly the anisotropy.

2.2. Boundary Conditions (BC)

Boundaries can be divided into inner- or outer-boundaries. Outer boundaries are the top and bottom of the domain as outer delimitation lines (surfaces). Examples of inner boundaries are discontinuity lines (surfaces) such as faults.

Generally, two types of boundary conditions (BCs) can be defined:

I. DIRICHLET type BC. - The potential is known at the boundary:

$$\Phi = \Phi_\Gamma(t)\,, \qquad \vec{x} \in \Gamma\,. \tag{2.49}$$

II. VON NEUMANN type BC. - The flow rate across the boundary is known:

$$u_{p\Gamma}(t) = -\lambda_p \bar{\bar{k}} \nabla \Phi_p \vec{n}_\Gamma\,, \quad \vec{x} \in \Gamma\,. \tag{2.50}$$

If the boundary is sealing (no-flow boundary) then:

$$u_{p\Gamma} = 0. \tag{2.51}$$

The top and bottom of the domain are sealing (no-flow) boundaries.

At the outer delimitations of the domain all kind of boundary conditions can be applied:

- In case of a grid aquifer this boundary is sealing.
- The flow rate as function of time is defined if an analytical aquifer model is used.
- Constant potential can be set for special cases.

At the well surfaces both BCs can be set. The flow rate or the potential at this boundary must be determined by a well model which considers the type of the well operation (constant rate, constant bottom-hole or wellhead pressure, etc.) and the pressure-drop within the well-bore. Such a well model can be analytical, numerical or semi-analytical.

An inner boundary separates and/or connects two continua. At any point *i* of the this boundary the flux must be continuous:

$$\bar{\bar{k}}_{ir}\nabla\Phi_{ir}\vec{n}_i = \bar{\bar{k}}_{il}\nabla\Phi_{il}\vec{n}_i, \tag{2.52}$$

where *ir* and *il* denote the right and left sides of the discontinuity surface, Φ_p is the potential of the phase *p* and $\vec{n}_i$ is the normal vector to the surface. The flow through the inner boundary can cause an additional pressure-drop (the choke effect), therefore, the potential is not continuous at this boundary:

$$\Phi_{pir} = \Phi_{pil} - \varepsilon_i\vec{u}_{pi}\vec{n}_i, \tag{2.53}$$

where ε is rather a function of the potential difference $\Phi_{pir} - \Phi_{pil}$ than a constant. The filtration velocity of phase *p* can be calculated from both sides of the boundary:

$$\vec{u}_{pi} = -\lambda_p\bar{\bar{k}}_{ir}\nabla\Phi_{pir}. \tag{2.54}$$

2.3. Discretized Mathematical Model

2.3.1 Discretized Mole Balance Equations

The discretization of the mole balances for dual continuum models, given by Equation 2.55 through Equation 2.56, follows the same scheme as for single-porosity ones, leading to the following expressions:

a) The balance equation for the fracture continuum:

$$\sum_{j=1}^{Nf}\sum_{p=1}^{P}\tau_{ij}(\Lambda_{pc})_{ij}^{n+1}(\Phi_{pj}-\Phi_{pi})^{n+1}+\sum_{p=1}^{P}(q_pD_px_{pc})_i^{n+1}+q_{cmf}^{n+1} = \frac{V_{if}}{\Delta t}\Delta_t\left[\phi\sum_{p=1}^{P}(S_pD_px_{pc})\right]_{i,f} \tag{2.55}$$

b) The balance equation for the matrix continuum:

$$\sum_{j=1}^{Nm}\sum_{p=1}^{P}\tau_{ij}(\Lambda_{pc})_{ij}^{n+1}(\Phi_{pj}-\Phi_{pi})^{n+1}+\sum_{p=1}^{P}(q_pD_px_{pc})_i^{n+1}-q_{cmf}^{n+1} = \frac{V_{im}}{\Delta t}\Delta_t\left[\phi\sum_{p=1}^{P}(S_pD_px_{pc})\right]_{i,m} \tag{2.56}$$

where q_{cmf} is matrix-fracture transfer term.

Equation 2.56 is valid, if the matrix grid system is continuous (i.e. the matrix block has matrix neighbors, $Nm > 0$). This is the case in a dual-porosity dual-permeability approach, but it is not the case for dual-porosity models. In the dual-porosity model, the matrix cell forms a noncontinuous medium and act solely as the source or sink term for the fractures (no wells perforated in the matrix and $Nm = 0$). Thus, for a dual porosity system the matrix mole balance equation is reduced to Equation 2.57, or in a discretized form to:

$$-q_{cmf}^{n+1} = \frac{V_{im}}{\Delta t}\Delta_t\left[\phi\sum_{p=1}^{P}(S_pD_px_{pc})\right]_{i,m}, \tag{2.57}$$

where the indices *m* and *f* are for matrix and fracture respectively. The terms are defined as follows:

N - number of neighboring blocks
τ_{ij} - interblock transmissibility, [m^3]
x_{pc} - mole fraction of component *c* in phase *p*, [-]
λ_p - mobility of the phase *p*, [1/cp]
D_p - specific mole density, [kmol/m^3]
Φ_p - phase potential, [bar]
q_p - source/sink term for phase, [m^3/day]
Δt - time step, [day]
V_i - grid block volume, [m^3]
Φ - porosity, [-]
S_p - phase saturation, [-]

Δ_t - time difference operator, $\Delta_t\Gamma = \Gamma^{n+1} - \Gamma^{n}$
n - subscript, denoting the time step, [-]
$n+1$ - subscript, new time step, [-]

2.3.2 Discretized Transfer Term

The discretized inter-porosity molar flux of component *c* for one cell is:

$$q_{cmf}^{n+1} = \tau_{mf} \sum_{p=1}^{P} [\Lambda_{pcmf}^{n+1} (\Phi_{pm} - \Phi_{pf})^{n+1}] \quad , \tag{2.58}$$

$$+ \delta_{mf} \sum_{p=1}^{P} [D_{pc} (S_p D_p)_m^{n+1} (x_{pcm} - x_{pcf})^{n+1}]$$

where

$$\tau_{mf} = k_m V \sigma \tag{2.59}$$

is the *matrix-fracture transmissivity* and

$$\delta_{mf} = \phi V \sigma \tag{2.60}$$

is the *matrix-fracture diffusivity.* The expression *diffusivity* is analogous to the transmissivity, but the permeability is replaced by the porosity. Note that *V* is the volume of the grid cell, means the control volume of the discretization and not the volume of the matrix block (see Section 5.2. for more details). It will be assumed that the grid block is identical for the fracture and matrix continua. The potential difference of phase *p,* between the matrix and the fracture grid block is:

$$\Phi_{pm} - \Phi_{pf} = p_{pm} - p_{pf} - \frac{1}{2}(\rho_{pm} + \rho_{pf}) g \Delta z_{mf} + P_{cpp'm} - P_{cpp'f}, \tag{2.61}$$

where *z* is the depth of grid points. The difference,

$$\Delta z_{mf} = z_m - z_{f}., \tag{2.62}$$

if not otherwise defined, will be zero $(\Delta z_{mf} = 0)$, as the two grid systems representing matrix and fractures are overlapping. Therefore, Equation 2.61 reduces to

$$\Phi_{pm} - \Phi_{pf} = p_{pm} - p_{pf} + P_{cpp'm} - P_{cpp'f}. \tag{2.63}$$

An additional potential difference can be created by the capillary force (see Section 4.1.2 for more details), the difference in the fluid density in the matrix blocks and the surrounding fractures (see Section 4.1.3 for more details) or by the pressure drop along the fractures caused by the flow and the static matrix (see Section 4.1.4 for more details).

2.3.3 Component Mobility

The component mobility is evaluated from single-point upstream weighting, based on the phase potentials, resulting in

$$\Lambda_{pc_{mf}} = \begin{cases} \Lambda_{pc_m}, \text{ if } \Phi_{pm} > \Phi_{pf} \\ \Lambda_{pc_f}, \text{ if } \Phi_{pm} \le \Phi_{pf} \end{cases}. \tag{2.64}$$

In general, single-point upstream weighting is used to evaluate the phase mobilities. Hence, when the flow goes from the matrix into the fracture, the relative permeability of the matrix is used for the calculation. When the flow goes from the fracture into the matrix, the flow is essentially also governed by the matrix properties. Therefore, options should be provided to combine matrix and fracture variables while calculating the phase mobility, even if the fracture is upstream. The following solutions could be imagined:

1. The matrix relative permeability is calculated for the fracture saturation.
2. Both the fracture-to-fracture flow and the fracture-to-matrix flow use the fracture relative permeability functions. Typically, they are straight lines with maximum values of 1.0, whereas the relative permeabilities in the matrix at the residual saturation of the displaced phase are considerably smaller. Therefore, the fracture relative permeability should be scaled up to using the maximum function values from the matrix. For the water phase the relative permeability is scaled as follows:

$$k_{rf}(S_{wf}) = k_{rf}(S_{wf})^{tab} \times (k_{rwm}^{max} / k_{rwf}^{max}), \tag{2.65}$$

   where.

   $k_{rf}(S_{wf})^{tab}$ is the fracture relative permeability looked up from the laboratory curves' table.

   k_{rwm}^{max} *and* k_{rwf}^{max} are the maximum relative permeability values for matrix and fracture respectively.

   The relative permeabilities for other phases (gas and oil) will be scaled in the same way. For the gas case the relative permeability is scaled to the matrix value at $S_g = 1\text{-}S_{org}$ and for the oil to $S_o = 1\text{-}max(S_{orw}, S_{org})$.
3. Using direction-dependent relative permeability functions. In addition to the relative permeability curves for matrix-matrix flow (laboratory curves) and fracture-fracture flow (usually straight lines), this option enables the treatment of matrix-fracture and fracture-matrix flow (pseudo-curves) and will therefore, always use the saturations from the upstream block.

2.4. The MINC method

Note: since it is not practically used, the following method is just explained here briefly to inform the reader about its existence and will not be referred to in any other section of this script.

In 1985 Pruess and Narasimhan[74] proposed the Multiple INteracting Continua (MINC) method for numerical simulations of heat and multiphase fluid flow in multidimensional fractured media. The MINC method is able to handle the transient flow of heat and fluids between matrix and fractures numerically. This is in contrast to the standard dual porosity model which uses an analytical expression, under the assumption of pseudo-steady state flow, for coupling the flow between matrix and fractures. Thus, the MINC model can be regarded as a generalization of the Barrenblatt *et al.*[8] and the Warren and Root[95] models. For most cases the pseudo-steady state flow description is sufficient. Only for some cases, such as a well test in a dual porosity system, the transient nature of the matrix-fracture flow is of importance for reservoir simulation.

The traditional dual porosity approach assumes that the matrix cell, within the fracture network, can be regarded as a single cell. But in the MINC approach it is different since two kinds of grid can be found:

1. A primary grid, which is the discretization of the reservoir volume into grid blocks.
2. A secondary grid, which is formed by nested sub-cells representing the matrix.

Such a MINC grid is illustrated in Figure 2.8. Figuratively speaking, each matrix grid cell could be regarded as a “Russian Doll” of nested sub-cells.

Even the MINC method, as a generalization of the dual-porosity models, it is based on some assumptions, namely:

1. The fractured reservoir is represented by uniform cubes, representing the matrix, which are bounded by fracture planes on all faces. A generalization to arbitrary fracture geometries is available, using a proximity function.
2. The depletion process is influenced by two aspects: First of all by the global movement of fluid and heat through the reservoir mainly taking place in the fracture system. Secondly by the fluid and heat flow between the matrix and the fracture. Thermodynamic conditions, such as temperatures, pressures, vapor saturations, in the matrix depend primarily on the distance from the nearest fracture. This leads to a discretization of the matrix into sub-volumes, where the interfaces between the matrix volume elements are parallel to the nearest fracture.
3. The equipotential surfaces of pressure, temperature and other thermodynamic state variables are assumed to be planes parallel to the nearest fracture. This assumption will hardly be the case for real flow problems. Nonetheless, some conditions can be imagined where a “distance-only” approximation leads to an accurate prediction of interporosity flow:
    3.1 Initial thermodynamic conditions in the matrix depend approximately only on the distance from the fracture. This includes the special case of uniform initial conditions in the matrix blocks.

3.2 The boundary conditions for the matrix blocks have to stay approximately constant at all times. If the transient conditions taking place in the fractures occur in a certain way, this condition will be satisfied.

However, the MINC method can be applied correctly to more than the latter conditions. As soon as the pressure, respectively the temperature gradient, calculated with the distance-only approximation leads to correct total flow rates over an sub-cell interface area, the MINC method can be regarded as accurate. With the distance-only approximation of MINC pressure, viscous and capillary force can be handled properly, but gravity forces, because of its directional dependency, would be problematic.

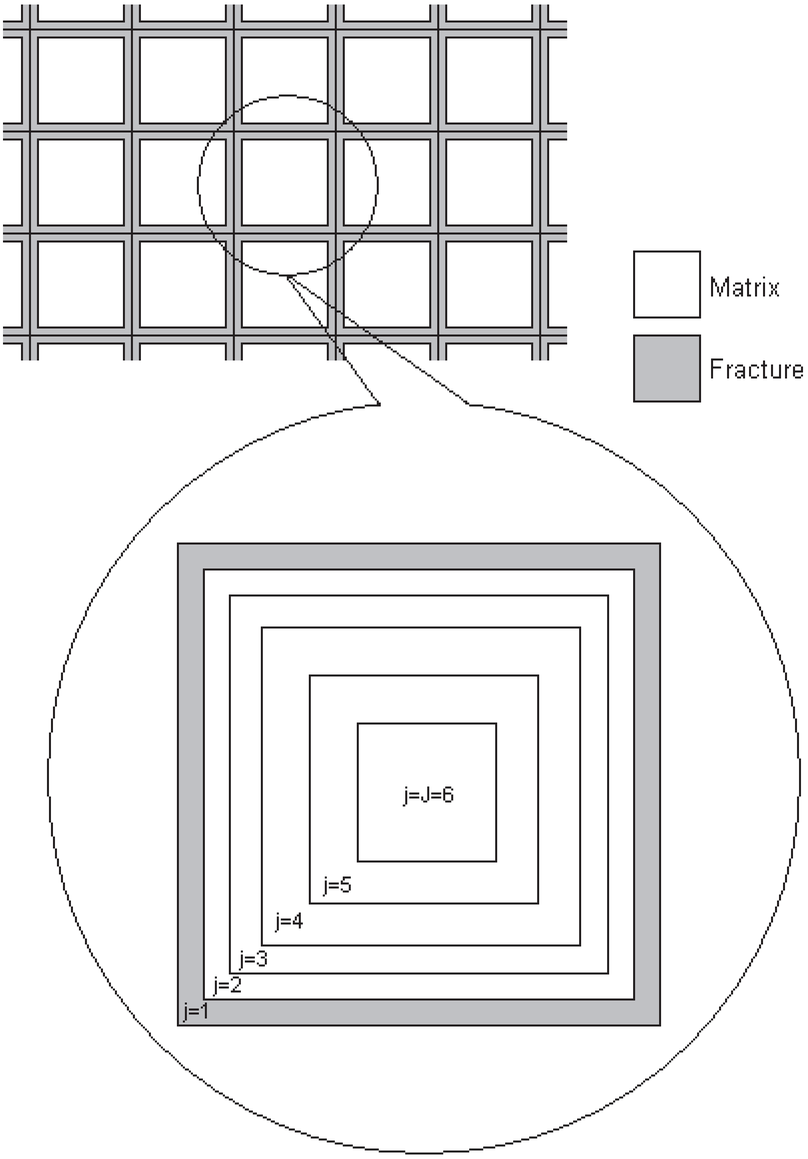

Figure 2.8: The MINC discretization

The grid generation for the MINC method can be described in three steps:

1. Firstly, the primary mesh has to be defined. This may be done by considering global reservoir geometry, global variations of reservoir properties and the desired spatial grid resolution. The global mesh will divide the reservoir into *N* elemental volumes V_n, where the subscript *n* ranges from 1 to *N*.
2. In the second step, the geometric parameters of the nested volume elements, V_j, within the primary volumes, V_n, have to be determined. In order to being able to do this, the volume fraction, f_j, of each individual sub-cell has to be known up front. The variable *j* is valid from 1 to *J*, where 1 refers to the fracture and *J* corresponds to the innermost matrix sub-cell. The volume fraction f_1 can easily be derived from the fracture spacing, *L*, and the fracture aperture, δ. Thus leading to:

$$f_1 = \frac{[L^3 - (L-\delta)^3]}{L^3} \approx \frac{3\delta}{L}. \tag{2.66}$$

   The other volume fractions can be chosen arbitrarily, only the constraint of $\sum_{j=1}^{J} f_j = 1$ has to be fulfilled. Of special interest is the region closest to the fractures. As a consequence, the outer matrix cub-cells having the indices *j = 2,3,...* will be more tightly-spaced than the elements far away from the fracture with the indices *j = J, J-1,....* This can be also seen in Figure 2.9.

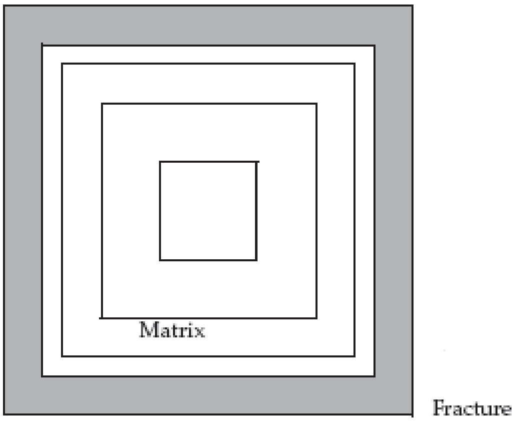

Figure 2.9: Nested matrix sub-cells with different spacing

   Based on the fracture spacing, *L*, and the volume fraction of the j^{th} continuum, f_j, the sub-cell volume can be calculated by

$$V_j = f_j L^3. \tag{2.67}$$

   Details on how the nodal distances and the interface areas are defined, as well as the used discretization scheme, integral finite difference formulation, for the MINC method can be found in the publication by Pruess and Narasimhan[74].
3. Usually the fracture spacing, *L*, is much smaller than the size of the grid cells of the

> primary grid. Thus, Pruess and Narasimhan[74] formulated scaling laws on how to partition the volume elements, V_n, of the primary grid into a sequence of interacting continua elements, V_{nj}, where j is indexing a continuum within V_n.

In a simulation grid cell with nested volume elements as outlined above, only one flow direction will be possible. This will be an outward flow from the matrix to the fracture, as production of reservoir fluids causing a pressure decline in the fracture system. This imposes a limitation to the MINC method. For instance, compositional problems arising in EOR operations require a modification of the method, which would allow flow through the matrix.

ECLIPSE[87] offers a method similar to the MINC method. Three different geometry options with increasing dimensional complexity are available. A linear (1D), a cylindrical (2D) and a spherical (3D) one. The cylindrical and the spherical geometries are respectively approximated by square cylinders and cubes

Chapter 3

Single Phase Flow in Naturally Fractured Rocks

3.1. The Warren-Root Model

The equation of continuity describes the law of mass conservation. For one phase flow in porous media the equation of mass conservation is written in the following form:

$$\nabla(\rho\vec{u}) = -\frac{\partial(\phi\rho)}{\partial t}, \tag{3.1}$$

where u is the filtration velocity, ϕ the porosity and ρ the fluid density. For a dual continua, Barenblatt *et al.*[8] introduced the term of interflow as a volume source and sink, and so Equation 3.1 can be written for matrix (subscript m) and fracture (subscript f) separately as:

$$\nabla(\rho\overrightarrow{u_f}) - q^{mf} = -\frac{\partial(\phi_f\rho)}{\partial t}. \tag{3.2}$$

$$\nabla(\rho\overrightarrow{u_m}) + q^{mf} = -\frac{\partial(\phi_m\rho)}{\partial t} \tag{3.3}$$

The interflow rate will be expressed as a linear relationship of the fracture-matrix pressure difference, assuming a pseudo-steady state flow from the matrix to the fracture:

$$q^{mf} = \rho^o \cdot \frac{\sigma k_m}{\mu}(p_f - p_m), \tag{3.4}$$

where σ is called shape factor. σ is a characteristic coefficient of the fractured rock, proportional to the specific surface of the matrix block (see Section 2.1.5 for more details). Note that the interflow rate has a dimension of $[m.t^{-1}.L^{-3}]$, and therefore, the dimension of σ is $[L^{-2}]$. The Barenblatt[8]'s assumption was proved by Kazemi *et al.*[45], concluding that in the practically interesting range of parameters the pseudo-steady state is reached quickly and, therefore, this assumption is reasonable. Note also that for the sake of convenience ρ^o is the fluid density at the reference pressure and therefore is constant.

Then the total compressibility for the matrix is:

$$c_m = c + c_{\phi m}, \tag{3.5}$$

where c is the fluid compressibility and c_ϕ the pore compressibility. Assuming low and constant compressibility for liquid and pores then the following approximation hold:

$$(\phi\rho)_m = (\phi\rho)_m^o\left\{1 + c_m(p_m - p^o)\right\}, \tag{3.6}$$

where the superscript, ^{o}, is for the reference state, preferably equal to the initial reservoir pressure p_i. Similarly for the fracture continuum:

$$c_f = c + c_{\phi f} \tag{3.7}$$

and

$$(\phi\rho)_f = (\phi\rho)_f^o\left\{1 + c_f(p_f - p^o)\right\}. \tag{3.8}$$

The filtration velocity will be calculated using Darcy's law:

$$\vec{u}_f = -\frac{k_f}{\mu}(\nabla p + \rho\vec{g}) . \tag{3.9}$$

Inserting Equation 3.9 and Equation 3.4 into Equation 3.2 results:

$$\frac{k_f}{\mu}\nabla^2 p_f + \frac{\sigma k_m}{\mu}(p_f - p_m) - \phi_f c_f \frac{\partial p_f}{\partial t} = 0, \tag{3.10}$$

where the term $\nabla^2(\rho^2\vec{g})$ was already neglected. Warren and Root[95] assumed no flow between the matrix blocks, therefore $\nabla(\rho\vec{u}_m) = 0$ and the Equation 3.2 is reduced to the following:

$$\frac{\sigma k_m}{\mu}(p_f - p_m) + \phi_m c_m \frac{\partial p_m}{\partial t} = 0. \tag{3.11}$$

Considering one dimensional radial symmetrical flow and using the relation given by Equation 3.11, Equation 3.10 becomes the following form:

$$\frac{k_f}{\mu}\left(\frac{1}{r}\frac{\partial}{\partial r}\left(r\frac{\partial p_f}{\partial r}\right)\right) + \phi_f c_f \frac{\partial p_f}{\partial t} - \phi_m c_m \frac{\partial p_m}{\partial t} = 0. \tag{3.12}$$

Note that here the special form of Laplace operator for radial symmetrical case as in Equation 3.13 is used.

$$\nabla^2 p_f = \frac{1}{r}\frac{\partial}{\partial r}\left(r\frac{\partial p_f}{\partial r}\right) \tag{3.13}$$

3.1.1 Pressure Draw-Down in the Infinite Acting Case

Consider the following conditions:

Initially the pressure is uniform:

$$p_m = p_f = p^o, \quad r \geq r_w, \quad t = 0 \tag{3.14}$$

The outer boundary is in infinitum, therefore:

$$p_m = p_f = p^o, \quad r \to \infty, \quad t \geq 0 \tag{3.15}$$

The well with radius r_w produces with constant rate:

$$\frac{2\pi r_w h k_f}{\mu}\frac{\partial p}{\partial r} = q, \quad r = r_w, \quad t > 0 \tag{3.16}$$

Warren and Root[95] applied the following dimensionless variables and parameters:

Dimensionless radius:

$$r_D = \frac{r}{r_w} \tag{3.17}$$

Dimensionless time:

$$t_D = \frac{k_f}{(\phi_m c_m + \phi_f c_f)\mu r_w^2} t \tag{3.18}$$

Dimensionless pressure:

$$P_D = \frac{2\pi h k}{\mu q}[p - p^o], \tag{3.19}$$

The dimensionless matrix-fracture transfer capacity λ is proportional to the ratio of the fracture and the matrix permeabilities:

$$\lambda = \frac{\sigma k_m r_w^2}{k_f}. \tag{3.20}$$

The dimensionless parameter

$$\omega = \frac{\phi_f c_f}{\phi_f c_f + \phi_m c_m} \tag{3.21}$$

is called storativity ratio and expresses the ratio between the storage capacity of the fracture network and the total storage capacity.

Using the dimensionless variables of Equation 3.17 through Equation 3.21, in Equation 3.11 and Equation 3.12, with the conditions Equation 3.14 through Equation 3.16, gives:

$$(1-\omega)\frac{\partial P_{Dm}}{\partial t_D} - \lambda(P_{Df} - P_{Dm}) = 0 \tag{3.22}$$

$$\frac{1}{r_D}\frac{\partial}{\partial r_D}\left(r_D\frac{\partial P_{Df}}{\partial r_D}\right) - \omega\frac{\partial P_{Df}}{\partial t_D} + (1-\omega)\frac{\partial P_{Dm}}{\partial t_D} = 0 \tag{3.23}$$

$$P_{Dm} = P_{Df} = 0, \quad r_D \geq 1, \quad t_D = 0 \tag{3.24}$$

$$P_{Dm} = P_{Df} = 0, \quad r_D \to \infty, \quad t_D \geq 0 \tag{3.25}$$

$$\frac{\partial P_{Df}}{\partial r_D} = -1, \quad r_D = 1, \quad t_D > 0 \tag{3.26}$$

The solution of the boundary condition problem Equation 3.22 through Equation 3.26, similar to the solutions of the Hurst-van Everdingen problems, can be obtained by a Laplace transformation. For r_D=1, i.e. for the well bottom pressure:

$$P_{Df}(1, t) = L^{-1}\left[\frac{K_0(\sqrt{sf(s)})}{s\sqrt{sf(s)}K_1(\sqrt{sf(s)})}\right], \tag{3.27}$$

where

$$f(s)) = \frac{\omega(1-\omega)s + \lambda}{(1-\omega)s + \lambda} \tag{3.28}$$

The inversion L^{-1} leads to an expression with infinite series containing K_0 and K_1, the second kind modified Bessel's functions of order zero and one. However, an asymptotic solution can be obtained if

$$t_D > 100\omega \text{ if } \lambda \ll 1 \quad \text{or} \tag{3.29}$$

$$t_D > 100\lambda - 1/\lambda \quad \text{if } \omega \ll 1\,. \tag{3.30}$$

These useful assumptions lead to the following approximation:

$$P_{Dfw}(t_D) = \frac{1}{2}\left[0.80907 + \ln t_D + Ei\left(-\frac{\lambda t_D}{\omega(1-\omega)}\right) - Ei\left(-\frac{\lambda t_D}{1-\omega}\right)\right] \tag{3.31}$$

or

$$P_{Dfw}(t_D) = \frac{1}{2}[0.80907 + \ln t_D + \Delta] \tag{3.32}$$

where Δ is the difference between Equation 3.31 and the single-porosity infinite acting solution (given also by Equation 3.37):

$$\Delta = \frac{1}{2}\left[Ei\left(-\frac{\lambda t_D}{\omega(1-\omega)}\right) - Ei\left(-\frac{\lambda t_D}{1-\omega}\right)\right]. \tag{3.33}$$

Equation 3.31 is plotted on Figure 3.1 while Equation 3.33 on Figure 3.2.

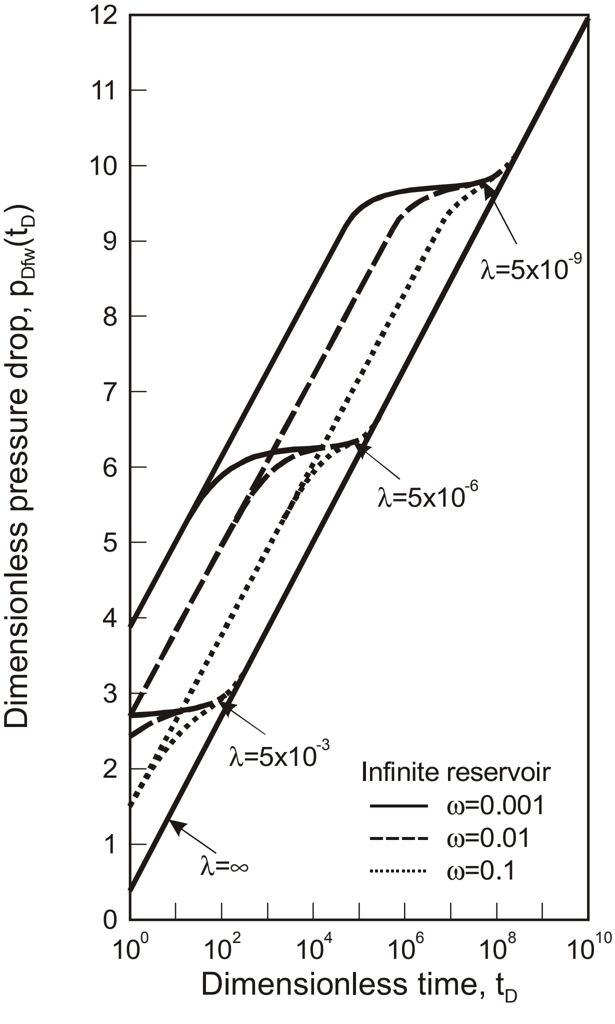

Figure 3.1: $P_{Dfw}(t_D)$ for pressure draw-down, infinite case, according Equation 3.31 (after Warren and Root[95]).

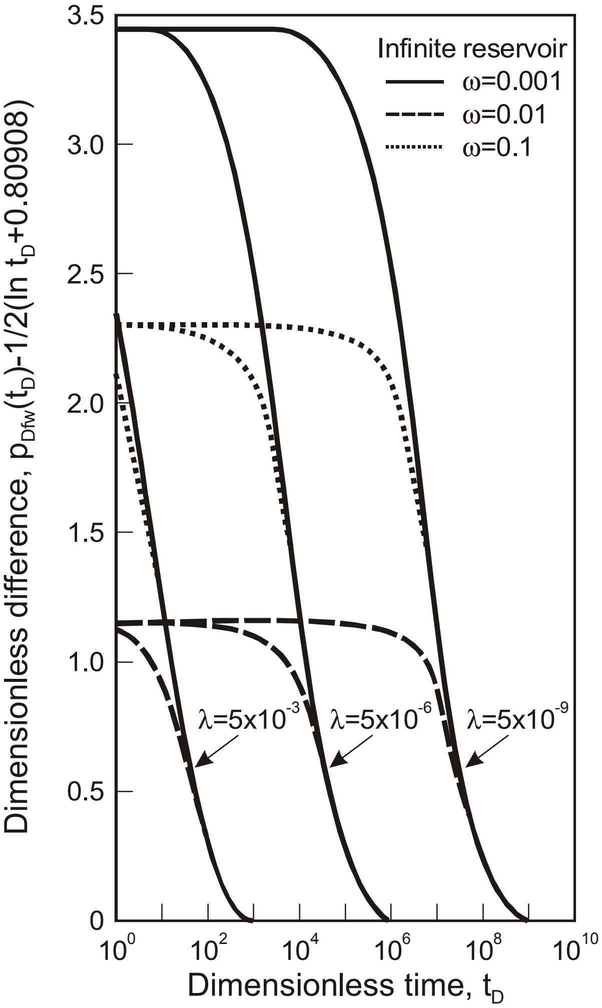

Figure 3.2: Difference curves $P_{Dfw}(t_D)-1/2(0.80907+\ln t_D)$ for pressure drowdawn, infinite case according Equation 3.33 (after Warren and Root[95]).

Both plots show three periods:

- The first period corresponds to the early stage of the production during which the liquid is produced mainly from the fracture system. For that first period, corresponding to a small argument of the *Ei* function, the logarithmic approximation:

  $$Ei(-\xi) = -\gamma - \ln\xi, \qquad \gamma = 0.5772\ldots \tag{3.34}$$

  can be used (γ is the Euler's number), leading to:

  $$P_{Dfw}(t_D) = \frac{1}{2}\left[0.80907 + \ln t_D + \ln\frac{1}{\omega}\right]. \tag{3.35}$$

- The second period is the transition between the first and third period and represents the interaction between ω *and* λ. Characteristic for this period is that the fracture pressure remains approximately constant. This corresponds to the concept that the large matrix pore volume has still the initial pressure and feeds the fracture system by quasi constant rate. Because $\omega \ll 1$ the argument of the first *Ei* expression is of a magnitude greater than that of the second, therefore Equation 3.33:

$$\Delta = \frac{1}{2}\left[Ei\left(-\frac{\lambda t_D}{\omega(1-\omega)}\right) - Ei\left(-\frac{\lambda t_D}{1-\omega}\right)\right] \approx -\frac{1}{2}Ei\left(-\frac{\lambda t_D}{1-\omega}\right) \tag{3.36}$$

- The third period is for a large $t_{D,}$ when the two *Ei* expressions in Equation 3.31 become the same and $\Delta = 0.$. Equation 3.31 becomes identical to that of the single porosity case:

  $$P_{Dfw}(t_D) = \frac{1}{2}[0.80907 + \ln t_D] \tag{3.37}$$

  In this period the matrix-fracture system communicates under pseudo-steady state conditions and the whole system produces as an equivalent homogeneous one. Since no flow exists between the matrix blocks the pressure drop of the equivalent homogenous reservoirs equals the permeability of the fractures.

The system parameters ω *and* λ can be easily determined from Equation 3.31 and Figure 3.2. At small t_D the difference Δ, which is the difference between the first and third period are straight lines in Figure 3.1, and therefore the index 13 is used:

$$\Delta_{13} = \ln\sqrt{1/\omega} = -\frac{1}{2}\ln\omega. \tag{3.38}$$

If t_D is small, which is the case for the transition (second) period, the logaritmical approximation (see Equation 3.31) can be applied to Equation 3.36:

$$\Delta = -\frac{1}{2}Ei\left(-\frac{\lambda t_D}{1-\omega}\right) = \frac{1}{2}\left[-\gamma - \ln\frac{\lambda t_D}{1-\omega}\right] \tag{3.39}$$

Note that the transition section of the difference curves has an average slope of -1.15/cycle, so a tangent drown through the inflection point which intersects the coordinate line at $t_D = 1$ at:

$$\Delta_2 = \frac{1}{2}\left[-\gamma - \ln\frac{\lambda}{1-\omega}\right] \tag{3.40}$$

gives the basis to calculate the parameter λ.

3.1.2 Pressure Draw-Down in a Finite Reservoir

The domain is closed at the outer radius r_{De}. The equations and conditions are the same as for the infinite case, given by Equation 3.22 through Equation 3.26, except for the boundary condition of Equation 3.25, which must be modified to:

$$\frac{\partial P_{Df}}{\partial r_D} = 0 \quad r_D = r_{De}, \quad t_D > 0\,. \tag{3.41}$$

The asymptotic solution valid at the conditions given by Equation 3.29 or Equation 3.30 is:

$$P_{Dfw}(t_D) = \left(\frac{2}{r_{De}^2}\right)\left[t_D + \frac{(1-\omega)^2}{\lambda}\exp\left(-\frac{\lambda t_D}{\omega(1-\omega)}\right)\right] + \ln r_{De} - \frac{3}{4} + s\,, \tag{3.42}$$

where the dimensionless skin factor is already added. Remember that the solution for the single porosity case is:

$$p_{Dw}(t_D) = \frac{2t_D}{r_{De}^2} + \ln r_{De} - \frac{3}{4} + s\,. \tag{3.43}$$

3.1.3 Pressure Build-Up, Infinite Case

The well’s shut-in pressure, may be directly obtained by superposition:

$$\Delta P_{Dfw} = P_{Dfw}(t_D + \Delta t_D) - P_{Dfw}(\Delta t_D) \tag{3.44}$$

By inserting the function according of Equation 3.31:

$$\Delta P_{Dsw} = \frac{1}{2}\left\{\ln\frac{t+\Delta t}{\Delta t} + Ei\left[-\frac{\lambda(t_D+\Delta t_D)}{\omega(1-\omega)}\right] - Ei\left[-\frac{\lambda\Delta t_D}{\omega(1-\omega)}\right] - \quad ,\right.$$
$$\left. Ei\left[-\frac{\lambda(t_D+\Delta t_D)}{1-\omega}\right] + Ei\left[-\frac{\lambda\Delta t_D}{1-\omega}\right]\right\} \tag{3.45}$$

For a large production time the *Ei* terms containing t_D will converge rapidly to zero and thus, the asymptotic solution of Equation 3.45 is reduced to:

$$\Delta P_{Dsw} = \frac{1}{2}\left\{\ln\frac{t+\Delta t}{\Delta t} + Ei\left[-\frac{\lambda\Delta t_D}{\omega(1-\omega)}\right] - Ei\left[-\frac{\lambda\Delta t_D}{1-\omega}\right]\right\}. \tag{3.46}$$

The limitation given by Equation 3.29 and Equation 3.30 are still valid.

Figure 3.4 shows some theoretical pressure build-up curves for constant λ and different ω. Note that the difference function to the single porosity case is the same as for pressure draw-down, given by Equation 3.33 and Figure 3.2. The same three periods as with pressure draw-down may be observed, and the parameters λ and ω can be determined in a similar way as by pressure draw-down, using the Equation 3.38 and Equation 3.40.

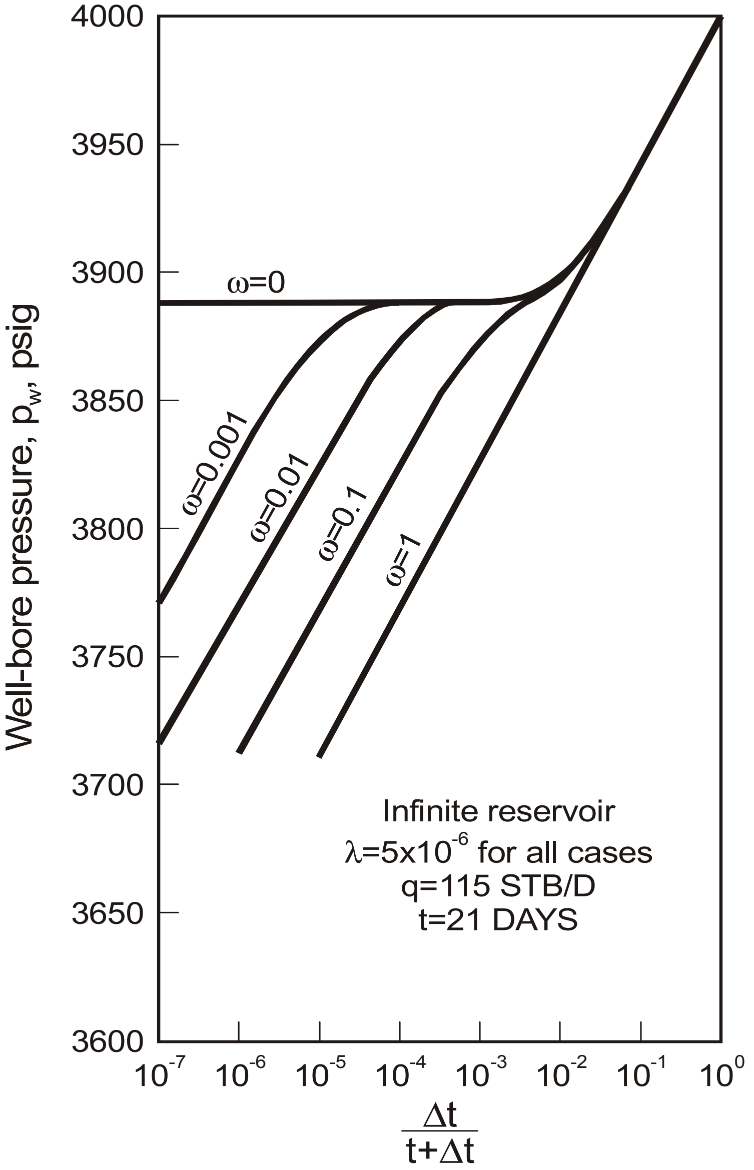

Figure 3.3: Theoretical pressure build-up curves (after Warren and Root[95])

Figure 3.4 shows the pressure build-up data for a naturally fractured reservoir. If both semilog straight lines develop, analysis of the total permeability-thickness product is estimated from the slope *m* of either straight line, for SI units:

$$hk_f = \frac{0.183qB\mu}{m} \text{ or in field units } hk_f = \frac{162.6qB\mu}{m} \tag{3.47}$$

Bourdet and Gringarten[11] showed that by drawing a horizontal line through the middle of the transition line (which is theoretically the inflexion point) to intersect with both semilog straight lines, as shown in Figure 3.5, the interporosity flow coefficient λ can be determined by reading the corresponding time at the intersection of either of the two straight lines, e.g. t_1 or t_2 and applying one of the following relationships:

a) For pressure draw-down:

$$\lambda = \left[\frac{\omega}{1-\omega}\right]\left[\frac{(\phi h c_t)_m \mu r_w^2}{1.781 k_f t_1}\right] = \left[\frac{1}{1-\omega}\right]\left[\frac{(\phi h c_t)_m \mu r_w^2}{1.781 k_f t_2}\right] \tag{3.48}$$

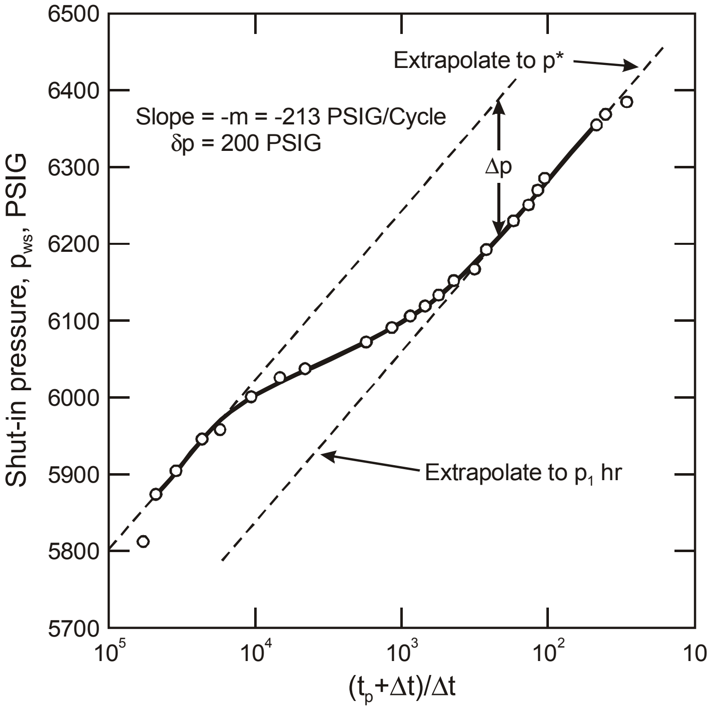

Figure 3.4: Typical dual porosity pressure buildup curve (after Warren and Root[95])

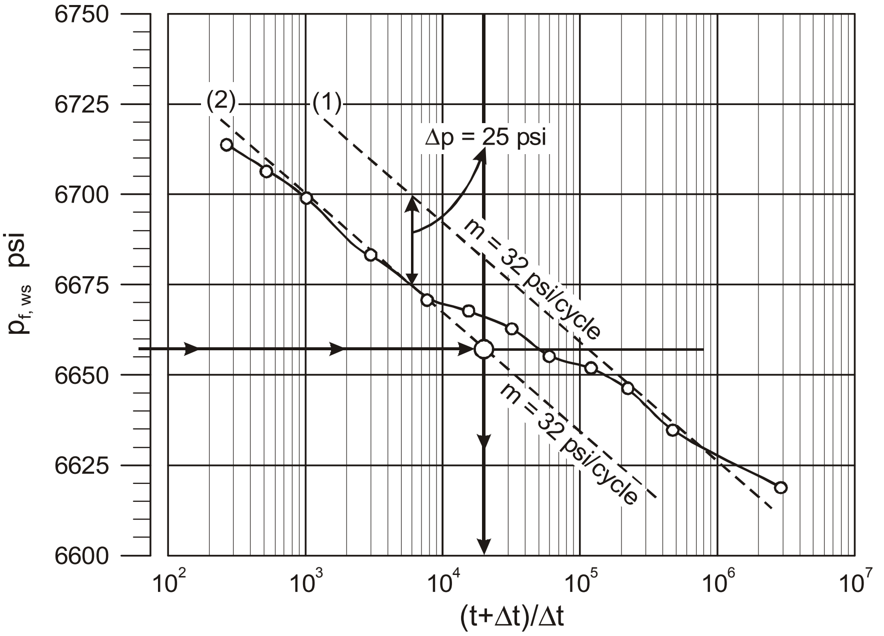

Figure 3.5: Horner plot of the buildup test data (after Sabet[82])

b) For pressure build-up:

$$\lambda = \left[\frac{\omega}{1-\omega}\right]\left[\frac{(\phi h c_t)_m \mu r_w^2}{1.781 k_f \cdot t_p}\right]\left(\frac{t_p + \Delta t}{\Delta t}\right)_1 = \left[\frac{1}{1-\omega}\right]\left[\frac{(\phi h c_t)_m \mu r_w^2}{1.781 k_f \cdot t_p}\right]\left(\frac{t_p + \Delta t}{\Delta t}\right)_2, \tag{3.49}$$

where t_p is the production time before shut-in. Equation 3.48 and Equation 3.49 are given in field units.

3.1.4 Remarks to Well Testing

Typical values of ω *and* λ are

$$\omega = 0.001 - 0.1 \quad \text{and} \quad \lambda = 10^{-3} - 10^{-9}.$$

The determination of the parameters λ and ω from well test is delicate and gives manifold possibilities for misinterpretation. Some of them should be mentioned here:

1. The initial pressure (or $p*$) will be determined by extrapolation to Horner time = *1*. If only the early portion of the pressure build-up curve were recorded, the value would be erroneously high by the quantity $-m\log\omega$ and the value of skin would be higher by $-1.15\log\omega$[1].
2. Dual-porosity fractured reservoirs exhibit double-slope type pressure draw-down and build-up performances. Unfortunately, this is characteristic of stratified reservoirs as well, so the evaluation of such data may be uncertain. If no other evidence for a fractured system exists, then it can be postulated only that the existence of pressure lag indicates the presence of macroscopic heterogeneity.
3. In cases of smaller values of λ ($\sim 10^{-8}$-10^{-9}) the build-up gives results that suggest the existence of a closed boundary.
4. Often significant parts of the pressure build-up curve is masked by the wellbore storage effect.

The two straight lines may or may not be present on the semilog plot, depending on the condition of the well and the duration of the test. Gringarten[35] concluded that the semilog plot is not an efficient or sufficient tool for identifying dual-porosity behavior. Log-log analysis represents a significant improvement over the conventional semilog analysis. In the log-log plot as shown in Figure 3.6, the dual-porosity behavior yields an S-shaped curve. The initial portion of the curve represents the homogeneous behavior resulting from depletion in the most permeable medium, i.e. fractures. A transition period follows and corresponds to the interporosity flow. Finally, the last portion represents the homogeneous behavior of both media when recharge from the least permeable medium (i.e.: matrix) is fully established and the pressures are equalized.

However, the S-shape behavior is difficult to see in highly-damaged wells and similar S-shape behavior may be found in irregularly-bounded well drainage systems.

Perhaps the most efficient means for identifying dual-porosity systems is to use pressure derivative plots. In Figure 3.6 the derivative shows a minimum between two pseudo-horizontal lines. The first represents the radial flow controlled by the fracture system and the second describes the stabilized behavior of the entire pore system. At an early time the typical wellbore storage effect can be seen also with the usual *45°* straight line.

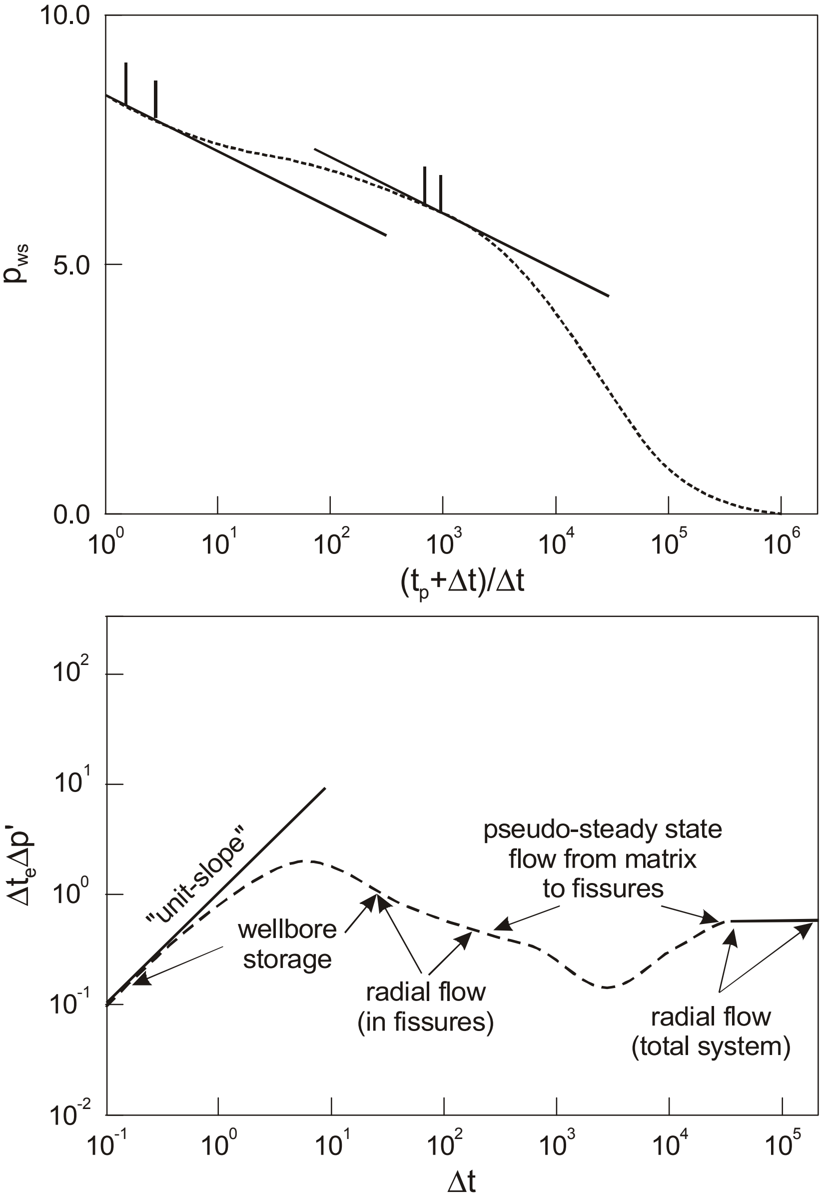

Figure 3.6: Dual-porosity behavior shows as two parallel semilog straight lines on a semilog plot, as a minimum on the derivative plot (from Ahmed and McKinney[1]).

3.2. Type Curve Matching

Based on the Warren and Root[95] theory, Bourdet and Gringarten[11] extended the method of type curve matching to dual porosity reservoirs, controlled by the variables of p_D, t_D/C_D and the parameters of C_De^{2s}, ω *and* λe^{-2s}. They developed two sets of pressure derivative type curves. The first set, given in Figure 3.7 is based on the assumption, that the interporosity flow is a pseudo-steady state one. The second set in Figure 3.8 is for transient flow conditions. The type curves are available in various books, company charts and special well test software. Detailed explanations and examples are given, among others, by Ahmed and McKinnley[1].

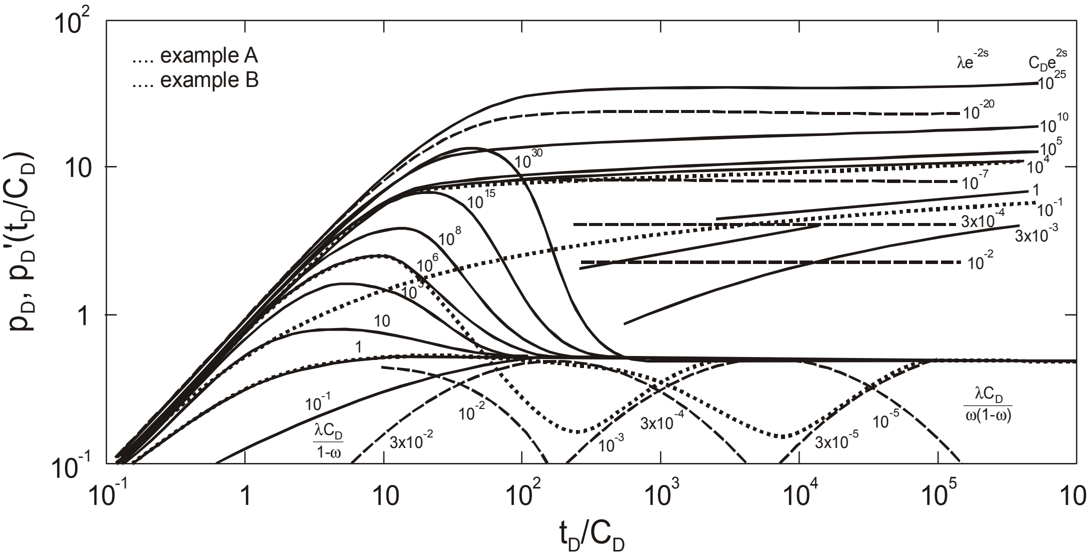

Figure 3.7: Type curves for dual porosity reservoirs, 1st set. (Bourdet *at al.*[11])

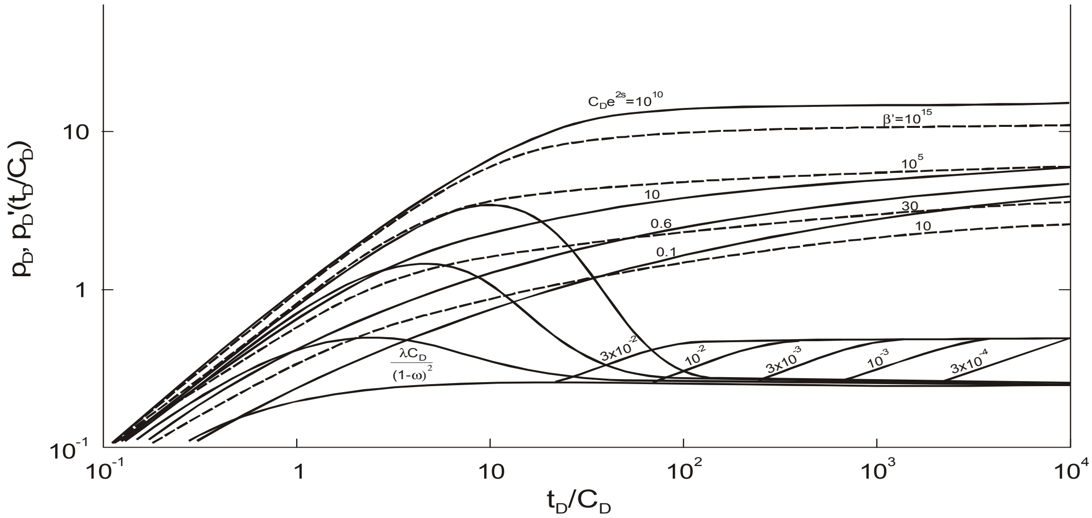

Figure 3.8: Type curves for dual porosity reservoirs, 2nd set. (Bourdet *at al.*[11])

3.3. Well Test Examples

The evaluation of well testing results is not really the topic of this section. The Warren-Root[95] model was presented because it provides the basis for the simulation models and it is suitable to introduce the dual continuum concept, explaining basic behaviors of dual porosity systems. The application to transient well tests should give the first link between the single phase and multi phase, multi component model descriptions. Practical examples are given, among others, by Ahmed and McKinnley[1].

3.3.1 Pressure build-up test

In the following the evaluation of a pressure build-up test is presented. The example shows the workflow of evaluating dual porosity reservoirs with a semi-log plot. The example is based on the example presented by Ahmed and McKinnely[1].

The task is to calculate estimates for the storativity ratio ω, the matrix-fracture transfer capacity λ and the shape factor σ based on the evaluation of a semi-log plot using pressure build-up data given in Table 3.1 and the general reservoir data given in Table 3.2.

Table 3.1: Pressure build-up data

Δt	p_{ws}	p_{ws}	$(t_p+\Delta t)/\Delta t$
[s]	[bar]	[Pa]	[-]
10.8	456.2	4.562E+07	2870334.3
61.2	457.3	4.573E+07	506530.4
118.8	458.1	4.581E+07	260940.4
241.2	458.5	4.585E+07	128523.4
478.8	458.8	4.588E+07	64745.4
961.2	459.3	4.593E+07	32251.9
1918.8	459.6	4.596E+07	16156.7
3841.2	459.8	4.598E+07	8071.3
7678.8	460.4	4.604E+07	4038.0
15361.2	460.9	4.609E+07	2019.0
30718.8	461.7	4.617E+07	1010.1
61441.2	462.2	4.622E+07	505.5
122878.8	462.8	4.628E+07	253.3

Table 3.2: Reservoir and fluid data

p_i	4.681E+07	[Pa]
$p_{wf(Dt=0)}$	4.380E+07	[Pa]
q_o	4.700E-03	[m³/s]
μ_o	0.001	[Pa.s]
B_o	2.3	[rm³/sm³]
t_p	30999600	[s]
r_w	0.1143	[m]
c_t	1.18496E-09	[1/Pa]
ϕ_m	0.21	[-]
k_m	9.87E-17	[m²]
h	5.2	[m]

1. At first the Horner time, $\left(\frac{t_p + \Delta t}{\Delta t}\right)$, has to be calculated based on the time t_p, the time of production before shut in and Δt, the time intervals after shut-in, where the well shut-in pressures, p_{ws}, where recorded. The calculated Horner times can be found in Table 3.1. Then a semi-log plot of p_{ws} versus $\left(\frac{t_p + \Delta t}{\Delta t}\right)$ can be drawn. This plot is displaced in Figure 3.9.

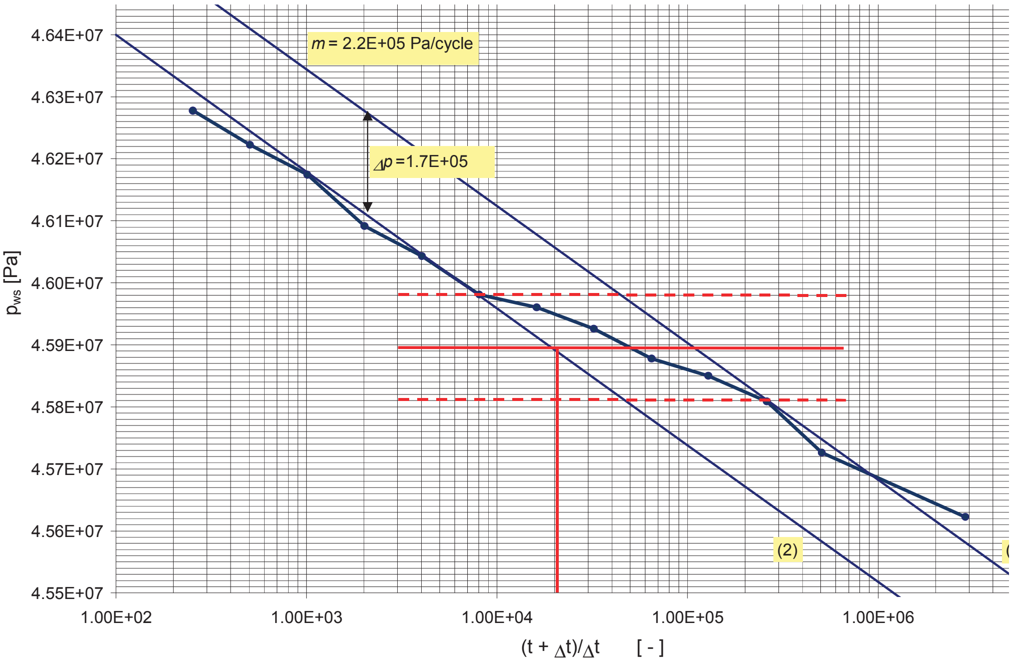

Figure 3.9: Semilog plot of pressure build-up test in NFR (from Ahmed and McKinney[1])

2. On the plot two parallel semi-log straight lines (1) and (2), with a slope of $m = 2.2E+05$ Pa/cycle can be identified. Applying Equation 3.47 the permeability-thickness product can be calculated:

$$hk_f = \frac{162.6 q_o B_o \mu_o}{m} = \frac{162.6 \cdot 4.7 \cdot 10^{-3}[m^3/s] \cdot 2.3[rm^3/sm^3] \cdot 0.001[Pa \cdot s]}{2.2 \cdot 10^5[Pa/cycle]}$$

$$hk_f = 8.966 \cdot 10^{-12}[m^3] \text{ or}$$

$$k_f = \frac{8.97 \cdot 10^{-12}[m^3]}{5.2[m]} = 1.730 \cdot 10^{-12}[m^2]$$

3. From the plot in Figure 3.9 the vertical distance, *Δp*, between the two parallel lines can be read to be $\Delta p = 1.7 \cdot 10^5[Pa]$. Based on this value and the slope, *m*, of the parallel lines the storativity ratio, ω, can be calculated.

$$\omega = 10^{\left(-\frac{\Delta p}{m}\right)} = 10^{\left(-\frac{1.7 \cdot 10^5[Pa]}{2.2 \cdot 10^5[Pa/cycle]}\right)} = 0.165$$

4. To determine the Horner time $\left(\frac{t_p + \Delta t}{\Delta t}\right)_2$, necessary for the calculation of the matrix-fracture transfer capacity λ, a horizontal line has to be drawn through the middle of the transition region. The intersection point of this horizontal line with the straight line (2) gives the reading of

$$\left(\frac{t_p + \Delta t}{\Delta t}\right)_2 = 2 \cdot 10^4 .$$

5. The matrix-fracture transfer capacity λ can be calculated now by Equation 3.49, where the constant 1.781, valid for field units, has to be replace by 2.059E+03 to account for SI units. Thus,

$$\lambda = \left[\frac{1}{1-\omega}\right]\left[\frac{(\phi h c_t)_m \mu_o r_w^2}{2.059 \cdot 10^3 k_f \cdot t_p}\right]\left(\frac{t_p + \Delta t}{\Delta t}\right)_2 .$$

$$\lambda = \left[\frac{1}{1-0.165}\right]\left[\frac{0.21 \cdot 5.2[m] \cdot 1.184[1/Pa] \cdot 0.001[Pa \cdot s] \cdot (0.1143[m])^2}{2.059 \cdot 10^3[m] \cdot 1.730 \cdot 10^{-12}[m^2] \cdot 30999600[s]}\right](2 \cdot 10^4)$$

$$\lambda = 3.655 \cdot 10^{-9}$$

6. The last step of this example is to calculate the shape factor σ using a rearranged form of Equation 3.20:

$$\sigma = \frac{\lambda k_f}{k_m r_w^2} = \frac{3.655 \cdot 10^{-9} \cdot 1.730 \cdot 10^{-12}[m^2]}{9.87 \cdot 10^{-17}([m^2] \cdot (0.1143[m])^2)} = 4.905 \cdot 10^{-3}[1/m^2] .$$

Chapter 4

Depletion of Matrices in Fractured Reservoirs

Initially, it is necessary to clarify some ambiguities in nomenclature and distinguish between matrix *blocks* and simulation *cells*. Figure 4.1 is the two-dimensional outcrop of a naturally fractured formation. In order to model it numerically, the space has to be discretized. The red squares in Figure 4.1 (or cubes in 3D) represent the control volumes, in other words, the "*simulation cells*". The dual continuum approach considers two simulation cells at each location (i.e. at the place of each red square), one is the "*matrix cell*" and the other is the "*fracture cell*". This will divide the space into two identically-shaped overlapping domains: the "*matrix domain*" and the "*fracture domain*". The fracture domain, consisting of fracture cells, usually has a much higher permeability and less porosity than the matrix domain. This means that the fracture cells, can exchange fluids easily with their neighboring fracture cells (along the black arrows in Figure 4.1). Matrix cells, may or may not be able to exchange fluids with their matrix neighbors resulting in dual permeability or dual porosity models respectively. The matrix cell and the fracture cell coexisting in the same location, are considered as neighbors which exchange fluids; this is called the matrix-fracture transfer term (explained in Section 2.1.5)

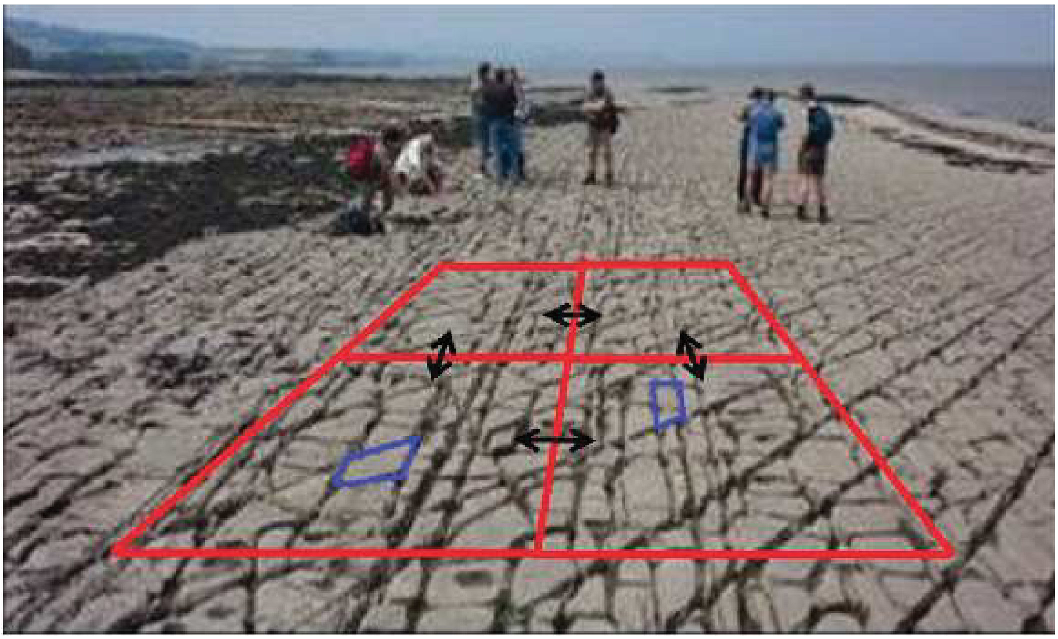

Figure 4.1: Matrix cell vs. matrix block, (by courtesy of Roxar training)[80]

In conventional models of fractured reservoirs, only one common averaged value is assigned to each property (e.g. porosity, pressure, saturation) of the whole simulation cell of the matrix and fracture domain respectively. It is equivalent with the assumption that the property is the same all over the simulation cell. For instance, in Figure 4.1, if each red square is a simulation cell (which makes a total of eight simulation cells: four matrix cells overlapping four fracture cells), it is assumed that each of these cells, has one common value for porosity, permeability, shape factor etc. which is obviously a wrong estimate: as it is clear from Figure 4.1 each cell consists of numerous small "*matrix blocks*" (e.g. the two marked purple blocks) of different shapes and sizes surrounded by fractures. Averaging some properties, such as the shape factor, over the entire simulation cell, results in an inherent error that will be cumulated for all the simulation cells that ultimately makes the conventional method of simulating fractured reservoirs inaccurate and uncertain.

Full field, sector/cross-section and single well model investigations usually are based on the dual continuum concept, using two co-located grid models, in which a greater number of matrix blocks is represented by a single simulation cell. The communication between the fracture system and the matrix is usually described using the Warren and Root[95] concept. Seldom the MINC[74] concept, presented in Section 2.4., is applied. The task of both (W&R and MINC) concepts is to establish the mass transfer between the two continua, namely the matrix and the fracture. None of them is really suitable to investigate the matrix depletion process itself. It can be recommended to perform detailed investigations, both laboratory and numerical, in this respect.

4.1. Recovery Processes in Fractured Reservoirs

The same processes that are active in non-fractured, single porosity systems are important in fractured reservoirs. These include rock compaction, fluid expansion, viscous drive, gravity displacement, capillary imbibition and diffusion. However, the majority of the oil is contained in the high porosity but low permeability matrix system while the wells drain the fluids directly from the high permeability fractures. Therefore, the degree of importance of the physical mechanisms may be quite different in the two systems.

Production from the matrix blocks can be associated with various physical mechanisms including:

- Rock compressibility and compaction,
- Single phase fluid expansion,
- Solution gas drive,
- Gravity drainage,
- Capillary Imbibition,
- Diffusion,
- Viscous displacement.

4.1.1 Expansion and Solution Gas Drive

As the pressure drops in the fracture system, as a consequence of production, fluid expands and flows out from the matrix to equilibrate the matrix pressure with the surrounding fracture pressure. Also the compressibility of rock or the secondary compaction can gain importance especially in the case of low fluid compressibility or low porosity. The pore compressibility for matrix and fracture are in most of the cases quite different.

Below bubble point pressure the solution gas liberates and expands. The efficiency of the matrix recovery under solution gas displacement can be calculated in a standalone way, using the well-known Muskat[57] or Pirson[72] methods. According to Pirson, the equations that describe the performance of the reservoir in case of solution gas drive can be written in finite difference form of the material balance:

$$\Delta\left[\frac{N_p}{N}\right] = \frac{\left[1-\frac{N_p}{N}\right]\Delta\left[\frac{B_o}{B_g}-R_s\right]-[1+m_{g,o}]B_{ob}\Delta\frac{1}{B_g}}{\left[\frac{B_o}{B_g}-R_s\right]_{i+1}+\bar{R}}. \tag{4.1}$$

The instantaneous gas-oil ratio is

$$R = R_s+\frac{B_o}{B_g}\cdot\frac{k_{rg}}{k_{ro}}\cdot\frac{\mu_o}{\mu_g}. \tag{4.2}$$

The oil saturation is

$$S_o = \left[1-\left(\frac{N_p}{N}\right)\right]\cdot\frac{B_o}{B_{ob}}(1-S_w). \tag{4.3}$$

Muskat[57] used also a differential form of the material balance equation to evaluate the performance of a reservoir with solution gas drive. The change in the oil saturation is:

$$\Delta S_o = \Delta p\left[\frac{S_o\lambda(p)+S_o\frac{k_g}{k_o}\eta(p)+(1-S_w-S_o)\varepsilon(p)}{\omega(p,S_o)}\right] \tag{4.4}$$

Where $\lambda(p)$, $\varepsilon(p)$, $\eta(p)$ and $\omega(p,S_o)$ are special Muskat functions[57]:

$$\lambda(p) = \frac{B_g}{B_o}\frac{dR_s}{dp} \tag{4.5}$$

$$\varepsilon(p) = B_g \frac{d}{dp}\left(\frac{1}{B_g}\right) \tag{4.6}$$

$$\eta(p) = \frac{1}{B_o}\frac{\mu_o}{\mu_g}\frac{dB_o}{dp} \tag{4.7}$$

$$\omega(p, S_o) = 1 + \frac{k_g \mu_o}{k_o \mu_g} \tag{4.8}$$

The cumulative amount of produced oil is then:

$$N_p = V_p \sum_{p_i}^{p} \Delta\left(\frac{S_o}{B_o}\right) = V_p\left[\left(\frac{S_o}{B_o}\right)_i - \left(\frac{S_o}{B_o}\right)\right] \tag{4.9}$$

The method proposed by Muskat[57] is advantageous if a larger number of calculations is required. The Muskat functions (Equation 4.5 - Equation 4.8) are readily available in tables and in form of curves (see Figure 4.2).

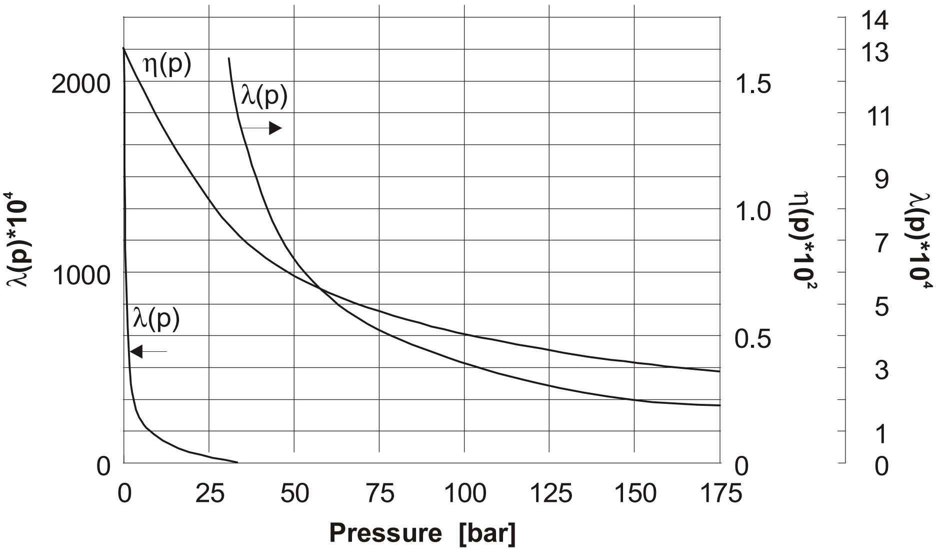

Figure 4.2: Muskat functions

Muskat and Taylor[58] analyzed the influence of the oil viscosity, the initial pressure, the solution GOR, the connate water saturation and the relative permeability ratio on oil production.

The pressures and GORs will develop similar to those shown in Figure 4.3, calculated by Muskat *et al.*[57]. The method can be applied to a single matrix block and to the whole matrix-fracture system as well. Note that in the first case the reservoir pressure and the recovery factor is valid for the matrix, and not for the entire porosity system including the fractures.

The numerical calculations of expansion mechanism are very accurate on every scale (also in full field models), while it is free of time truncation, numerical dispersion and grid orientation errors.

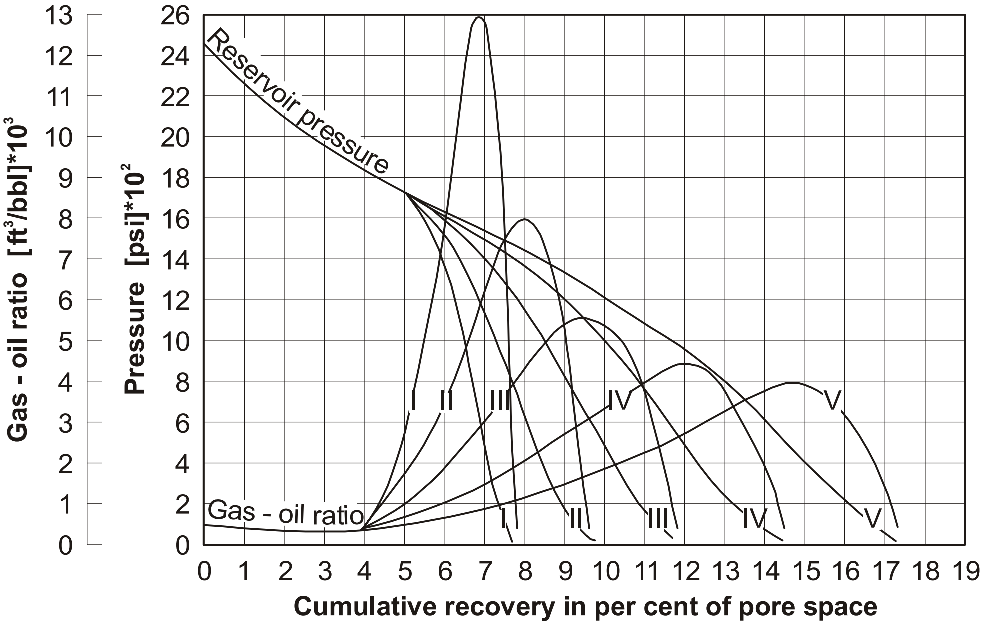

Curve I: atmospheric-pressure viscosity = 11.04 cp.
Curve II: atmos. pres. viscosity = 5.52 cp.
Curve III: atmos. pres. viscosity = 2.76 cp.
Curve IV: atmos. pres. viscosity = 1.38 cp.
Curve V: atmos. pres. viscosity = 0.69 cp.
Gas solubility at 2500 lb. per sq. in. = 534 cu. ft. per bbl. in all cases

Figure 4.3: Pressure and gas oil ratio histories of solution gas-drive reservoirs producing oil of different viscosities (after Muskat and Taylor[57])

4.1.2 Capillary Imbibition

Let’s imagine a piece of porous rock, called matrix, surrounded by fractures. The matrix is assumed to be water wet. The water invading the fractures flows, driven by capillary forces, into the matrix, displacing oil in countercurrent way, which means that water imbibes the matrix from the same side where oil is expelled. Depending on the fracture configuration, the displacement has two or three dimensional character, but it can be examined on a simplified one dimensional model.

Now let's consider a core sealed on all sides except the bottom surface, as shown in Figure 4.4. The core is saturated by oil and the initial water saturation is equal with the connate water saturation S_{wm}. At the bottom side the core is contacted with the wetting phase. Due to capillary forces the wetting phase - in our case the water - tends to intrude at the bottom side and thus displaces the nonwetting phase - in our case the oil - in counter flow.

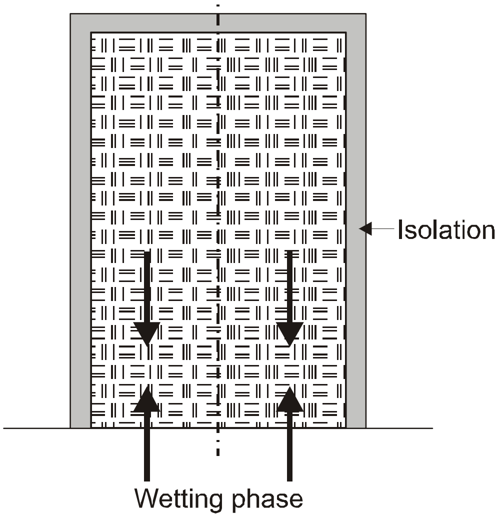

Figure 4.4: Countercurrent imbibition

To calculate the displacement process the following assumptions will be made:

1. The rock is homogenous.
2. The displacement is one dimensional.
3. The two phases are incompressible and immiscible.
4. Multiphase Darcy's equation is valid.

As consequence of these assumptions the overall fluid velocity must be everywhere zero:

$$u_w + u_o = 0, \tag{4.10}$$

where:

$$u_w = -\frac{kk_{rw}}{\mu_w}\left(\frac{\partial p_w}{\partial x} + \rho_w g\right) \tag{4.11}$$

and:

$$u_o = -\frac{kk_{ro}}{\mu_o}\left(\frac{\partial p_o}{\partial x} + \rho_o g\right) \tag{4.12}$$

The difference of the phase pressures is the capillary pressure:

$$p_o - p_w = P_c(S_w)\,. \tag{4.13}$$

The continuity equation for the water and oil are:

$$\frac{\partial u_w}{\partial x} + \phi\frac{\partial S_w}{\partial t} = 0 \tag{4.14}$$

$$\frac{\partial u_o}{\partial x} + \phi\frac{\partial S_o}{\partial t} = 0 \tag{4.15}$$

The saturation constraint is:

$$S_w + S_o = 1\,. \tag{4.16}$$

Then Equation 4.11 is divided by $k_{\mathrm{rw}}/\mu_{\mathrm{w}}$ and Equation 4.12 by $k_{\mathrm{ro}}/\mu_{\mathrm{o}}$. Afterwards they are subtracted one from another:

$$u_w\left(\frac{\mu_w}{k_{rw}} + \frac{\mu_o}{k_{ro}}\right) = k(\rho_w - \rho_o)g + k\frac{dP_c}{dS_w}\cdot\frac{\partial S_w}{\partial x} \tag{4.17}$$

or written it in a more compact form:

$$u_w = \varphi_w + \psi_w \cdot \frac{\partial S_w}{\partial x}, \tag{4.18}$$

where:

$$\varphi_w = \frac{k(\rho_w - \rho_o)g}{\dfrac{\mu_w}{k_{rw}} + \dfrac{\mu_o}{k_{ro}}} \tag{4.19}$$

$$\psi_w = \frac{k}{\dfrac{\mu_w}{k_{rw}} + \dfrac{\mu_o}{k_{ro}}} \cdot \frac{dP_c}{dS_w}\,. \tag{4.20}$$

Substituting of Equation 4.18 into Equation 4.14 leads to:

$$\frac{\partial}{\partial x}\left[\varphi_w + \psi_w\frac{\partial S_w}{\partial x}\right] + \phi\frac{\partial S_w}{\partial t} = 0 \tag{4.21}$$

or

$$\frac{1}{\phi}\left[\frac{\partial \varphi_w}{dS_w}\cdot\frac{\partial S_w}{\partial x} + \frac{\partial}{\partial x}\left(\psi_w\frac{\partial S_w}{\partial x}\right)\right] + \frac{\partial S_w}{\partial t} = 0 \tag{4.22}$$

The boundary conditions are:

At the outlet $x = L$:

$$u_w = \left[\varphi_w + \psi_w \frac{\partial S_w}{\partial x}\right]_{x = L} = 0 \tag{4.23}$$

At the inlet $x = 0$, the capillary pressure is zero, thus:

$$(S_w)_{x = 0} = S_{wM} = 1 - S_{or} \tag{4.24}$$

where S_{or} is the residual oil saturation and S_{wM} is the maximum possible water saturation. The solution of the above boundary value problem (Equation 4.22 – Equation 4.24) is the saturation as a function of the location and time:

$$S_w = S_w(x, t), \tag{4.25}$$

which can be found by applying numerical methods only.

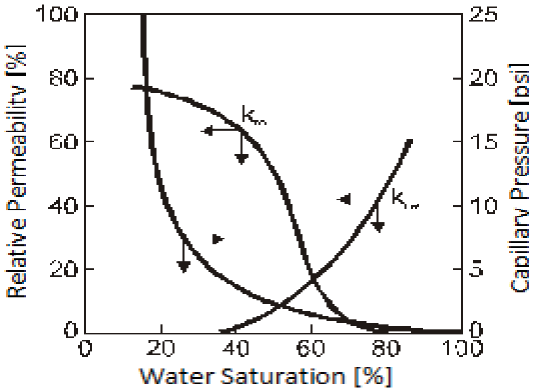

Figure 4.5: Capillary pressure and relative permeability functions used in the calculations (Blair[10])

Blair[10] presented numerical solution for the model defined by Figure 4.4. Figure 4.5 shows the capillary pressure and relative permeability curves used in the calculations. The results showed similarity to a concurrent linear displacement, which means that a relative narrow transition zone, interpreted as water front, was formed between the displacing and displaced phases.

Figure 4.6 shows the pressure and saturation profile when the water front has reached approximately half the length of the sample. The water saturation is high at the open end of the core, but decreases then abruptly. The pressure gradient in the water phase is highest near the front. The greatest pressure gradient in the oil phase occurs near the open end of the core, because of the fact that with the maximum oil flow rate the oil relative permeability is the minimum. In case of strongly water wet rock the process of spontaneous imbibition lasts theoretically until the oil saturation in the matrix reaches its residual value. The results of the calculations showed that the rate of imbibition depends strongly on rock and fluid properties.

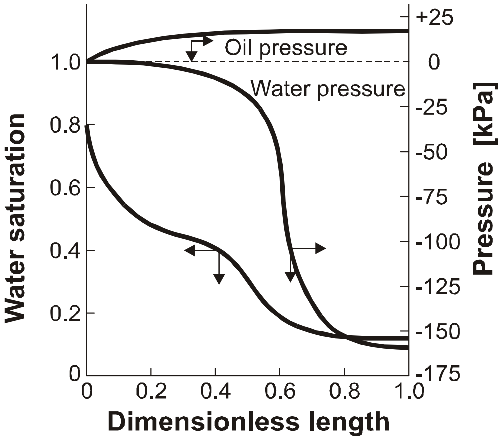

Figure 4.6: Distribution of pressure and saturation after 6.6 hours. (by Blair[10])

The numerical results from Blair[10] were verified by experiments of Graham and Richardson[34]. They measured the oil production as function of the time. One result is shown in Figure 4.7 where all parameters, except the core lengths, were constant. The results give a feeling to the time dependence of the imbibition process.

The results presented above are strictly valid for one dimensional displacement of two incompressible fluids. The matrix recovery processes under real conditions are more complicated, and therefore the applicability of the Blair[10] model is limited. General mathematical models, as used in reservoir simulation practise, make it possible to investigate the mechanisms in fully complexity. Such an approach will be presented in Section 5.3.

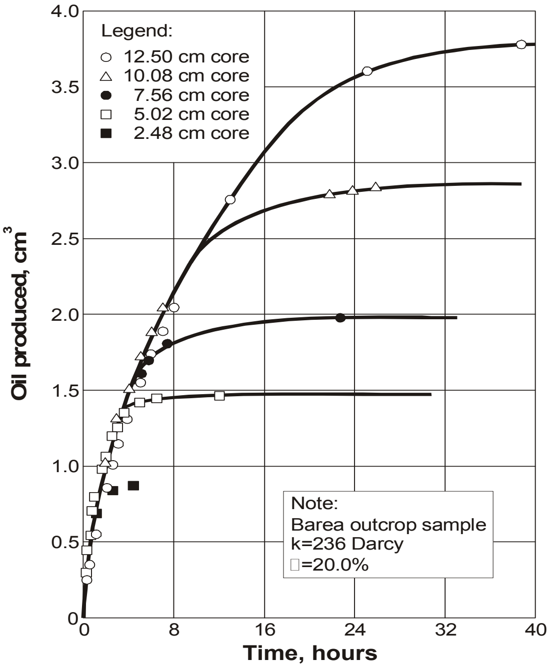

Figure 4.7: Recovery in case of linear counterflowing imbibition and the experimental determination of the influence of a certain in core-length. (by Graham and Richardson[34])

Mattax and Kyte[55] demonstrated that the recovery behavior of a large reservoir matrix block can be predicted from an imbibition test on a small core sample. The oil recovery can be scaled for a given rock type and oil-to-water ratio by a dimensionless rate parameter:

$$t = \sqrt{\frac{k}{\phi}}\frac{\sigma_{ow}}{\mu_w L^2} \qquad (4.26)$$

where t is the imbibition time, k is the permeability, ϕ is the porosity, σ_{ow} is the interfacial tension, μ_w is the water viscosity and L is a characteristic length for a matrix block. From Equation 4.26 can be concluded that in an imbibition displacement the time of recovery is proportional to the square of the block height, L. Mattax and Kyte[55] showed that if the imbibition oil recovery is plotted against the dimensionless scaling parameter the same recovery curve will be obtained for the model and all reservoir matrix blocks of the same rock type and geometry:

$$\left(t\sqrt{\frac{k}{\phi}}\frac{\sigma}{\mu_w L^2}\right)_{\text{model}} = \left(t\sqrt{\frac{k}{\phi}}\frac{\sigma}{\mu_w L^2}\right)_{\text{matrix block}} \qquad (4.27)$$

Figure 4.8 shows the results of the verification of the scaling parameter.

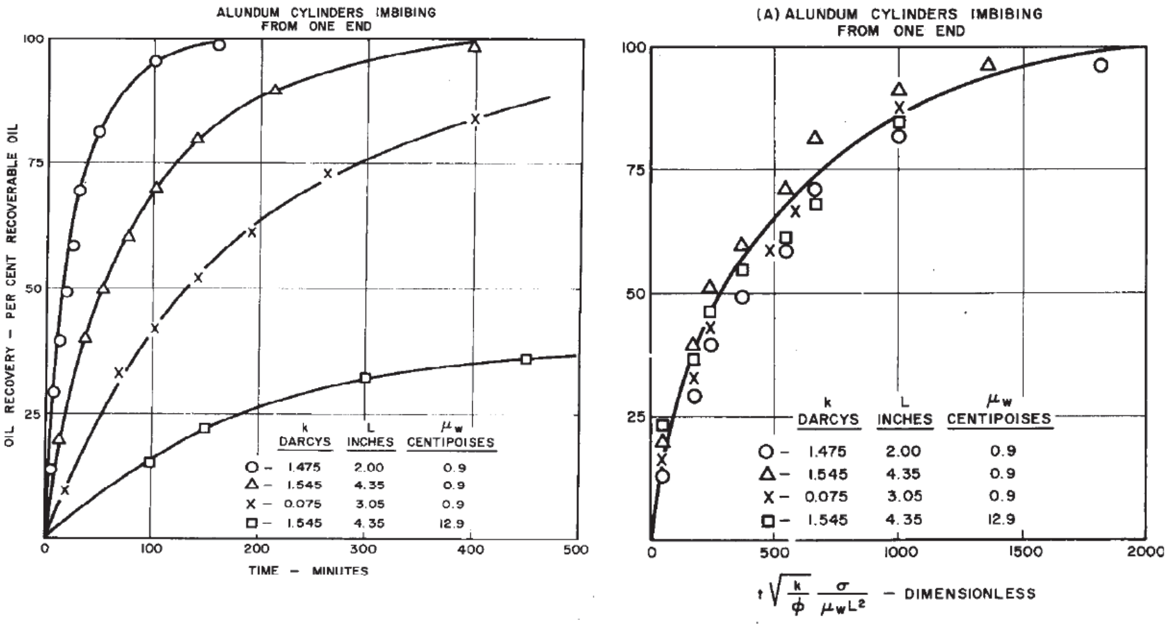

Figure 4.8: Verification of imbibition scaling[55]

In gas-oil systems the oil is the wetting phase and tends to imbibe into the matrix. In practice this means in absence of gravity drainage no oil production occurs from the matrix block when the associated fracture block is filled by gas.

4.1.3 Gravity Drainage

When the fluid contents of the matrix and fracture are not the same (e.g. fracture is filled with gas or water), a difference in the hydrostatic head due to gravitational force exists between the matrix and the fracture. This additional potential difference, may force water or gas from the fracture into the matrix and expel the oil out of the matrix; this process is called gravity drainage.

4.1.3.1 Gravity drainage assuming homogenous vertical saturation

Regard a matrix block surrounded by vertical fractures. The matrix is saturated by oil and the fracture is filled by (a) water or (b) by gas. In absence of capillary forces there would be no difference between the phase pressures: $p = p_o = p_g = p_w$. The pressures at the middle depth of the matrix block and in the fracture are in a pseudo-steady state situation equal. During a transient process such as well testing, the pressures could be different at this point but then they will be equalized within a short time. The different hydrostatical gradients create a pressure difference above and bellow the midpoint as it is shown in Figure 4.9.

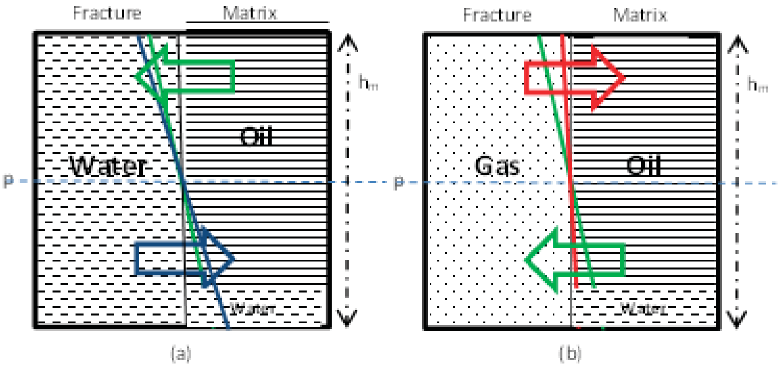

Figure 4.9: Vertical pressure distributions in matrix and in fracture (a) filled with water, (b) filled with gas

In the case that the fracture is filled by water the water will enter in the matrix at the lower half and the oil will be expelled at the upper one. The average hydrostatic pressure difference between the matrix and the fracture are the same for both phases:

$$P_{hwof} = \frac{1}{2} h_m (\rho_w - \rho_o) g \tag{4.28}$$

where h_m is the vertical extension of the matrix block. This pressure difference acts on the half length of the matrix block which has to be considered while calculating the effective potential differences for the water and for the oil phases:

$$\Phi_{wm} - \Phi_{wf} = p_{om} - p_{of} - P_{cwom} + P_{cwof} - \frac{1}{4} P_{hwof} \tag{4.29}$$

$$\Phi_{om} - \Phi_{of} = p_{om} - p_{of} + \frac{1}{4} P_{hwof} \tag{4.30}$$

Similar for the gas filled fracture case:

$$P_{hgof} = \frac{1}{2} h_m (\rho_g - \rho_o) g \tag{4.31}$$

and the potential differences for the gas and for the oil phases:

$$\Phi_{gm} - \Phi_{gf} = p_{om} - p_{of} + P_{cogf} - P_{cogf} - \frac{1}{4} P_{gof} \tag{4.32}$$

$$\Phi_{om} - \Phi_{of} = p_{om} - p_{of} + \frac{1}{4} P_{hogf} \tag{4.33}$$

The gas enter at the upper half of the matrix and the oil expels at the lower one.

Above it was assumed that the fracture is entirely filled by water or gas. In this case the fracture capillary pressures are zero per definition:

$$P_{cwof} = P_{cogf} = 0 \tag{4.34}$$

This remains valid also if not *100%* water or gas but a homogeneous vertical fluid saturation in the fracture is assumed. As it was shown in Section 1.3.2 Equation 4.34 remains valid in this case too.

4.1.3.2 Gravity drainage assuming phase segregation

4.1.3.2.1 Two phase water-oil case

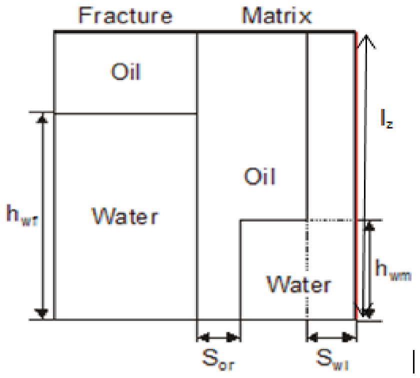

Figure 4.10: Matrix block partially merged in water

Figure 4.10 illustrates an idealized matrix block surrounded by fractures. Both the matrix and corresponding fractures contain oil and water. Assuming perfect phase separation both in the fracture and in the matrix, the hydrostatic pressure difference can be calculated for the matrix and for the fracture:

$$P_{hwof} = h_{wf}(\rho_w - \rho_o)g, \tag{4.35}$$

$$P_{hwom} = h_{wm}(\rho_w - \rho_o)g. \tag{4.36}$$

The difference in the hydrostatic head is a supplementary driving force for the interporosity flow and must be incorporated in Equation 4.35.

$$\Phi_{wm} - \Phi_{wf} = p_{om} - p_{of} - P_{cwom} + P_{cwof} + P_{hwom} - P_{hwof} \tag{4.37}$$

$$\Phi_{om} - \Phi_{of} = p_{om} - p_{of} - P_{hwom} + P_{hwof} \tag{4.38}$$

The hydrostatic heads h_f and h_m can be expressed using the saturations. For the fracture:

$$h_{wf} = L_z \cdot \left(\frac{S_w - S_{wi}}{1 - S_{wi} - S_{orw}}\right)_f \approx L_z \cdot S_{wf}, \tag{4.39}$$

and for the matrix:

$$h_{wm} = L_z \cdot \left(\frac{S_w - S_{wi}}{1 - S_{wi} - S_{orw}}\right)_m \tag{4.40}$$

Inserting Equation 4.39 and Equation 4.40 into Equation 4.36 and Equation 4.35 the hydrostatical pressure differences become functions of the saturation too, and so they are formally similar to the well-understood capillary pressure:

$$P_{hwof}(S_{wf}) = L_z \cdot S_{wf} \cdot (\rho_w - \rho_o)g \tag{4.41}$$

$$P_{hwom}(S_{wm}) = L_z \cdot \left(\frac{S_w - S_{wi}}{1 - S_{wi} - S_{orw}}\right)_m (\rho_w - \rho_o)g \tag{4.42}$$

For this reason, the hydrostatic pressure difference usually is referred to as pseudo-capillary pressure and the fluid exchange induced by the gravitation as gravity imbibition and drainage.

4.1.3.2.2 Two phase gas-oil case

Figure 4.11 illustrates an idealized matrix block surrounded by fractures. Both the matrix and corresponding fractures contain oil and gas.

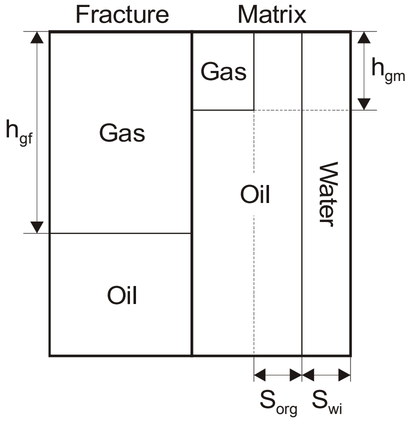

Figure 4.11: Matrix block partially invaded by gas

Similarly to the water/oil case, the following is valid for oil and gas:

$$P_{hgof}(S_{gf}) = L_z \cdot S_{gf} \cdot (\rho_o - \rho_g)g \tag{4.43}$$

$$P_{hgom}(S_{gm}) = L_z \cdot \left(\frac{S_g}{1 - S_{wi} - S_{org}}\right)_m (\rho_o - \rho_g)g \tag{4.44}$$

and

$$\Phi_{gm} - \Phi_{gf} = p_{om} - p_{of} + P_{cogm} - P_{cogf} + P_{hgom} - P_{hgof} \tag{4.45}$$

$$\Phi_{om} - \Phi_{of} = p_{om} - p_{of} - P_{hgom} + P_{hgof} \tag{4.46}$$

4.1.3.2.3 Three phase case

The three phase case with segregated fluid saturation model can be handled as a combination of the two-phase cases described in the previous two sections. Note that the gravity term (pseudo-capillary pressure) depends on the calculated free fluid level and thus on the saturation distribution model. Figure 4.12 shows one example for a three phase case.

The segregated flow assumption is also commonly applied to single porosity models. The methods to determine the relative permeabilities used there are applicable for dual porosity systems without any modifications.

The saturation distribution in the matrix can be naturally more complicated, especially if different displacement mechanisms act one after the other. For instance, a solution gas drive followed by water displacement and then gas displacement.

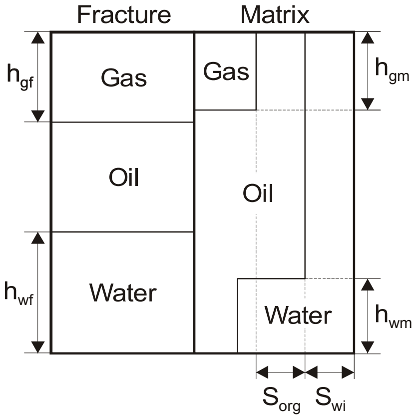

Figure 4.12: A possible three phase saturation distribution in the matrix, assuming segregated flow (SF)

4.1.3.3 Quandalle and Sabathier Gravity Drainage Model

An alternative gravity drainage model was suggested by Quandalle and Sabathier[66]. The matrix-fracture flow is taken to be the sum of three flows from the center of the matrix to the fractures: one horizontal one vertical upwards and one vertically downwards[87] as shown in Figure 4.13. Theoretically this model has the following advantages:

- The shape factor can be different in vertical and horizontal directions,
- The vertical anisotropy can be considered,
- The gravity force (in vertical direction) can be considered,
- The relative permeability depends on the direction.

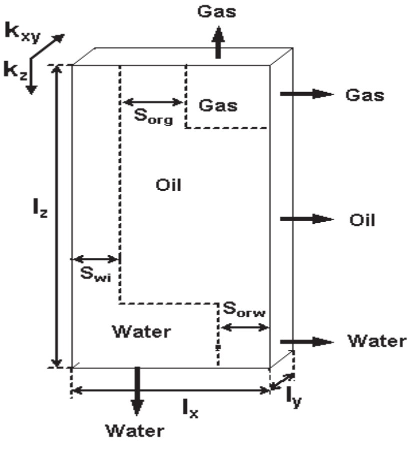

Figure 4.13: Modified gravity drainage model (after Quandalle and Sabatier[66])

Nevertheless the practical advantage of this method is questionable. There is no way to determine the necessary parameters for the Quandalle and Sabatier[66] approach in a reliable way. On top of that, calculation of the lateral oil, water and gas rates (showed by horizontal arrows in Figure 4.13) requires an estimate for the apparent fluid density in the fracture. While this can be done explicitly[66], the numerical stability of method is reduced and therefore the applicable time step length is limited.

4.1.3.4 The Matrix Column

Fractures open to fluid flow are mostly vertical. The matrix blocks, also if horizontal fractures exist, are pressed to each other by the overburden pressure and if no tight (styololites) intervals exists then they are in capillary contact. This means that the vertical extension of the matrix blocks can be assumed equal to those of the simulation cell. Therefore, the previous sections assumed that the matrix column heights are equal to those of the simulation cells ($L_z = h$). However, this is the case if the gridding strictly follows the geological layering and changes in rock quality or discontinuities caused by interbeddings or erosion surfaces are represented by layers or layer boundaries. Additionally, two situations must be considered:

1. The matrix column (more accurately, the matrix tranche) height is greater than the simulation cell thickness. In this case the column is represented by more than one simulation cell. The matrix-matrix fluid exchange is then possible which can be described by dual-porosity dual-permeability model rather than by the usual dual-porosity single-permeability one. Equation 4.35 through Equation 4.46 remain valid.
2. The matrix column height is less than the block thickness. This can be caused typically by building styololites, hampering the vertical fluid movement. Styololites can even reduce the vertical permeability practically to zero. In such a layer splitting ($L_z < h$), the saturation distribution is more or less homogenous within the matrix slices and the gravitational drainage cannot act. No gravitational drainage is possible if the capillary threshold pressure is greater than then maximum possible hydrostatical pressure head:

$$L_z \le \frac{P_c^{tres}}{g\Delta\rho} \tag{4.47}$$

The gravity drainage process strongly depends on the height of the matrix block but also on the density contrast between the phases and the interfacial tension between the wetting and the nonwetting phase. Gravity drainage is an important recovery mechanism if the gravitational head can overcome the capillary restraining forces of the rock. The ultimate recovery depends on the balance between gravity forces and capillary forces. To displace the oil in a gas/oil system, the gas pressure must exceed the threshold pressure to enter the matrix. The ratio of capillary forces to gravitational forces for a single matrix block can be written[59] as:

$$CGR = \frac{P_c}{P_g} = \sqrt{\frac{k}{\phi}}\frac{\sigma_{pp'}\cos\theta}{\Delta\rho g h_f} \tag{4.48}$$

In Equation 4.48, $\sigma_{pp'}\cos\theta$ accounts for the capillary force of the system and the wettability of the rock surface, whereas the gravity forces of the denser hydrocarbon across the rock surface is $\Delta\rho gh_f$. It is obvious that for $CGR<1$, the gravity drainage process from the matrix block can start (i.e. the capillary force effect is less than the gravity drainage effect) as discussed by Schechter *et al.*[85] in more details.

4.1.3.5 Oil Displacement by Water

The phase potential difference between matrix and fracture is given by Equation 4.35. Note that Equation 4.35 is valid for homogenous saturation distribution only, and does not take any gravitational force into account. This is a consequence of the dual continuum concept and the discretisation method in use. The fracture grid point is in the same location as the grid point of the corresponding matrix cell, therefore the depth difference between the two cells ($\Delta z_{mf} = 0$). The saturations within the cells are not uniform but they are determined by the gravitational, capillary and viscous forces. The distribution in the fracture and matrix columns are fundamentally different from the following reasons:

- The vertical extension of the fractures can be considerable. They can also connect permeable intervals trough compact and impermeable interbeddings. The fracture permeability is high, the capillary pressure is there zero and the residual saturations are also near to zero. A complete phase segregation in the fracture system is a reasonable assumption.
- The permeable parts of matrix can be separated by interbeddings or styololites. The matrix permeability is normally by magnitudes less than the permeability of the fractures. The wettability, the capillary pressures and the residual saturations have considerable influence on the phase distribution. If the oil viscosity is not unusually high (e.g. < 10 cP) and the permeability not extremely low (> 0.1 md), then the saturation distribution will be near to the one corresponding to the capillary-gravitational equilibrium. Figure 4.14 show some possible cases with and without vertical capillary continuity.

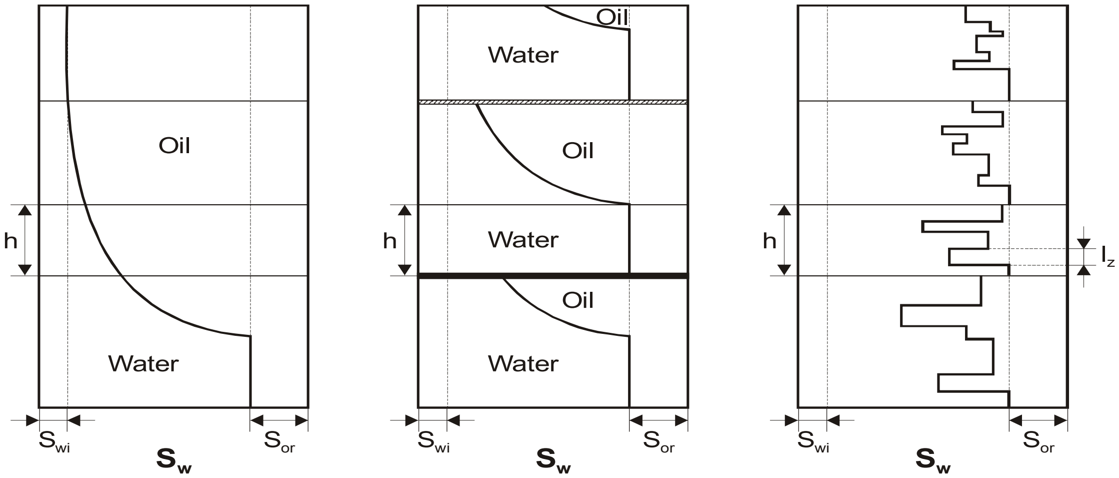

Figure 4.14: Vertical saturation distribution within the matrix column: a) complete vertical communication, b) the vertical communication is hampered by interbeddings, c) the vertical permeability is zero.

Under certain conditions and by excluding case c) in Figure 4.14 phase segregation can also be assumed within the matrix cells. Figure 4.10 illustrates such an idealized situation. Note that the catch shows a possible simulation cell and not a matrix block. The later ones are smaller than the simulation cell, but it is assumed that they are vertically in capillary contact to each other. In the first approach the matrix column should have the same height (L_z) as the simulation block (h) and it is surrounded by vertical fractures. Both the matrix and corresponding fractures contain oil and water.

4.1.3.6 Pseudocapillary Pressure Model

When using the pseudo-functions the standard transfer Equation 4.37 can be used, where the phase potential differences are entered as

$$(\Phi_{wm}-\Phi_{wf}) = \left(p_{om}-p_{of}-\frac{1}{2}(\rho_{wm}+\rho_{wf})gz_{mf}-\tilde{P}_{cow,m}+\tilde{P}_{cow,f}\right) \tag{4.49}$$

$$(\Phi_{om}-\Phi_{of}) = \left(p_{om}-p_{of}-\frac{1}{2}(\rho_{om}+\rho_{of})gz_{mf}\right) \tag{4.50}$$

$$(\Phi_{gm}-\Phi_{gf}) = \left(p_{om}-p_{of}-\frac{1}{2}(\rho_{gm}+\rho_{gf})gz_{mf}-\tilde{P}_{cgo,m}+\tilde{P}_{cgo,f}\right) \tag{4.51}$$

where $\tilde{P}_{cgo}$ and $\tilde{P}_{cow}$ are the gas-oil and oil-water pseudocapillary pressures, respectively.

Assuming instantaneous vertical gravity-capillary equilibrium, the pseudocapillary pressure can be derived as proposed by Coats[20] with:

$$\int_{\tilde{P}_{cog}-(\gamma_o-\gamma_g)L_z/2}^{\tilde{P}_{cog}+(\gamma_o-\gamma_g)L_z/2} S_g d\tilde{P}_{cog}-(\gamma_o-\gamma_g)L_z S_g = 0 \tag{4.52}$$

and

$$\int_{\tilde{P}_{cow}-(\gamma_w-\gamma_o)L_z/2}^{\tilde{P}_{cow}+(\gamma_w-\gamma_o)L_z/2} S_w d\tilde{P}_{cow}-(\gamma_w-\gamma_o)L_z S_w = 0 \tag{4.53}$$

4.1.3.7 Modified Pseudocapillary Pressure Model

Assuming that the matrix-fracture transfer term can be split into (1) a convective term, and (2) a separate contribution accounting for the drainage, then:

$$q_{cmf} = q_{cmf,c}+q_{cmf,d} \tag{4.54}$$

The drainage term can be derived under the assumption that capillary-gravity equilibrium is instantaneously reached within the matrix block and the gas drains into the matrix block from the top and from the part of the four sides of the ideal matrix block filled with gas Figure 4.15.

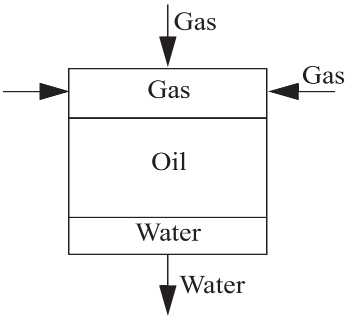

Figure 4.15: Single Matrix Block

In this case the matrix-fracture transmissibility, calculated in Equation 4.53 can be modified to:

$$\tau_{mafr} = k_{z,m}\frac{L_x L_y}{L_z/2} + S_{g,m} \cdot 2\left(k_{x,m}\frac{L_y L_z}{L_x/2} + k_{y,m}\frac{L_x L_z}{L_y/2}\right) \tag{4.55}$$

where S_g is the matrix block gas saturation and the equation refers to a phase-segregated block model description. Following Equation 4.52, the matrix-fracture transfer term is given by:

$$q_{cmf}^{n+1} = \tau_{mf} \sum_{p=1}^{P} [(x_{pc}\lambda_p D_p)_{mf}^{n+1} (\Phi_{pm} - \Phi_{pf})^{n+1}] \tag{4.56}$$

where for the gas potential difference:

$$(\Phi_{gm} - \Phi_{gf}) = \left\{p_{om} - p_{of} + \left[S_{g,m} + \frac{\sigma_z}{\sigma}\left(\frac{1}{2} - S_{g,m}\right)\right] \cdot (\tilde{P}_{cog,m} - \tilde{P}_{cog,f})\right\} \tag{4.57}$$

and:

$$\sigma_z = 4 \cdot \frac{k_{z,m}}{L_z^2} \tag{4.58}$$

$\tilde{P}_{cog,m}$, $\tilde{P}_{cog,f}$ are the gas-oil pseudocapillary pressures in the matrix and the fracture respectively.

Using a similar analysis, the matrix transfer function for the water, draining from the bottom of the matrix block can be derived. In this case the water potential difference should be:

$$(\Phi_{wm} - \Phi_{wf}) = \left\{ p_{om} - p_{of} - (P_{cow,\,m} - P_{cow,\,f}) - \frac{1}{2}\frac{\sigma_z}{\sigma}\cdot[(\tilde{P}_{cow,\,m} - \tilde{P}_{cow,\,f}) - (P_{cow,\,m} - P_{cow,\,f})]\right\} \tag{4.59}$$

4.1.4 Viscous Displacement

4.1.4.1 Unstructured Grid

Consider a representative matrix block as shown in Figure 4.16. The average pressure in the matrix cell and in the fracture will equalize due to the capillary and gravitational forces. In the isolated matrix cell the fluid does not move therefore, the pressure is uniform. Contrary, there is a pressure gradient in the fracture system while the fluid is moving towards the production wells (and away from the injection wells). Therefore, there is a pressure difference Δp between the two edges of the block.

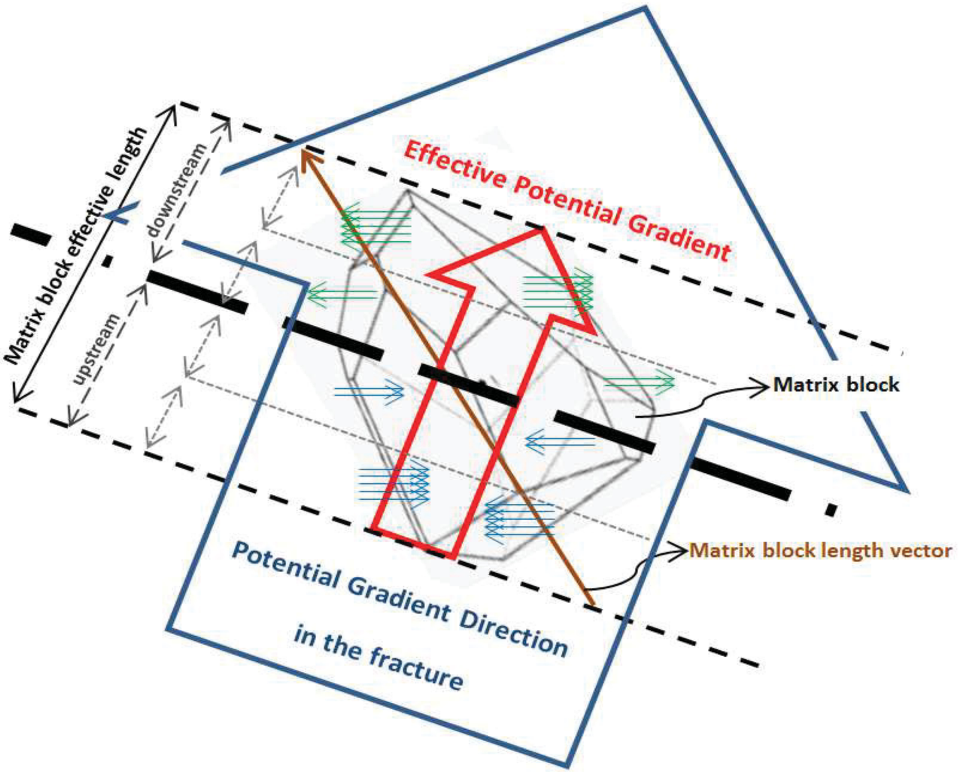

Figure 4.16: Schematic of the viscous effect in fluid exchange between the matrix block (in the center) and the surrounding fracture

A pressure difference of $\Delta p/4$ acts in average at the upstream half and $-\Delta p/4$ at the downstream half of the matrix block. Consequently, fluid enters from the fracture into the matrix at the upstream half and flows out from the matrix to the fracture at the downstream half. This additional driving force can contribute to the matrix recovery process.

The pressure gradient for the phase p at the grid point i is

$$\overrightarrow{\nabla\Phi}_p = \Phi'_{px}\vec{i} + \Phi'_{py}\vec{j} + \Phi'_{pz}\vec{k}, \tag{4.60}$$

where Φ' are the partial derivatives. The potential difference between the grid point i and the neighbor j is given by the scalar product of the neighbor's position vector

$$\vec{r}_{ij} = \Delta x_{ij}\vec{i} + \Delta y_{ij}\vec{j} + \Delta z_{ij}\vec{k} \tag{4.61}$$

and the potential gradient. In the case of N neighboring grid points a linear equation system of N equations with 3 unknowns can be created:

$$\Phi'_{px}\Delta x_{ij} + \Phi'_{py}\Delta y_{ij} + \Phi'_{pz}\Delta z_{ij} = \Phi_{pj} - \Phi_{pi}, \; j = 1, N \tag{4.62}$$

To achieve the three components of the potential gradient $\Phi'_{p\alpha}$; $\alpha = x, y, z$ the Gauss normal equations have to be created and solved:

$$\begin{aligned}
\Phi'_{px}\sum\Delta x_{ij}^2 + \Phi'_{py}\sum\Delta y_{ij}\Delta x_{ij} + \Phi'_{pz}\sum\Delta z_{ij}\Delta x_{ij} &= \sum(\Phi_{pj} - \Phi_{pi})\Delta x_{ij} \\
\Phi'_{px}\sum\Delta x_{ij}\Delta y_{ij} + \Phi'_{py}\sum\Delta y_{ij}^2 + \Phi'_{pz}\sum\Delta z_{ij}\Delta y_{ij} &= \sum(\Phi_{pj} - \Phi_{pi})\Delta y_{ij} \\
\Phi'_{px}\sum\Delta x_{ij}\Delta z_{ij} + \Phi'_{py}\sum\Delta y_{ij}\Delta z_{ij} + \Phi'_{pz}\sum\Delta z_{ij}^2 &= \sum(\Phi_{pj} - \Phi_{pi})\Delta z_{ij}
\end{aligned} \tag{4.63}$$

The summation is over the neighbors $j=1,...,N$. Assuming that the matrix block has the size of L_x, L_y, L_z, the potential difference between matrix and fracture at the two sides of the matrix block is:

$$\Delta\Phi_{pv} = \frac{1}{4}\overrightarrow{\nabla\Phi_p} \bullet (L_x\vec{i} + L_y\vec{j} + L_z\vec{k}) \tag{4.64}$$

The potential difference at the grid point is

$$\Delta\Phi_{pmf} = \Phi_{pm} - \Phi_{pf}. \tag{4.65}$$

If

$$\Delta\Phi_{pmf} + \Delta\Phi_{pv} \ldots and \ldots \Delta\Phi_{pmf} - \Delta\Phi_{pv} \tag{4.66}$$

have the same sign then at both halves of the matrix block either the matrix or the fracture is the upstream side and the term $\Delta\Phi_{pv}$ will be cancelled out in the flow equation, consequently the viscous force has no effect. If both $\Delta\Phi_{pmf} + \Delta\Phi_{pv} > 0$ and $\Delta\Phi_{pmf} - \Delta\Phi_{pv} < 0$ then the phase

p enters the matrix block at the upstream side (if $\lambda_{pf} > 0$) and expels at the downstream one. Finally, the matrix fracture fluid exchange rate for the phase p with considering of the viscous force is:

$$q_{mfp} = \frac{\tau_{mf}}{2}\lambda_{pf}(\Delta\Phi_{pmf} + \Delta\Phi_{pv}) - \frac{\tau_{mf}}{2}\lambda_{pm}(\Delta\Phi_{pmf} - \Delta\Phi_{pv}) . \tag{4.67}$$

Note that the Equation 4.67 is applicable only if the mentioned inequalities are valid.

In the derivation above, no restriction regarding the positions of the neighboring grid point were made, so the approach can be applied on unstructured grid too. The disadvantage is that the calculation time is very high. A simpler approach can be applied only on a structured grid as it is used by ECLIPSE[87] using a viscous displacement model, based on a technique described by Gilman and Kazemi[31] is described in the following section.

4.1.4.2 Structured Grid

A viscous displacement of fluid takes place when the fluid movement is caused by a pressure differential. In a dual porosity system the moving of the fluids towards the production wells will cause a pressure gradient within the fractures. Usually the fracture has a very high effective permeability and thus the pressure gradient inside the fractures will be small. As a consequence the viscous forces acting between the fracture and the matrix can be neglected. If the fracture system has a permeability of moderate magnitude, then fluid flow between matrix and fractures will be affected significantly by viscous forces. The following paragraphs describe the ECLIPSE[87] viscous displacement model.

Consider a representative matrix block, with known dimensions, that is surrounded by fractures, such as the block illustrated in Figure 4.17, where fluid movement takes place from the left to the right side. Then the fracture pressure will be higher at the inlet (p_1) and lower at the outlet (p_2) than the average fracture pressure (p_f), therefore fluid enters from the fracture into the matrix at the inlet and fluid enters from the matrix into the fracture at the outlet. If water is flowing in the fracture then a greater pressure gradient can help to recover oil from the matrix.

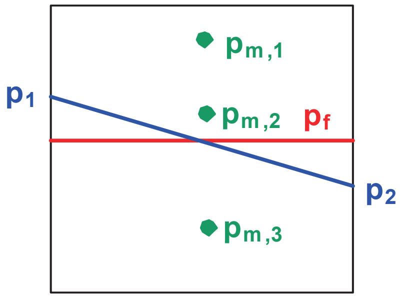

Figure 4.17: Explanation of the effect of viscous force

Three distinct cases of pressure inside the matrix can be considered:

1. The pressure in the matrix, p_{m1}, is greater than the pressures in the fracture p_1 and p_2. As a consequence flow will take place from the matrix to the fracture at the inlet and at the outlet if we consider the 1D case of Figure 4.17. Then the matrix-fracture flow, q_{mf}, can be expressed by:

$$q_{mf} = \frac{\tau_{mf}}{2}\lambda_m(p_{m1}-p_1) + \frac{\tau_{mf}}{2}\lambda_m(p_{m1}-p_2), \tag{4.68}$$

   where λ_m is the matrix mobility.
   Usually the pressures, p_1 and p_2, at the inlet and at the outlet of a matrix block are not known, but the average fracture pressure which is:

$$p_f = \frac{p_1+p_2}{2}. \tag{4.69}$$

   Using Equation 4.69 Equation 4.68 can be simplified to:

$$q_{mf} = \tau_{mf}\lambda_m(p_{m1}-p_f). \tag{4.70}$$

2. The pressure in the matrix, p_{m2}, is smaller than the fracture pressure at the inlet p_1 and larger than the fracture pressure at the outlet p_2. Expressed in mathematical terms this means $p_1 > p_{m2} > p_2$. As a consequence fluid flows from the fracture to the matrix at the inlet and from the matrix to the fracture at the outlet. The overall matrix-fracture flow, q_{mf}, will be then:

$$q_{mf} = \frac{\tau_{mf}}{2}\lambda_f(p_1-p_{m2}) - \frac{\tau_{mf}}{2}\lambda_m(p_{m2}-p_2), \tag{4.71}$$

   where λ_f is the fracture mobility.
   Inserting the average fracture pressure, p_f, defined in Equation 4.69, Equation 4.71 can be modified to:

$$q_{mf} = \frac{\tau_{mf}}{2}\lambda_f\left(p_f+\frac{p_1-p_2}{2}-p_{m2}\right) - \frac{\tau_{mf}}{2}\lambda_m\left(p_{m2}-p_f+\frac{p_1-p_2}{2}\right). \tag{4.72}$$

   The unknown pressure difference between the inlet and the outlet of the matrix block can be expressed by a pressure gradient G along the fracture spacing L,

$$p_1-p_2 = G\cdot L \tag{4.73}$$

   For our simple example presented in Figure 4.17 two neighboring blocks one on the left and the other on the right side will be introduced, as shown in Figure 4.18.

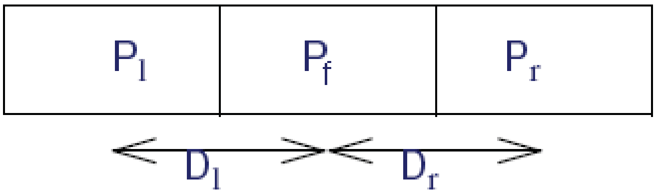

Figure 4.18: Neigboring grid blocks to the representative

Then the fracture pressure gradient can be estimated from the fracture block pressure,p_l, of the left and the fracture block pressure, p_r, of the right neighbor of our central block having a fracture block pressure p_f. D_l and D_r are the distances between the grid points.

$$G = \frac{|p_l - p|}{2D_l} + \frac{|p - p_r|}{2D_r} \tag{4.74}$$

Finally the matrix-fracture flow taking into consideration viscous forces can be written as:

$$q_{mf} = \frac{\tau_{mf}}{2}\lambda_f(p_f - p_{m2}) - \frac{\tau_{mf}}{2}\lambda_m(p_{m2} - p_f) + \frac{\tau_{mf}}{4}G \cdot L(\lambda_f - \lambda_m), \tag{4.75}$$

for the case that the condition $p_1 > p_{m2} > p_2$ is fulfilled.

3. Both pressures p_1 and p_2, valid at the inlet and the outlet of the representative matrix block, are higher than the pressure in the matrix, p_{m3}. As a consequence flow will be directed from the fracture to the matrix. For such a case the matrix-fracture flow term is:

$$q_{mf} = \tau_{mf}\lambda_m(p_f - p_{m3}). \tag{4.76}$$

For a three dimensional case, the matrix-fracture flow terms can be derived in a similar fashion.

4.1.5 Treatment of Molecular Diffusion

In naturally-fractured reservoirs, as opposed to unfractured reservoirs, molecular diffusion may be very important, because the dispersive flux through fractures rapidly increases the contact area for diffusion. Similarly, Fick's molecular diffusion potential may even override viscous forces when hydrocarbon or inert gases are injected and the fracture spacing is small.

The following method is used to calculate the diffusion between fracture and matrix blocks. However, it is not used for grid blocks within the same grid system. The method can also be used to calculate gas-gas and gas-liquid diffusion rates. This approach was described by Da Silva and Belery[24].

When hydrocarbon gas is injected at pressures below the oil bubble point pressure, two-phase diffusion can take place. For example, the injected gas dispersed throughout the fractures may contact large areas with two-phase saturated matrix blocks. Due to concentration differences, the injected gas tends to diffuse through both hydrocarbon phases, which simultaneously cause counter flow to the fractures. However, the gas-gas diffusion is approximately ten times faster than the gas-liquid diffusion.

The mixing process observed during multicomponent fluid displacements in porous media is typically of convection-diffusion type. Convection arises from the heterogeneity of the medium inducing local bulk velocity differences, while diffusion refers to the random motion of the molecules. The combination of the two types of molecular motion causes dispersion (i.e., a mechanism which will tend to abrogate any spatial concentration differences).

In principle, the dispersive flux of a particular fluid component depends upon the concentration gradients of all other components. The use of effective coefficients eliminates all the cross terms. The following simulation approach can be proposed based on the work described by Coats[20] and Da Silva[24]:

Diffusion is only calculated between matrix and fracture blocks (and not between blocks that are lying in the same grid system). Only the gas-gas diffusion or the gas-liquid diffusion is taken into consideration (if both are taken into consideration, an equilibrium-state dilemma arises which would require all matrix component K-values to be equal). Furthermore, the effective diffusion coefficient must be known for each component. The diffusion coefficients are calculated from a static variable group as reservoir temperature, component molecular weights and critical properties of the components and from dynamic variables as pressure and composition. When dealing with black-oil models it is only possible to calculate the liquid-gas diffusion rate since the gas phase consists of a single component. In compositional simulation more components exist for the gas phase, therefore the gas-gas diffusion rate can also be calculated. If, for example, gas with a different composition than the reservoir gas is injected into a reservoir the gas-gas diffusion should be taken into account. Figure 4.19 shows a schematic of gas-gas and liquid-gas diffusion between a matrix and a fracture grid block.

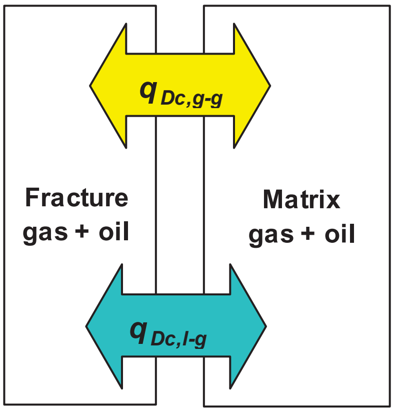

Figure 4.19: Schematic of gas-gas and liquid-gas diffusion

The matrix-fracture diffusion transfer is given for gas-gas diffusion as

$$q_{Dc,\,g-g} = \tau_D S_{gm} j_{gc}[(D_g x_{gc})_m - (D_g x_{gc})_f] \cdot (1 - S_{wf}) \tag{4.77}$$

and for the gas-liquid diffusion as

$$q_{Dc,\,o-g} = \tau_D S_{om} j_{oc}[(D_o x_{oc})_m - (D_g x_{gc})_f] \cdot (1 - S_{wf}), \tag{4.78}$$

with

$$\tau_D = V_m \cdot 8\left[\frac{1}{L_x^2} + \frac{1}{L_y^2} + \frac{1}{L_z^2}\right] \cdot \frac{\phi_m}{\tau_{or}} \tag{4.79}$$

where

$q_{Dc,\,g-g}$ - gas-gas diffusion rate for component *c*, [mol/d]
$q_{Dc,\,o-g}$ - liquid-gas diffusion rate for component *c*, [mol/d]
τ_D - diffusion'transmissibility', [m]
j_{gc} - effective gas diffusion coefficient for component *c*, [m^2/d]
j_{oc} - effective liquid diffusion coefficient for component *c*, [m^2/d]
τ_{or} - tortuosity (porous medium correction factor), [-]

The multiplication by (1-S_{wf}) (Equation 4.77 and Equation 4.78) is performed to prevent the requirement for a diffusion calculation for immersed matrix blocks by water. The contribution of the diffusion will be added to the matrix-fracture transfer term.

4.2. Transfer Functions

The transfer function and the so-called dual continuum concept were formulated initially by Barenblatt et al (1960) assuming single phase flow under pseudo steady state conditions. Kazemi et al. (1976) extended it to multiphase flow. Gilman and Kazemi (1883), Gilman (1986) and Sonier et al. (1988) continued improving this model by adding a gravity term and making it saturation depended. However, all the six matrix faces of the Warren and Root sugar cubes were considered, which overestimate the speed of recovery, when gravity is the dominant mechanism. Quandalle and Sabathier (1989) corrected it by separating the horizontal and vertical flows. They also added a viscous recovery term.

$$q_{pmf} = \Sigma k_a \frac{k_{rp}}{\mu_p B_p}(\Phi_{pf} - \Phi_{pm}) \quad , \quad p = w, o, g \tag{4.80}$$

where p stands for oil, water and free gas. k_a is the apparent matrix permeability, μ the viscosity, B the formation volume factor, k_r the relative permeability and Φ the phase potential in the fracture (f) and in the matrix (m). The shape factor, Σ, is a characteristic value of the matrix block. It will be calculated based on the size and form of the individual matrix blocks. The most complete version is the generalized Kazemi-Gilman-ElSharkawy (1992) shape factor as derived by Heinemann and Mittermeir (2012).

4.3. Numerical Investigation of Matrix Depletion Processes

4.3.1 Objectives

The approaches and investigations regarding fracture-matrix fluid transfer presented in the previous Section have the weakness that, among other issues, they do not account for an inhomogeneous fluid distribution within the matrix. Calculating numerically the same processes on fine gridded single porosity models promise more appropriate solutions. Such a calculation can be done for small scale laboratory measurement on cores, but also for imaginary matrix blocks situated in the reservoir. The comparison with laboratory data is necessary to increase for the conclusions the level of confidence.

Different applications of matrix block models can be found in the literature e.g[19],[28],[36],[50],[79]. These publications deal with recovery mechanism in fractured reservoirs, primarily with water/oil countercurrent imbibition and gas/oil drainage, and the matrix-fracture transfer. In all cases the internal grid cells build the matrix, surrounded by the high permeable fracture cells or connected to a boundary. The first solution is the only posibility while using commercial simulators, placing production and injection wells in fracture cells. Such a workaround is impractical, CPU intensive and often numerically instable. In the second case constant pressure or constant flux is set at the outer boundary (Mora and Wattenbarger (2009a).

In Pirker[71] approach the fracture cells represent the boundary with defined pressure and saturations. These cells inject fluids into the matrix and adsorb the fluids expelled from the matrix without altering its pressures and its saturation. The fracture cells will be re-initialized anyway at the beginning of every time step. Along these boundaries, i.e. in the fracture no fluid is flowing, but setting the cell pressures accordingly, a pressure gradient caused by moving fluid can be emulated. In our opinion this is the right and practical solution operating a single matrix block model.

Also Abushaikha and Gosselin (2008) used standard (single porosity) commercial flow simulators (Eclipse and Athos) in which the matrix block and the surrounded fractures are explicitly represented. They set constant fluid saturation and pressure in the large fractures surrounding the matrix. Unfortunately they did not explained how the fine gridded model was operated.

4.3.2 Model Building

4.3.2.1 The SMB Grid

In the first guess, to get reliable results, both the volume and the shape of the of the investigated matrix block should be identical with the real one. Heinemann and Mittermeir[43] showed that in the case of uniform boundary conditions not the shape itself but the shape factor is decisive. Consequently any arbitrarily-shaped matrix block can be mapped to any other shape as long the shape factors remain the same. The shape factor depends on the matrix-fracture connection surfaces, its distances from the point of gravity, the orientation of principle permeability axes (see Section) and the surface to volume ratio. For isotropic rock this means that the surface-to-volume ratios have to be identical. The boundary conditions are uniform when the pressure and the saturations are identical at every open side of the of the matrix block and the driving forces are limited to compression and capillary forces. Mora and Wattenbarger (2009a) conducted numerical experiences with irregularly shaped single matrix block using fine-grid simulation with constant pressure boundary conditions. From these various results they derived an expression for the shape factor depending solely on the block's volume *V* and the outer surface area *S*. For all the cases analyzed the numerical derived shape factors were within a limit of +/-10% difference. They concluded that the general expression for estimating the shape factor of irregularly shaped matrix blocks would be formed by the intersection of realistic, non-orthogonal fracture networks. The conclusions of Mora and Wattenbarger are neither surprising nor new.

In cases where also gravitational and/or viscose forces are considered the boundary conditions cannot be uniform and therefore, the equivalency is given only if the matrix block lengths in given directions are also the same. By accounting only for the gravitational force, this direction is vertical, and the condition reduces to claiming the same matrix block heights. Regarding the viscous force the potential gradient in the flow direction is decisive. These driving forces were discussed in Section 4.1.3 and in Section 4.1.4 respectively. These classical approaches suggest that in case of similarity, investigations can be performed on a simpler geometry, irrespective of the matrix block shape. All geometries, shown in Figure 4.20, should show the same matrix-fracture fluid transfer behavior.

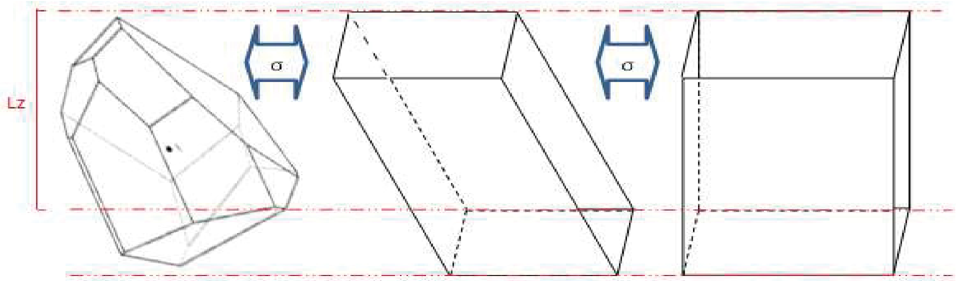

Figure 4.20: Simplifying the irregular matrix block shapes to a vertical cuboid with the same transfer behavior (same shape factor and height).

Nevertheless it is impossible to elicit the individual shapes of all native matrix block, therefore the question addressing second order differences has no practical importance. We accept two matrix blocks as being similar (in point of view of the fluid transfer) if their shape factor and height are identical.

Note that non of the principal permeability direction are necessarily vertical. It should be seen that all parameters in the single matrix examination are highly hypothetical. Nevertheless, in order to keep it simple, it is advisable to have the model vertical and assume that the permeability coordinate axes are identical with the geometrical ones.

The matrix block model is discretized into grid cells. Fracture planes are added to the sides of the matrix block. The simple geometrical shapes of the cubic single matrix block models do not require any special gridding technique, therefore simple Cartesian grids are used to discretize the matrix block and the surrounding fracture planes.These fracture planes can be set up in different combinations. They can surround the entire matrix block or only the (vertical) sides. Figure 4.21 shows a quarter of the model for the two patterns of possible fracture constellations. Fracture cells are marked in green and matrix cells in red. On the left vertical fractures are set along *x*- and *y*-planes, on the right also horizontal fractures exist at the top and the bottom

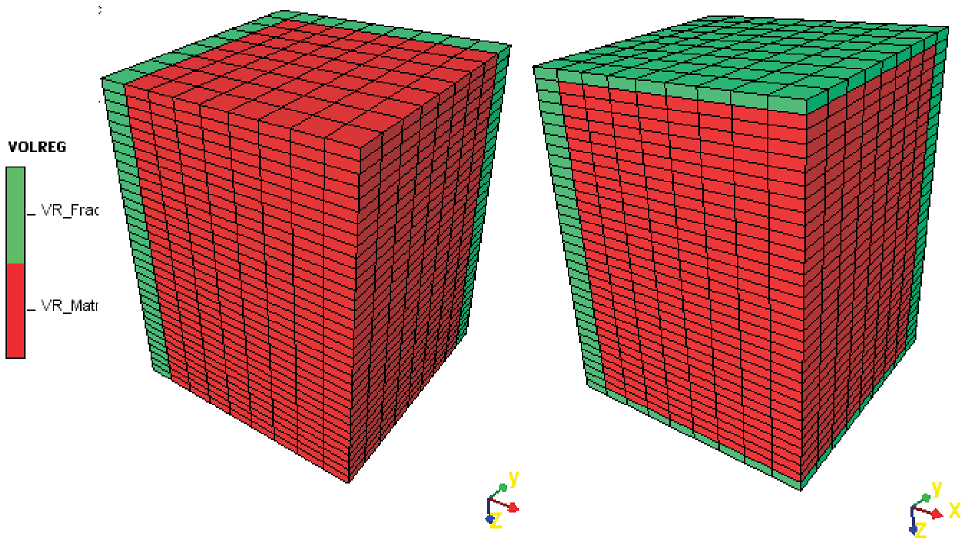

Figure 4.21: Single matrix blocks with different fracture constellations.

Due to the symmetry of the block model it is sufficient to calculate only one quarter of the model, therefore the side length of the cube is reduced in *x*- and *y*-direction to $L_x/2$ and $L_y/2$ respectively. The dimension in *z*-direction remains the same as in the vertical direction the gravity is in action making it not feasible to halve the block height. Figure 4.21 shows a single matrix block model as used in the further investigations with two- and three-dimensional fracture networks (*2D* or *3D*).

Pirker[71] recommends the *9*x*9*x*36* grid cells for the quarter model as generally applicable. However her investigations were limited to solution gas and linear water drive without phase separation. Gharsalla (2015) performed more extended investigations. The question was not only the limit beyond that the grid resolution has no more influence on the results but also which is the overall optimum by considering the CPU time too. The investigated x/y/z grids were

6x6x11, 7x7x21, 9x9x37 and 12x12x51. The Figure 4.22 compare the recovery curves for water drive, the Figure 4.23 for gas drive. The results show that the conclusions of Pirker where right, but also a more coarse grid could offer applicable result with considerable CPU time saving. A resolution of 7x7x21 is certainly satisfactory for most of the practical cases.

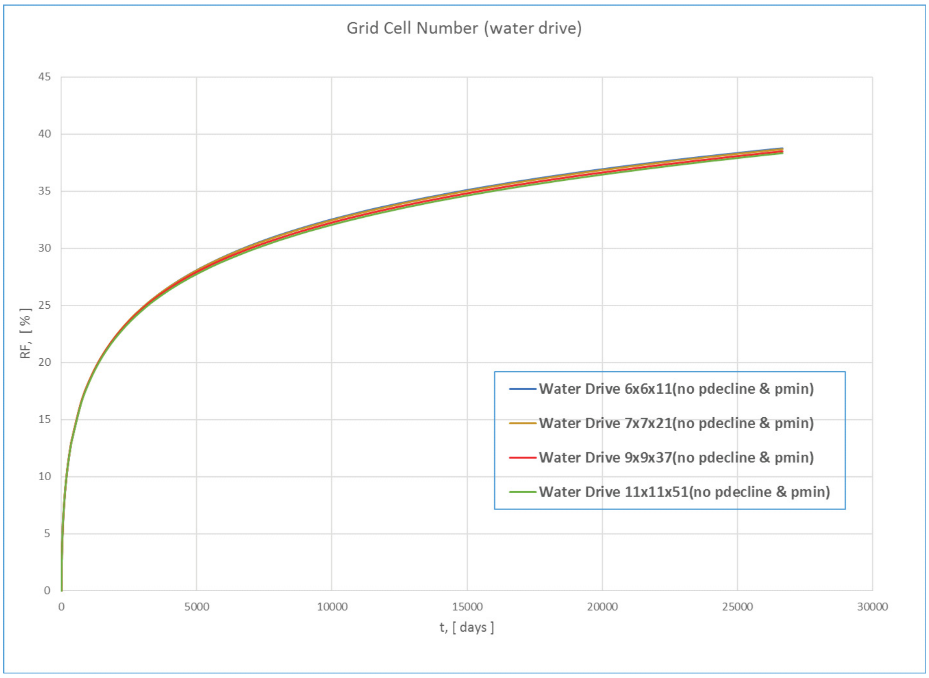

Figure 4.22: Sensitivity analysis on grid cell number, water drive.

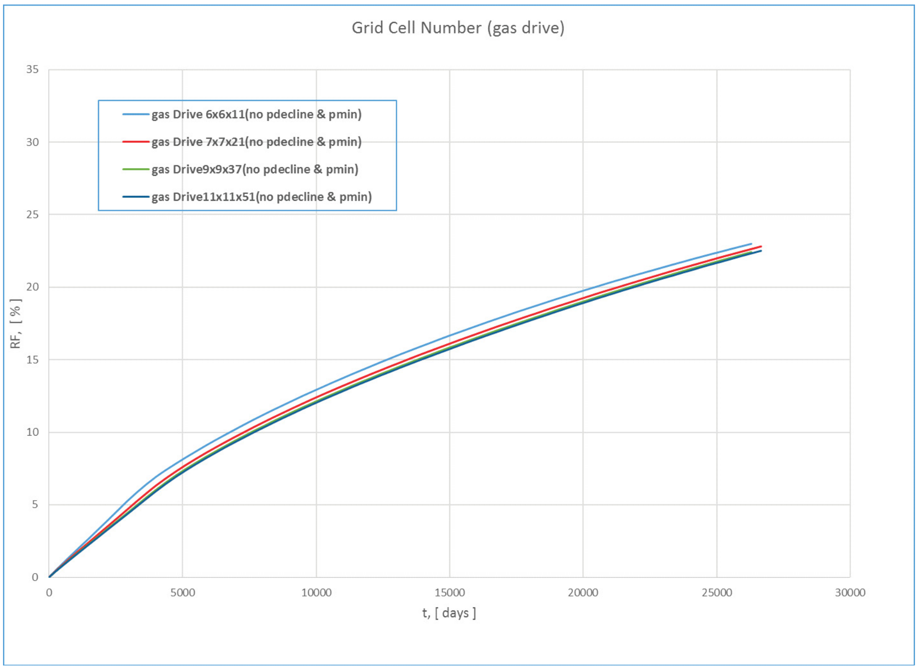

Figure 4.23: Sensitivity analysis on grid cell number, gas drive.

4.3.2.2 Grid Cell Properties and Parameters

The matrix domain is considered being homogeneous. The usual properties have to be assigned to the grid model: porosity, pore compressibility, permeability values in x-, y- and z-direction: (k_x, k_y, k_z). The net-to-gross ratio is considered to be 1.0 for obvious reasons.

The capillary and relative permeability functions in the matrix domain have to originate from the object under investigation. There are no restrictions regarding the PVT data, except that the PVT data for both the matrix and the fracture domains have to be the same. In our implementation both black-oil as well as compositional fluid models can be used.

As already mentioned. it is assumed that the permeability coordinate axes are identical with the geometrical ones. The permeability is defined by the apparent permeability k_a and the anisotropy coefficients k'_x, k'_y, k'_z . In isotropic case the values of the last ones are uniformly equal to 1. *The equivalent isotropic permeability*[59] $k_a = \sqrt[3]{k_x k_y k_z}$, would give the actual directional matrix permeability values (of $k_x = k_a * k'_x$, $k_y = k_a * k'_y$ and $k_z = k_a * k'_z$) in x-, y- and z-direction in the principle Cartesian coordinate system. In the case where the vertical permeability $k_z = 0$, the *equivalent isotropic permeability*[59] is $k_a = \sqrt{k_x k_y}$.

The fracture cells represents a boundary therefore their properties do not effect the matrix displacement process. A fracture cell communicates with a single matrix cell but not with the neighboring fracture cells. That means that no flow take place within the fracture plans. From technical reason parameters are defaulted to the fracture cells: E.g.: extension in direction of the matrix neighbor 0.001 m and pore volume 10000- times of a matrix cell. In this case the matrix-fracture transmissibility is determined by the matrix side only and fluid expelling from the matrix does not change the saturation in the fracture cell. The fracture cells will be re-initialized anyway at the beginning every time step.

4.3.2.3 Shape Factor

Note that the shape factor is not used in the course of calculations in the single matrix block model. However, the apparent matrix permeability, k_a, and the normalized permeability anisotropy tensor are related to each other through the shape factor, as it is evident from Equation 4.81 and Equation 4.82. Here, the shape factor is used to determine the geometry and size of the studied matrix block (as described in Section 4.3.2.4) as well as for outputting purposes and for further analysis. This means that when creating the model with *2D* or *3D* fracture network (i.e. without and with horizontal fracture planes respectively), the matrix block size is calculated from the correct simplification of Equation 2.38, as for the *3D* case:

$$\sigma = 4\left(\frac{k'_x}{L_x^2}+\frac{k'_y}{L_y^2}+\frac{k'_z}{L_z^2}\right) \Rightarrow L_x = L_y = \sqrt{\frac{k'_x + k'_y}{\frac{\sigma}{4}-\frac{k'_z}{L_z^2}}} \tag{4.81}$$

and for the *2D* case:

$$\sigma = 4\left(\frac{k'_x}{L_x^2}+\frac{k'_y}{L_y^2}\right) \Rightarrow L_x = L_y = \sqrt{\frac{k'_x + k'_y}{\frac{\sigma}{4}}} \tag{4.82}$$

In this way, the effect of different fracture constellations will be considered in the matrix block size. Note that if the shape factor after Kazemi *et al.*[45] is used instead of Heinemann and Mittermeir[43] shape factor, the values of k'_x, k'_y and k'_z are equal to *1* in Equation 4.81 and Equation 4.82 as the model is considered to be isotropic.

The vertical cuboid can also be created by specifying the matrix block side lengths, L_x, L_y and L_z (note that L_z is here also the effective matrix block height in the direction of the gravitational force). The shape factor can be calculated from Equation 4.81.

4.3.2.4 Model Operation

The initial saturation in the matrix is homogenous. The master phase can be oil, gas or water. The saturations of the other phases are equal to the critical one or are zero. The initial pressure is assigned to the middle layer (there the pressure will be the same for both, the matrix and the fracture) and vertically corresponds to the particular hydrostatic gradient of the matrix, respectively the fracture. In most of the cases the matrix will be fully oil-saturated with connate water saturation.

The fracture is filled with a single fluid, water, gas or oil, depending on the investigated displacement scenario.

The fracture inject the displacement fluid into the matrix and adsorbs those fluids expelled from the matrix. Due to the huge volumes of the fracture cells neither the pressure nor the saturation changes over a time step. The pressure and the saturation (equal to 1.0 for the displacing fluid) will be reset.

In depletion drive the fracture is filled with slightly undersaturated oil and the pressure will be lowered according a predefined rate. The expanding oil flows out from the matrix. Bellow the bubble point pressure gas will be deliberated and when exceeding the critical gas saturation it will also flow out into the fracture.

In case of water drive the fracture is filled with water, in case of gas drive with gas. Both of them can be combined with depletion, this means by gradually decreasing fracture pressure.

For investigations of oil re-saturation, the matrix is filled initially by gas and the oil saturation within the matrix equals the residual one. Due to the gravitational force the oil of the fracture will displace the gas modelling the well known oil re-saturation process.

The different displacement mechanisms can be combined as desired. E.g: Depletion followed by water drive and finally by gas drive and oil re-saturation.

4.3.3 Recovery Curve

In two recovery curves calculated with single matrix block models are displayed. The underlying single matrix block models are identical (PVT and SCAL data, initial pressure, drive mechanism, permeability, porosity and shape factor). The only difference is that for one model only vertical fractures are considered and for the second model also horizontal, this top and bottom fracture planes are considered. As was shown in Equation 4.81and Equation 4.82 the block dimensions will be consequently different.

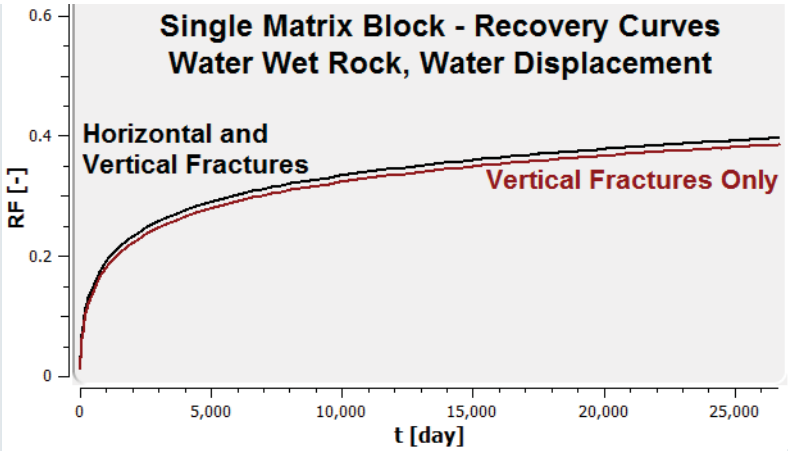

Figure 4.24: Recovery curves of a 2D and 3D single matrix block model

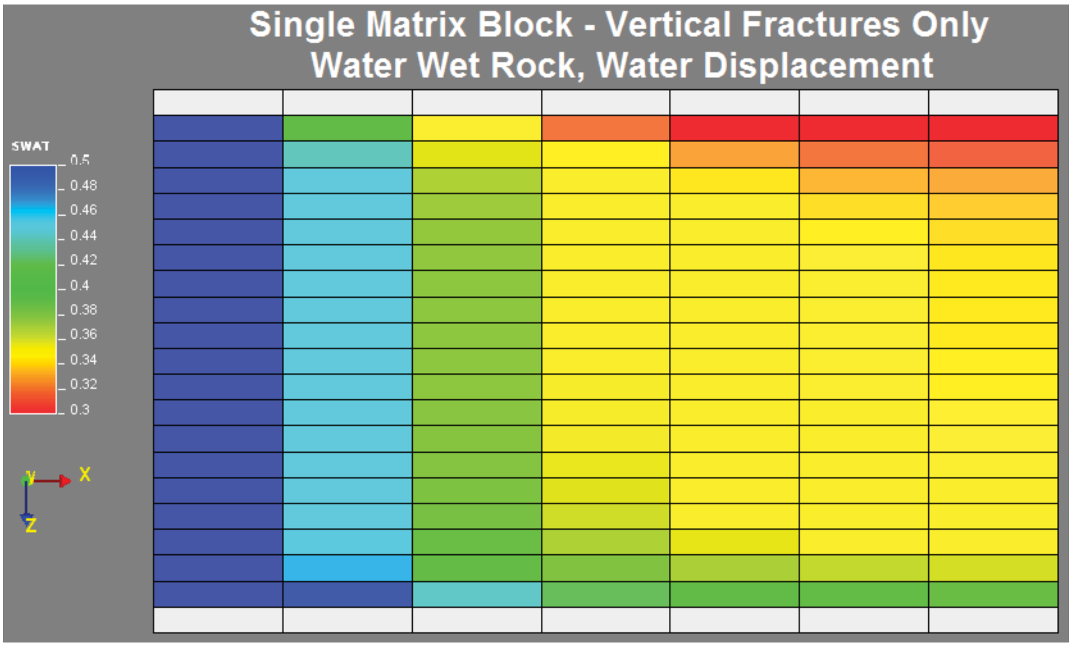

Figure 4.25: Single matrix block model showing water saturation distribution with vertical fractures only

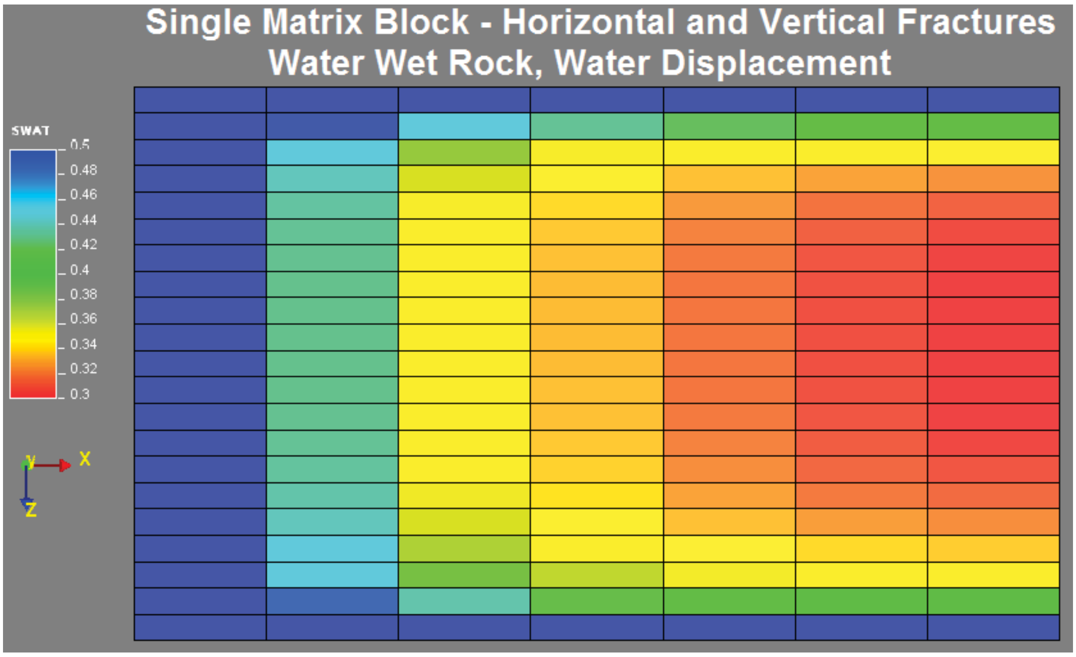

Figure 4.26: Single matrix block model showing water saturation distribution with vertical and horizontal fractures

4.3.4 Matrix Displacement - Basic Mechanisms

4.3.4.1 Expansion and solution gas drive

Without phase separation
With phase separation

4.3.4.2 Water drive

- Oil wet case
  Without phase separation
  With phase separation

- Water wet case
  Without phase separation
  With phase separation

4.3.4.3 Gas drive

Without phase separation
With phase separation

4.3.4.4 Oil re-saturation

4.3.5 Combined driving mechanisms

4.3.5.1 Water drive with depletion

4.3.5.2 Gas drive with depletion

4.3.5.3 Water drive followed by gas drive

4.3.5.4 Gas drive followed by water drive

4.4. Comparison of the SMB results with the transfer functions.

4.4.1 Calculating the Shape Factor

The shape factor can be calculated at every time step (n) by solving the transfer function for σ:

$$\sigma = \frac{q_{cmf}}{V_{cell} k_a \sum_{p=1}^{P} \Lambda_{pc}(\Phi_{pf} - \Phi_{pm})}. \tag{4.83}$$

$$\sigma = \frac{kmol \cdot s^{-1}}{V_{cell} m^2 \sum_{p=1}^{P} kmol \cdot m^{-3} \cdot Pa^{-1} \cdot s^{-1} Pa}$$

where,

$$\Lambda_{pc} = \lambda_p D_p x_{pc},$$

P	is the number of phases,
q_{cmf}	mole rate of the component c is the apparent permeability [kmol/s],
k_a	is the apparent permeability [m^2],
λ_p	is the mass mobility of component *c* in phase *p* [(Pa.s)$^{-1}$],
D_p	is the specific molar density [kmol/m^3],
x_{pc}	is the mole fraction of component *c* in phase *p* [-],
$(\Phi_{pf} - \Phi_{pm})$	is the potential difference of phase *p* between fracture and matrix [Pa].

Writing for oil phase:

$$\sigma = \frac{q_{omf}/V_b}{k_a \Lambda_{oc}(\Phi_{of} - \Phi_{om})}. \tag{4.84}$$

Replacing, $q_{omf} = OOIP \times (RF^n - RF^{n-1})$ and expanding the potential difference between the matrix and fracture we have, for the water drive case:

$$\sigma = \frac{OOIP}{k_a} \times \frac{(RF^n - RF^{n-1})/V_b^n}{\Lambda_{oc}^n[(\bar{p}_{of} - \bar{p}_{om}) - (P_{cowf} - P_{cowm}) - (P_{hwof} + P_{hwom})]^n}, \tag{4.85}$$

$$P_{hwof}(S_{wf}) = L_z \cdot S_{wf} \cdot (\rho_w - \rho_o)g, \tag{4.86}$$

$$P_{hwom}(S_{wm}) = L_z \cdot \left(\frac{S_w - S_{wi}}{1 - S_{wi} - S_{orw}}\right)_m (\rho_w - \rho_o)g, \tag{4.87}$$

and for the gas drive:

$$\sigma = \frac{OOIP}{k_a} \times \frac{(RF^n - RF^{n-1})/V_b^n}{\Lambda_{oc}^n[(\bar{p}_{of} - \bar{p}_{om}) + (P_{cogf} - P_{cogm}) - (P_{hgof} + P_{hgom})]^n}, \tag{4.88}$$

$$P_{hgof}(S_{gf}) = L_z \cdot S_{gf} \cdot (\rho_o - \rho_g)g, \tag{4.89}$$

$$P_{hgom}(S_{gm}) = L_z \cdot \left(\frac{S_g}{1 - S_{wi} - S_{org}}\right)_m (\rho_o - \rho_g)g, \tag{4.90}$$

and for expansion drive:

$$\sigma = \frac{OOIP}{k_a} \times \frac{(RF^n - RF^{n-1})/V_b^n}{\Lambda_{oc}^n[(\bar{p}_{of} - \bar{p}_{om}) - P_{cogm} - P_{hgom}]^n}. \tag{4.91}$$

Chapter 5

Material Balance Calculation for Dual Porosity Reservoirs

5.1. Introduction

The material balance (MB) calculation is one of the oldest reservoir engineering methods which made it possible to understand the natural recovery procedure of oil and gas reservoir. The first formulation was published by Schilthuis (1936), followed by Tarner (1944) and Muskat and Tayor (1946). The most comprehensive discussion of the MB method is given by Pirson (1950,1957). Initially the MB was applied to determine the oil in place, but due to introducing more sophisticated analytical aquifer models by van Everdingen and Hurst (1949), Carter and Tracy (1960), and Fetkovich (1971) the MB method could be used increasingly for production forecast too.

In classical Material Balance (MB) calculations the reservoir is treated as a single barrel analogue. The dual porosity nature of the reservoir could be preserved by creating two barrels, one representing the fracture and the other the matrix pore volume. Assigning different pressures to both volumes (matrix and fracture) and calculating the mass transfer between the two systems is not possible for two reasons: First, the pressure of the matrix cannot be measured and second, the mass transfer is governed by capillary, gravitational and viscous forces rather than by the force of compression. Penuela et al. (2001), Sandoval et al. (2009) and Bashiri and Kasiri (2011) distinguished between the matrix and fracture systems but considered only the difference in the pore compressibility. Such an approach differs only slightly from a single porosity model using averaged pore compressibility and therefore cannot be regarded as a valid extension of MB calculation to dual porosity reservoirs. This could probably be the reason why no petroleum software provider offers material balance tools especially suited for dual porosity reservoirs.

Since the work of Buckley and Leverett (1942), recovery curves are used to describe the efficiency of any displacement process. A recovery curve displays the recovery factor either versus time, injected pore volume or boundary pressure. Figure 5.1 shows the recovery curve as function of injected pore volumes for a Buckley-Leverett (1942) type linear displacement with constant injection rate. In a dual porosity reservoir the fracture system provides the local boundary condition for any individual matrix block, injects the displacing phase into the matrix, and the matrix block feeds the fracture system. Heinemann (2003) suggested to elaborate recovery curves for the matrix blocks and to use those curves directly in numerical modeling (simulation) of NFRs. Instead of considering individual properties for calculation of the matrix-fracture transfer terms, the recovery curves should be predefined and assigned to simulation cells directly. Heinemann (2013) showed the applicability and advantages of this approach in comparison to the classical dual porosity/permeability methods. The concept of the recovery curve method was adapted by Mittermeir (2015) to MB calculations and so 80 years after Schilthuis (1936) a comprehensive MB method for naturally fractured dual porosity reservoirs was borne. This method fully accounts for the fracture-matrix mass transfer, governed by the capillary, gravitational and viscous forces. No similar approach has been published up to date.

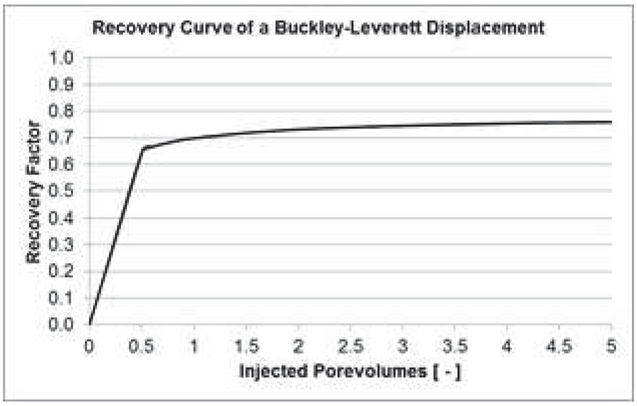

Figure 5.1: Recovery curve of Buckley-Leverett type linear displacement

Material balance calculation is a proxy method offering fast results and does not replace numerical simulation models. For both, conventional (single porosity) material balance calculation and the herein introduced dual porosity method, certain limitations exist: The MB model operates on homogenized reservoir data. This is true for all kind of data (PVT, rock, production, etc.). Furthermore, MB calculations apply only one average reservoir pressure as a function of time. MB models cannot predict individual well performances and thus, cannot be used to optimize production strategies on well level. Naturally, so called multi-tank MB calculations allow to consider areal variations. But the data of a single tank is homogenized nevertheless. For capturing the (apparent entire) heterogeneity of a reservoir and for modeling individual well performances numerical reservoir simulation has to be applied.

On the other hand MB calculation has also its merits. It is a rapid screening tool, especially applicable to an early stage of a reservoir engineering project. Moreover, MB calculations can be used to reduce the uncertainty of original hydrocarbons in place determinations. In addition MB calculations are required for determining analytical aquifer models. Those can be either used for predicting future field (not well) performance with MB calculations or for providing the required water influx in subsequent reservoir simulation. The herein introduced dual porosity MB approach allows additionally the matching of phase contact movements and recovery curves, which describe the matrix-fracture transfer. Those recovery curves can be used to replace the classical Warren-Root transfer term in the reservoir simulation model.

5.2. The Twin Barrels

Both – simulation models and MB calculations – are based on a geocellular model that usually contains millions of cells. Such a model is initialized by assigning pressures, saturations and mole fractions (for compositional fluid description) to each grid cell. Based on this model, the original fluids (oil; free and dissolved gas; water) in place for each cell are calculated. The term "tranche" is used in the following to distinguish between the subdivision of an aggregate and a slice, which has geometric connotations. Starting at the initial Oil Water Contact (OWC) horizontal tranches of unit thickness are set throughout the geocellular model. Alternatively, the tranches could be also of arbitrary thickness. Summing up the fluid contents of the tranches results in two columns of barrels. One column represents the matrix and the second the fracture continuum. This is illustrated in **Figure 5.2**. As a consequence of the vertical resolution, the distribution of the fluids and the position of the initial OWC and the Oil Gas Contact (OGC) are known.

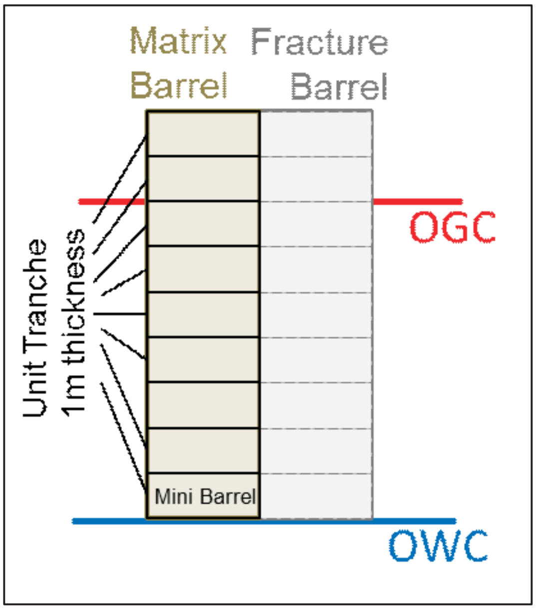

Figure 5.2: The twin barrel for dual porosity material balance calculation

The reservoir model for the dual porosity material balance calculation is built by two columns, one representing the fracture, the other one the matrix continuum. The columns are divided in tranches, which are numbered (k=1, 2, .., M) starting from the initial OWC upwards. M corresponds to the top of the reservoir. The vertical distributions of oil in place and other properties and variables (e.g.: pore volume, initial water saturation, etc.) are obtained similarly. The extensive values (e.g.: OOIP, pore volume) are the sum of the horizontal tranches throughout the reservoir. The intensive values (e.g. S_{wi}, which is the initial water saturation) are the averaged sum of them. The fracture column defines the boundary condition for the matrix column.

In the following different indices will be used:

- *o, g, w* denote the phases oil, gas and water,
- *i* is the initial value,
- *m* and *f* denote the matrix and fracture respectively,
- *k* is the serial number of the unit tranches, measured from the original OWC upwards,
- *j* is the time step counter, t_j is the production time.

In the geocellular model every cell has its own pressure, whereas In the MB model only one average pressure is considered. Besides the fluids in place, also the pore volume within the individual tranches can be summed up. It has to be corrected accordingly, taking into account the reservoir volume of the fluids at the average pressure. The fluid in a tranche *k* has to be flashed at the average pressure giving the pore volume (V_k):

$$V_k = N_k B_o(p_i, R_{si}) + G_k B_g(p_i) + W_k B_w(p_i) \tag{5.1}$$

where N_k, G_k, W_k are original amounts of oil, free gas and water in the tranche *k*. B_o, B_g and B_w, are the formation volume factors for the three phases oil, gas and water, p_i is the average initial pressure and R_{si} the average solution gas/oil ratio (GOR). Index *i* denotes the initial state. It should be noted that the initial pressure p_i corresponds to the entire MB model and not only to one tranche. **Equation 5.1** has to be applied to both the matrix (index *m*) and the fracture (*f*) continuum.

5.2.1 Pressure Match and Water Encroachment

As stated previously, it is not possible to determine different average pressures for the fracture and the matrix domain. The overall material balance (as it was already presented by Tarner (1944)) has to consider both domains in one common barrel. From **Equation 5.30** in Appendix A the water influx can be expressed as a function of time, calculated for every time step by inserting the cumulative production/injection of oil, gas and water and by calculating the PVT values at the actual average reservoir pressure p_j.

$$\begin{aligned} W_e(t_j) = -\frac{1}{B_{wj}} \Big\{ & N\left[B_{oj} - B_{oi} + B_{gj}\left(R_{si} - R_{sj}\right)\right] + NB_{oi}c_{\varphi a}\left(p_i - p_j\right) + mNB_{oi}\left(B_{gj}/B_{gi} - 1\right) \\ & - N_{pj}\left[B_{oj} + B_{gj}\left(R_{pj} - R_{sj}\right)\right] - W_{pj}B_{wj} + \left(W_{Ij}B_{wj} + G_{Ij}B_{gj}\right) \Big\} \end{aligned} \tag{5.2}$$

It has to be emphasized that *N* is the overall OOIP of the fracture and the matrix. Based on the function $W_e(t_j)$ one of the well-known analytical aquifer models, such as Fetkovich (1971), Van Everdingen and Hurst (1949) or Carter and Tracy (1960), can be identified as the best fitting one and their parameters can be determined. The Fetkovich model has two governing parameters, the other two models have three of them.

Such models can be used to predict the future water inflow and pressure development. It is clear that the water enters in the fracture system and subsequently invades parts of the matrix.

Equation 5.2 does not provide any information about the fluid transfer between the two continua or distinguishes between its actual fluid contents.

5.2.2 Application of the Recovery Curve in Material Balance Calculation

After production startup the average pressure of the reservoir will drop. Water encroachment at the bottom and expansion of a (primary or secondary) gas cap will cause a movement of the phase contacts (OWC and OGC). The pressure and saturation changes in the fracture will alter the boundary conditions at any elementary matrix tranche. Depending on the governing recovery mechanism, the recovery increment is either determined by the pressure change (depletion – single phase expansion and solution gas drive) or the elapsed time (water imbibition and gas drainage – water and gas drive).

5.2.2.1 Assumptions

The herein introduced dual porosity material balance method is based on the following assumptions:

- The model is based on the dual porosity – single permeability approach; the fluid distribution is balanced vertically in the fracture but not in the matrix column.
- The matrix permeability is large enough so that the fracture-matrix pressures can equalize. In other words the matrix permeability is greater than 0.01 mD and the pressure differences are less than 1 bar (14.7 psia).
- Full phase segregation is considered in the fracture column.
- Three matrix recovery mechanism are considered:

1. Depletion (single phase expansion, solution gas drive). This drive mechanism is active in the entire model. Those parts of the model, in which depletion is the sole drive mechanism are referred to Zone 1 in the following.
2. Water displacement. Water drive is active only for those portions of the matrix where the belonging fracture is water filled. This water zone – later also referred to Zone 3 – is below the dynamic OWC.
3. Gas displacement. Analogously to the water drive, this drive mechanism is active only for those matrix cells in which the belonging fracture contains free gas only. This gas zone is above the dynamic OGC and is referred to Zone 2.

- The phenomenon of oil re-saturation is handled by the recovery method analogously. The oil former displaced by gas at a structural higher position descents in the fracture and gets into contact with the matrix blocks which are already depleted. The fracture cell injects now oil instead of gas or water into the matrix.
- Production occurs from the fracture domain and the rates are defined for oil, gas and water independently. No outside production constraints (maximum water cut, maximum GOR, minimum pressure, etc.) are applied. Naturally, the phase conditions

inside the fracture must fit to the imposed target production, leading to inherent production constraints. Considering the production GOR two cases must be considered. First, it cannot be less than the solution GOR and second, it cannot be greater than the solution GOR in absence of free gas in the fracture. The water cut (WC) has to be zero as long as no water exists in the fracture.

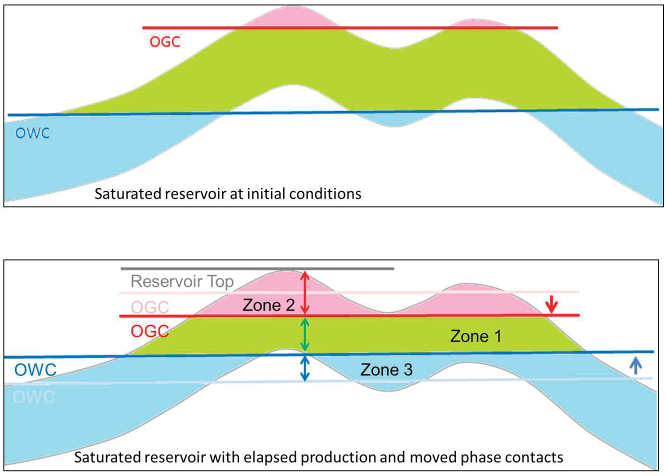

Figure 5.3: Schematics of an initially saturated reservoir and how the phase contacts will move due to production

A saturated reservoir with an initial gas cap is considered. **Figure 5.3** sketches this reservoir at initial state where $t_j = 0$, and at a state of elapsed production time $t_j > 0$. For $t_j > 0$ the average pressure has dropped from p_i to p_j. Three zones can be distinguished. They are determined by the phase contacts in the fracture system. The corresponding dual porosity MB model is sketched in **Figure 5.4**.

At the time point j the actual state of any tranche k is defined by the uniform pressure p_j, the recovery factor E_{kj} and concerning the water invaded zone eventually also by the gas saturation S_{gkj}. The recovery factor itself determines the oil saturation for all tranche $k = 1, M$:

$$S_{okj} = (1 - S_{wki}) \cdot (1 - E_{kj}) B_{oj} / B_{oi} \tag{5.3}$$

where S_{wik} is the initial water saturation, considered also as irreducible. It should be noted that the initial water saturation resulting from the geocellular model will not be uniform for the tranche $k = 1, M$.

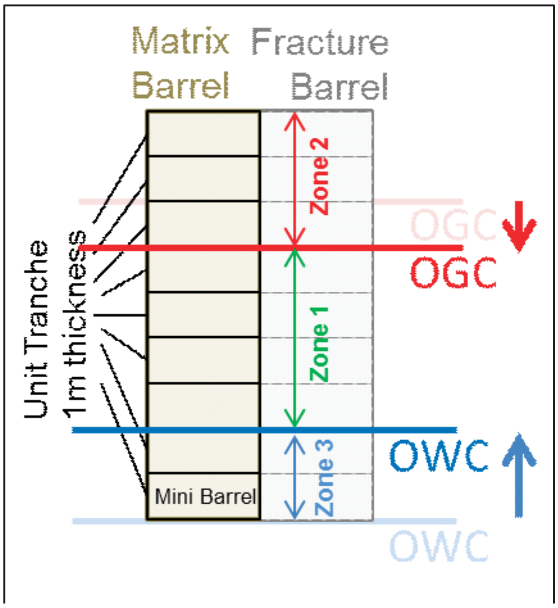

Figure 5.4: Dual porosity MB model with moving phase contacts

5.2.2.2 Oil recovery from the matrix in Zone 1

For Zone 1 depletion drive is active only. As long as the oil of the matrix is undersaturated (above bubblepoint) the expansion of rock and liquid phases (consisting of the irreducible initial water and oil saturation) expels the oil. Afterwards, the oil is recovered by solution gas drive. In this zone the water is regarded as immobile. The recovery factor is solely a function of pressure and therefore it is uniform for the entire Zone 1. It can be calculated using the finite difference material balance introduced by Pirson (1958, 508, his Eq. 10-45). The derivation and its adoption for the current publication can be found in Appendix A, **Equation 5.39** respectively. The matrix tranche has no gas cap (m=0), neither water influx ($w_e = 0$), nor water production ($w_p = 0$) nor water and gas injection ($w_I = 0$ and $g_I = 0$) take place. For one time step $\Delta t = t_{j+1} - t_j$ the pressure change is $\Delta p = p_{j+1} - p_j$. Applying those assumptions to **Equation 5.41**the recovery factor increment of one matrix tranche is given by:

$$\Delta_{j+1}E_k = \frac{(1-E_{kj})\Delta_{j+1}\left(\frac{B_o}{B_g}-R_s\right)+B_{oi}\Delta_{j+1}\left(\frac{1}{B_g}\right)(p_i c_{\phi ak}-1)-B_{oi}c_{\phi ak}\Delta_{j+1}\left(\frac{p}{B_g}\right)}{\left[\left(\frac{B_o}{B_g}-R_s\right)_{j+1}+\overline{R_{pk}}\right]} \tag{5.4}$$

Where Δ_{j+1} denotes the change of the subsequent entity during the time interval $\Delta t = t_{j+1} - t_j$. In the undersaturated case ($p_j > p_b$), R_s will be constant ($R_{sj} = R_{sj+1} = R_{si}$) and no free gas will be flowing between the matrix and the fracture, therefore the average production gas/oil ratio will be equal to the initial solution gas/oil ratio ($\overline{R_p} = R_{si}$). In the saturated case ($p_j < p_{bi}$), the apparent pore compressibility can be neglected. Therefore **Equation 5.4** simplifies to:

$$\Delta_{j+1}E_k = \frac{\left(1 - E_{kj}\right)\Delta_{j+1}\left(\frac{B_o}{B_g} - R_s\right) - B_{oi}\Delta_{j+1}\left(\frac{1}{B_g}\right)}{\left[\left(\frac{B_o}{B_g} - R_s\right)_{j+1} + \overline{R_{pk}}\right]} \tag{5.5}$$

The recovery values E_k can be different for the tranches of Zone 1 because the initial water saturations S_{wki} resulting from the geocellular model will not be uniform and so the numerical values of apparent pore compressibility and relative permeability can be slightly different. Those differences have no practical importance. The oil saturation S_{okj} is given in **Equation 5.3** and the gas saturation is:

$$S_{gkj} = 1. - S_{wki} - S_{okj} \tag{5.6}$$

As result of the fluid expansion and the gas liberation only oil will expel from the matrix until the critical gas saturation is reached. Then gas is flowing from the matrix to the fracture additionally. It is assumed that the water content in the matrix remains unchanged, thus $w_e = w_I = w_p = 0$ in **Equation 5.41**. The gas transfer from the matrix to the fracture is governed by the GOR, which is determined by the relative permeability and so by the gas saturation:

$$R_{pkj} = R_{sj} + \left(\frac{B_o}{B_g}\frac{\mu_o}{\mu_g}\frac{k_{rg}}{k_{ro}}\right)_{kj} \tag{5.7}$$

The relative permeability values are calculated based on the saturations. The average outflow gas-oil-ratio for the time interval $\langle j, j+1\rangle$ is

$$\overline{R_{pk}} = \left(R_{pkj+1} + R_{pkj}\right)/2 \tag{5.8}$$

5.2.2.3 Oil recovery from the matrix in Zone 2

Zone 2 is directly located above Zone 1. Now the fracture is invaded by gas. Oil recovery from the matrix happens also due to expansion drive, but it is overloaded by gas displacement. τ_{gk} is the moving OGC arrival time for the tranche k, which is measured as the vertical distance from the original OWC. At this date the recovery factor equals E_{kj}. From this time onwards the fracture can inject gas into the matrix as soon as the gravitational force exceeds the capillary threshold. With the presence of free gas the oil is saturated. The water content in the matrix remains, thus $w_e = w_I = w_p = 0$ in **Equation 5.41.** The material balance given in **Equation 5.5** has to be extended by the injected gas amount, $\Delta_{j+1}g_k$:

$$\Delta_{j+1}E_k = \frac{(1-E_{kj})\Delta_{j+1}\left(\frac{B_o}{B_g}-R_s\right)-B_{oi}\Delta_{j+1}\left(\frac{1}{B_g}\right)+\Delta_{j+1}g}{\left[\left(\frac{B_o}{B_g}-R_s\right)_{j+1}+\overline{R_{pk}}\right]} \tag{5.9}$$

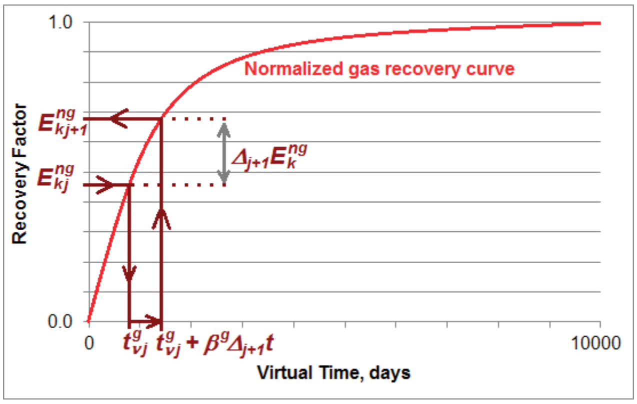

Figure 5.5: Determination of gas recovery increment based on apparent time

The increment of gas flowing from the fracture into the matrix, $\Delta_{j+1}g_k$, has to be obtained from the gas displacement recovery curve in a nomogram-like manner as it is shown in **Figure 5.5**

Figure 5.5 represents a schematic normalized gas recovery curve. The curves for water and gas drive are usually different. Each of them is elaborated by individual numerical single matrix block investigations setting the appropriate boundary conditions. E_{kj} is the actual recovery from tranche k at time j. The normalized recovery factor values of $\alpha^g E_{kj}$ correspond to the virtual time t^g_v on the normalized gas recovery curve. Adding an arbitrary time step $\Delta_{j+1}t$ and reading the normalized recovery factor at the new virtual time yield:

$$t^g_{vj+1} = t^g_{vj} + \beta^g \Delta_{j+1}t \tag{5.10}$$

results in the recovery factor increment:

$$\Delta_{j+1}E^g_k = \left(E^{ng}_k(t^g_{vj+1}) - E^{ng}_k(t^g_{vj})\right)/\alpha^g \tag{5.11}$$

Such an increase in the recovery factor causes a change of the in situ gas volume (i.e. gas saturation) which can be converted to standard volume at the actual reservoir pressure:

$$\Delta_{j+1}g_k = \Delta_{j+1}E^g_k \cdot (B_o/B_g)_{j+1}. \tag{5.12}$$

Inserting **Equation 5.12** into **Equation 5.9** provides the recovery increment considering the combination of depletion and gas drive:

$$\Delta_{j+1}E_k = \frac{\left(1-E_{kj}\right)\Delta_{j+1}\left(\frac{B_o}{B_g}-R_s\right)-B_{oi}\Delta_{j+1}\left(\frac{1}{B_g}\right)+\Delta_{j+1}E_k^g\left(\frac{B_o}{B_g}\right)_{j+1}}{\left[\left(\frac{B_o}{B_g}-R_s\right)_{j+1}+\overline{R_{pk}}\right]} \tag{5.13}$$

5.2.2.4 Oil recovery from the matrix in Zone 3

In this zone the fracture injects water into the matrix. The oil can be both either undersaturated or saturated. The undersaturated case is similar to the gas displacement described beforehand in Zone 2 since only two mobile phases (oil and water) exist in the matrix. Applying the appropriate conditions (m=0, $g_I = 0$, $w_p = 0$ and $w_e = 0$) to **Equation 5.41** the material balance for tranche k is:

$$\Delta_{j+1}E_k = \frac{\left(1-E_k\right)\Delta_{j+1}\left(\frac{B_o}{B_g}-R_s\right)+B_{oi}\Delta_{j+1}\left(\frac{1}{B_g}\right)\left(p_i c_{\phi ak}-1\right)-B_{oi}c_{\phi ak}\Delta_{j+1}\left(\frac{p}{B_g}\right)}{\left[\left(\frac{B_o}{B_g}-R_s\right)_{j+1}+\overline{R_{pk}}\right]}$$

$$+\frac{w_{Ikj}\Delta_{j+1}\left(\frac{B_w}{B_g}\right)+\Delta_{j+1}w_{Ik}\left(\frac{B_w}{B_g}\right)_{j+1}}{\left[\left(\frac{B_o}{B_g}-R_s\right)_{j+1}+\overline{R_{pk}}\right]} \tag{5.14}$$

It is assumed that the amount of injected water can be estimated from the water drive recovery curve which was elaborated for a two phase water displacement. $\Delta_{j+1}E_k^w$ is the oil recovery increment of the water drive case for the time step interval $\Delta t=t_{j+1}-t_j$. The specific water inflow during the same time is then:

$$\Delta_{j+1}w_{Ik} = \Delta_{j+1}E_k^w \cdot (B_o / B_w)_{j+1} \; . \tag{5.15}$$

In the saturated case (below the initial bubblepoint pressure) a free gas saturation exists already in the matrix. The water injected by the fracture into the matrix tranche is also displacing the free gas flowing from the matrix to the fracture.

$$\Delta_{j+1}w_{Ik} = \Delta_{j+1}E_k^w \cdot \left[B_{oj+1} + B_{gj+1}(\overline{R}_{pk} - R_{sj+1})\right] / B_{wj+1} \; . \tag{5.16}$$

The production GOR $\overline{R}_{pk}$ is calculated using **Equation 5.8**.

For the calculation of relative permeability the gas saturation in the matrix has to be estimated based on the known oil saturation and cumulative intruded water:

$$\begin{aligned} S_{gkj} &= 1.-S_{okj}-S_{wkj} \\ &= 1.-S_{wki}-(1.-S_{wki})\left(E_{kj}B_{oj}/B_{oi}+w_{Ikj}\right) \\ &= (1.-S_{wki})\left(1.-E_{kj}B_{oj}/B_{oi}-w_{Ikj}\right) \end{aligned} \quad . \tag{5.17}$$

The cumulative intruded water is the sum of all increments:

$$w_{Ikj}=\sum_{n=1,j}\Delta_n w_{Ik} \quad . \tag{5.18}$$

The applicability of **Equation 5.16** is unfortunately limited. The reason is that small inaccuracies have already a great impact on the gas saturation value and the error propagates via **Equation 5.7** and **Equation 5.17** exponentially. It is better to create a composite recovery curve by modeling water displacement in single matrix blocks with predefined pressure decline. Such a calculation will produce not only the recovery curve but also an estimate of the gas saturation over a period of time.

5.3. Monitoring of Phase Contacts

Having the recovery factor E_{kj} the cumulative transferred oil from the matrix into the fracture can be easily calculated:

$$Q_{mf}(t_j)=\sum_{k=1}^{M}OOIP_k\cdot E_{kj} \quad . \tag{5.19}$$

The actual amount of the oil in the fracture is:

$$N_{fj}(t_j)=N_{fi}+Q_{mf}(t_j)-Q_o(t_j) \quad . \tag{5.20}$$

where Q_o is the cumulative oil production and N_{fi} is the original amount of oil in the fracture situated between the initial water and gas oil contacts (OWC and OGC).

In the fracture system complete phase segregation is assumed. If the vertical distribution of the fracture volume V_{fk} with $k = 1, M$ is known then also the positions of the phase contacts can be determined. The volume of the oil column between the actual phase contacts is given by the following relation:

$$\sum_{k=K_{owc}}^{K_{ogc}} V_{fk} \approx \left[N_{fi} + Q_{mf}(t_j) - Q_o(t_j)\right]B_{oj} \quad . \tag{5.21}$$

For the presented approach the tranche thickness equals 1m. Due to this resolution a maximum deviation of ±1m between the physical phase contact and the one of the model located at tranche *k* can be identified. This is expressed by the ≈ sign. The fracture oil column is situated in the interval K_{owc} and K_{ogc}. Above the K_{ogc} level the fracture column is filled with free gas. Below K_{owc} the fracture column contains only water. For reasons of simplicity it is assumed that the connate and residual saturations of the fracture equal zero. In absence of water inflow the same is valid for the OGC determination. If both free gas and water inflow exist, then the position will be more uncertain and will need supplementary considerations, which will be explained later.

5.3.1 Undersaturated Reservoirs

Determining the position of the OWC is easy in the case of no free gas. Therefore, in an undersaturated case the position of the actual OWC is defined by the following relation:

$$\sum_{k=K_{owc}}^{M} V_{fk} \geq \left[N_{fi} + Q_{mf}(t_j) - Q_o(t_j)\right]B_{oj} > \sum_{k=K_{owc}+1}^{M} V_{fk} \quad . \tag{5.22}$$

The actual OWC is then situated between the depth K_{owc} and K_{owc}+1, measured upwards from the original OWC. k=0 corresponds to the depth of the original OWC and M to the top depth of the reservoir.

5.3.2 Absence of Aquifer/Water Encroachment

The determination of the OGC position in absence of water influx is similarly simple:

$$\sum_{k=1}^{K_{ogc}} V_{fk} \geq \left[N_{fi} + Q_{mf}(t_j) - Q_o(t_j)\right]B_{oj} > \sum_{k=1}^{k=K_{ogc}-1} V_{fk} \quad . \tag{5.23}$$

The actual OGC is then situated between the depth K_{ogc} and K_{ogc}-1, measured upwards from the original OWC.

5.3.3 Three Phase Case

Concerning the three phase case – gas on top of the fracture column (Zone 2), oil in the middle

(Zone1) and water at the bottom (Zone3) – placement of the phase contacts (OWC and OGC) is no longer trivial. For evaluating the OWC it is necessary to consider **Equation 5.16** for the calculation of the water amount intruding into the matrix. As already explained, this is burdened by the uncertainty of the gas saturation estimation. Summing up **Equation 5.16** for the interval between the first tranche above the initial OWC and the actual OWC (K_{owc}), the cumulative water intrusion in the matrix system is given by:

$$W_{mj} = \sum_{k=1}^{K_{owc}} w_{kj} \quad . \tag{5.24}$$

The cumulative water influx (W_{ej}) of the entire reservoir (matrix and fracture) is calculated from **Equation 5.1** similar to the single porosity case according to the pressure history. The aquifer, being the source of the water encroachment W_e, is only connected to the fracture system. Therefore, the amount of water residing within the fracture pore volume at the time j is:

$$W_{ej} - W_{mj} - Q_w(t_j) \quad . \tag{5.25}$$

The following relation has to be satisfied:

$$\sum_{k=1}^{K_{owc}} V_{fk} \le \left[W_e - W_{mj} - Q_w(t_j)\right] B_{wj} < \sum_{k=1}^{K_{owc}+1} V_{fk} \quad . \tag{5.26}$$

The actual OWC is then situated between the depth K_{owc} and $K_{owc}+1$, measured upwards from the original OWC.

The amount of gas in the matrix is the sum of the free and dissolved gas:

$$G_{mj} = \sum_{k=1}^{M} V_{mk} \left(\frac{S_{gk}}{B_g} + \frac{S_{ok}}{B_o} R_s\right)_j \quad . \tag{5.27}$$

G_i is the original gas amount in the entire model. The actual amount of free gas in the fracture is then:

$$G_{fj} = G_i - G_{mj} - N_{fj} R_{sj} - Q_g(t_j) \quad . \tag{5.28}$$

$$\sum_{k=K_{ogc}}^{M} V_{fk} \le G_{fj} B_{gj} < \sum_{k=K_{ogc}-1}^{M} V_{fk} \quad . \tag{5.29}$$

Naturally, between the estimated OWC and OGC the fracture volume must be equal to the volume of the oil column given by **Equation 5.21**. Satisfying this requirement is a difficult matter and it needs a careful and critical estimation of the relative permeability functions.

5.4. Nomenclature

Symbols:

B	formation volume factor, L^3/L^3, STB/res bbl
c	compressibility, Lt^2/m, 1/psia
E	efficiency/recovery factor
G	gas amount, L^3, scf
G_I	cumulative injected gas, L^3, scf
g	specific gas amount, scaled to unit oil in place
J_w	aquifer productivity index, L^4t/m
K_{ogc}	tranche containing the actual OGC
K_{owc}	tranche containing the actual OWC
k	permeability, L^2, m^2
k_r	relative permeability
L	characteristic dimension, L, m
m	gas cap factor
N	original oil in place, L^3, STB
N_p	cumulative oil production, L^3, STB
p	pressure, m/L^3, psia
Q	cumulative production, L^3, STB
Q_{mf}	cumulative matrix-fracture oil transfer, L^3, STB
R	gas/oil ratio, L^3/L^3, scf/STB
t	time, t, day
S	saturation
SF	shape factor, $1/L^2$, $1/m^2$
V	pore volume, L^3, res bbl
W_I	cumulative injected in place, L^3, STB
W_e	water encroachment, L^3, STB
W_{ei}	maximum encroachable water, L^3, STB
W_p	cumulative water production, L^3, STB
w	specific water amount, scaled to unit oil in place

Greek symbols:

α	reciprocal of ultimate recovery
β	time scaling factor
Δ	difference operator
ϕ	porosity
μ	viscosity, m/Lt, cp
τ	arrival time, t, d
σ	interfacial tension, m/t^2, N/m
ω	weighting factor

Subscripts:

a	apparent
b	bubblepoint
f	fracture
g	gas phase
i	initial
j	time point index
k	tranche index
m	matrix
M	tranche for top of reservoir
N	time index for end of history
o	oil phase
p	production
R	recovery
r	residual
s	solution
w	water phase

Greek Subscripts:

ϕ	pore

Superscripts:

a	analytical
g	gas
n	normalized
w	water

5.5. References

[1] Aronofsky, J. S., Masse, L., and Natanson, S. G. 1958. A Model for the Mechanism of Oil Recovery from the Porous Matrix Due to Water Invasion in Fracture Reservoirs. Paper SPE 932-G. *Transactions of the AIME* **213**: 17-19.

[2] Amiry, M.T. 2014. Modeling Flow Behavior in Naturally-Fractured Reservoirs. PhD Thesis, Montanuniversität Leoben, Leoben, Austria (February 2014).

[3] Bashiri, A. and Kasiri, N. 2011. Revisit Material Balance Equation for Naturally Fractured Reservoirs. Paper SPE 150803-MS presented at the Nigeria Annual International Conference held in Abuja, Nigeria, 30 July-3 August. http://dx.doi.org/10.2118/150803-MS

[4] Buckley S.E. and Leverett M.C. 1942. Mechanism of Fluid Displacement in Sands. In *Transactions of the AIME* **146** (1): 107-116. http://dx.doi.org/10.2118/942107-G

[5] Carter, R.D. and Tracy, G.W. 1960. An Improved Method for Calculating Water Influx. In *Petroleum Transactions*, AIME, Vol.219, 415-417.

[6] Davis, G.B. and Hill, J. M. 1982. Some Theoretical Aspects of Oil Recovery From

Fractured Reservoirs. *Trans IChemE* **60**: 352-358.

[7] de Swann, A. 1978. Theory of Waterflooding in Fractured Reservoirs. *SPE Journal*. **18** (2): 117-122. SPE-5892-PA. http://dx.doi.org/10.2118/5892-PA

[8] Di Donato, G., Lu, H. Tavassoli, Z. and Blunt, M.J. 2007 Multirate-Transfer Dual-Porosity Modeling of Gravity Drainage and Imbibition. Paper SPE 93144-PA. *SPE Journal* **12** (1): 77-88. http://dx.doi.org/10.2118/93144-PA

[9] Fetkovich, M.J. 1971. A Simplified Approach to Water Influx Calculations-Finite Aquifer Systems. Journal of Petroleum Technology **23** (7): 814-828. SPE-2603-PA. http://dx.doi.org/10.2118/2603-PA

[10] Gilman, J. R. and Kazemi, H. 1988. Improved Calculation for Viscous and Gravity Displacement in Matrix Blocks in Dual-Porosity Simulators. Journal of Petroleum Technology **40** (1): 60-70. Paper SPE 16010. http://dx.doi.org/10.2118/16010-PA

[11] Heinemann, Z. E., Mittermeir, G.M. and Gharsalla, M.M. 2014. Successful Application of Material Balance Calculation to a Fractured Dual Porosity Field. Paper SPE 172325-MS presented at the Annual Caspian Technical Conference and Exhibition held in Astana, Kazakhstan, 12-14 November. http://dx.doi.org/10.2118/172325-MS

[12] Kazemi, H., Gilman, J.R. and Elsharkawy, A.M. 1992. Analytical and Numerical Solution of Oil Recovery from Fractured Reservoirs Using Empirical Transfer Functions. Paper SPE 19849-PA *SPE Reservoir Engineering* **7** (2): 219-227. http://dx.doi.org/10.2118/19849-PA

[13] Mattax, C.C. and Kyte, J.R. 1962. Imbibition Oil Recovery from Fractured, Water-Drive Reservoirs. *SPE Journal* **2** (2): 177-84 SPE-187-PA. http://dx.doi.org/10.2118/187-PA

[14] Mittermeir, G.M., Pichelbauer J., and Heinemann Z.E. 2004. Automated Determination of Aquifer Properties from Field Production Data. Paper presented at the 9th European Conference on Mathematics of Oil Recovery (ECMOR IX), Cannes, France, 30 August –2 September.

[15] Mittermeir, G.M. 2015. Material Balance Method for Dual Porosity Reservoirs using Recovery Curves to Model the Matrix-Fracture Transfer. Paper SPE-174082-PA accepted for publication in SPE Reservoir Evaluation.

[16] Penuela, G., Eduardo, A., Idrobo, A. et al. 2001. A new Material-Balance Equation for Naturally Fractured Reservoirs Using a Dual System Approach. Paper SPE 68831-MS presented at the SPE Western Regional Meeting held in Bakersfield, California, 26-30 March. http://dx.doi.org/10.2118/68831-MS

[17] Pirker, B., Mittermeir G.M., and Heinemann Z.E. 2007. Numerically Derived Type Curves for Assessing Matrix Recovery Factors. Paper SPE 107074-MS presented at the EUROPEC/EAGE Conference and Exhibition held in London, U.K., 11-14 June. http://dx.doi.org/10.2118/107074-MS

[18] Pirker, B. and Heinemann Z. E. 2008. Method to Preliminary Estimation of the Reserves and Production Forecast for Dual Porosity Fractured Reservoirs. Paper SPE 113378-MS presented at the EUROPEC/EAGE Conference and Exhibition held in Rome, Italy, 9-12 June. http://dx.doi.org/10.2118/113378-MS

[19] Pirker, B., Harrer A. W., and Heinemann Z.E. 2008.Reserve Estimation for Naturally Fractured Reservoirs Using Numerically Derived Recovery Curves. In *EAGE Proceedings of the 11th European Conference on the Mathematics of Oil Recovery*, held in Bergen, Norway, 8-11 September.

[20] Pirker, B. 2008. A New Approach for Modeling Dual Porosity Reservoirs Using Recovery Curves. PhD dissertation, Montanuniversität Leoben, Leoben, Austria (November 2008).

[21] Pirson, S.J. ed. 1958. *Oil Reservoir Engineering*, 508 .New York City: McGraw-Hill Book Company

[22] Sandoval, P., Calderon, Z., and Ordonez A. 2009. A new, Generalized Material Balance Equation for Naturally Fractured Reservoirs. Paper SPE 122395-MS presented at the Latin American and Caribbean Petroleum Engineering Conference held in Cartagena de Indias, Columbia, 31 May-3June. http://dx.doi.org/10.2118/122395-MS

[23] Schilthuis, R.J.: "Active Oil and Rerservoir Engergy", Trans., AIME, 118, (1936), 33-52.

[24] Tarner, J. 1944. How Different Size Gas Caps and Pressure Maintenance Programs Affect Amount of Recoverable Oil. Oil Weekly **144** (June 12): 32-34.

[25] Warren, J.E. and Root, P.J. 1963. The Behavior of Naturally Fractured Reservoirs. *SPE J.* **3** (3): 245-255. SPE-426-PA. http://dx.doi.org/10.2118/426-PA

[26] Van Everdingen, A.F. and Hurst W. 1949. The Application of the Laplace Transformation to Flow Problems in Reservoirs. Journal of Petroleum Technology 1 (12): 305-324. SPE-949305-G. http://dx.doi.org/10.2118/949305-G

[27] Vogt, J.P. and Wang, B. 1987. Accurate Formulas for Calculating the Water Influx Superposition Integral, Paper SPE 17066 presented at the SPE Eastern Regional Meeting geld in Pittsburgh, Pennsylvania, 21-23 Oct. http://dx.doi.org/10.2118/17066-MS

Appendix A – Material Balance (MB)

The Material Balance (MB) given in **Equation 5.30** is valid for saturated and undersaturated oil reservoirs, for gas reservoirs with and without water influx from an aquifer considering the compressibility of the rock and the connate water and possible water and gas injections.

$$\begin{aligned} &N\left[B_o - B_{oi} + B_g(R_{si} - R_s) + \frac{B_{oi}(c_\phi + S_{wi}c_w)(p_i - p)}{1 - S_{wi}}\right] + G(B_g - B_{gi}) + W_e B_w \\ &= N_p\left[B_o + B_g(R_p - R_s)\right] + W_p B_w - (W_I B_w + G_I B_g) \end{aligned} \tag{5.30}$$

Usually the constant term for the rock and water compressibility is replaced by an apparent pore volume compressibility factor $c_{\phi a}$ given by:

$$c_{\phi a}=\frac{c_\phi+S_{wi}c_w}{1-S_{wi}}=\frac{c_\phi+S_{wi}c_w+c_w-c_w}{1-S_{wi}}=\frac{c_\phi+c_w}{1-S_{wi}}-c_w \tag{5.31}$$

The initial free gas volume G can be also expressed by the gas cap factor m, the original oil in place N and the formation volume factors of oil (B_{oi}) and gas (B_{gi}).

$$G=\frac{mNB_{oi}}{B_{gi}} \tag{5.32}$$

Inserting the relations of **Equation 5.31** and **Equation 5.32** in **Equation 5.30**:

$$\begin{aligned}&N\left[B_o-B_{oi}+B_g\left(R_{si}-R_s\right)\right]+NB_{oi}c_{\phi a}\left(p_i-p\right)+mNB_{oi}\left(\frac{B_g}{B_{gi}}-1\right)+W_eB_w\\&=N_p\left[B_o+B_g\left(R_p-R_s\right)\right]+W_pB_w-\left(W_IB_w+G_IB_g\right)\end{aligned} \tag{5.33}$$

Dividing **Equation 5.33** by the gas formation volume factor B_g gives:

$$\begin{aligned}&N\left[\frac{B_o}{B_g}-\frac{B_{oi}}{B_g}+\left(R_{si}-R_s\right)\right]+\frac{NB_{oi}}{B_g}c_{\phi a}\left(p_i-p\right)+mNB_{oi}\left(\frac{1}{B_{gi}}-\frac{1}{B_g}\right)+\frac{W_eB_w}{B_g}\\&=N_p\left[\frac{B_o}{B_g}-R_s\right]+N_pR_p+\frac{W_pB_w}{B_g}-\left(\frac{W_IB_w}{B_g}+G_I\right)\end{aligned} \tag{5.34}$$

Equation 5.34 can now be written for time points j and j+1. Writing **Equation 5.34** for time point j will lead to:

$$\begin{aligned}&N\left[\frac{B_{oj}}{B_{gj}}-\frac{B_{oi}}{B_{gj}}+\left(R_{si}-R_{sj}\right)\right]+\frac{NB_{oi}}{B_{gj}}c_{\phi a}\left(p_i-p_j\right)+mNB_{oi}\left(\frac{1}{B_{gi}}-\frac{1}{B_{gj}}\right)+\frac{W_{ej}B_{wj}}{B_{gj}}\\&=N_{pj}\left[\frac{B_{oj}}{B_{gj}}-R_{sj}\right]+N_{pj}R_{pj}+\frac{W_{pj}B_{wj}}{B_{gj}}-\left(\frac{W_{Ij}B_{wj}}{B_{gj}}+G_{Ij}\right)\end{aligned} \tag{5.35}$$

For writing **Equation 5.34** at time point j+1 the index j of **Equation 5.35** simply has to be replaced by j+1. Please note that for variables of cumulative production/injection (N_p for produced oil, W_I for injected water, etc.) the increment Δ_{j+1} of the production/injection for the time step will be written.

$$N\left[\frac{B_{oj+1}}{B_{gj+1}}-\frac{B_{oi}}{B_{gj+1}}+\left(R_{si}-R_{sj+1}\right)\right]+\frac{NB_{oi}}{B_{gj+1}}c_{\phi a}\left(p_i-p_{j+1}\right)+mNB_{oi}\left(\frac{1}{B_{gi}}-\frac{1}{B_{gj+1}}\right)+\frac{\left(W_{ej}+\Delta_{j+1}W_e\right)B_{wj+1}}{B_{gj+1}}$$
$$=\left(N_{pj}+\Delta_{j+1}N_p\right)\left[\frac{B_{oj+1}}{B_{gj+1}}-R_{sj+1}\right]+N_{pj}R_{pj}+\Delta_{j+1}N_p\overline{R}_p$$
$$+\frac{\left(W_{pj}+\Delta_{j+1}W_p\right)B_{wj+1}}{B_{gj+1}}-\left(\frac{\left(W_{Ij}+\Delta_{j+1}W_I\right)B_{wj+1}}{B_{gj+1}}+\left(G_{Ij}+\Delta_{j+1}G_I\right)\right)$$

(5.36)

It should be noted that for time point *j* the cumulative gas production G_{pj} could be expressed by the cumulative oil production N_{pj} and the overall production gas/oil ratio R_{pj}. This means:

$$G_{pj}=N_{pj}R_{pj} \tag{5.37}$$

Therefore at time point $j+1$ the cumulative gas production G_p is equal to:

$$G_{pj+1}=G_{pj}+\Delta_{j+1}G_p=G_{pj}+\Delta_{j+1}N_p\overline{R_p} \tag{5.38}$$

where R_p is the average production gas/oil ratio for the time period t_j, t_{j+1}. Subtracting **Equation 5.35** from **Equation 5.36** results in the differential form of the material balance:

$$N\Delta_{j+1}\left(\frac{B_o}{B_g}-R_s\right)-NB_{oi}\Delta_{j+1}\left(\frac{1}{B_g}\right)+NB_{oi}p_ic_{\phi a}\Delta_{j+1}\left(\frac{1}{B_g}\right)-NB_{oi}c_{\phi a}\Delta_{j+1}\left(\frac{p}{B_g}\right)$$
$$+mNB_{oi}\Delta_{j+1}\left(\frac{1}{B_g}\right)+W_{ej}\Delta_{j+1}\left(\frac{B_w}{B_g}\right)+\Delta_{j+1}W_e\left(\frac{B_w}{B_g}\right)_{j+1}$$
$$=N_p\Delta_{j+1}\left(\frac{B_o}{B_g}-R_s\right)+\Delta_{j+1}N_p\left[\left(\frac{B_o}{B_g}-R_s\right)_{j+1}+\overline{R_p}\right]$$
$$+W_{pj}\Delta_{j+1}\left(\frac{B_w}{B_g}\right)+\Delta_{j+1}W_p\left(\frac{B_w}{B_g}\right)_{j+1}-W_{Ij}\Delta_{j+1}\left(\frac{B_w}{B_g}\right)-\Delta_{j+1}W_I\left(\frac{B_w}{B_g}\right)_{j+1}-\Delta_{j+1}G$$

(5.39)

From**Equation 5.39** the incremental oil production ΔN_p for the time period t_j, t_{j+1} is expressed as:

$$
\begin{aligned}
\Delta_{j+1} N_p = {} & \frac{(N - N_P)\Delta_{j+1}\left(\frac{B_o}{B_g} - R_s\right) + NB_{oi}\Delta_{j+1}\left(\frac{1}{B_g}\right)\left(p_i c_{\phi a} - 1\right) - NB_{oi} c_{\phi a}\Delta_{j+1}\left(\frac{p}{B_g}\right) + mNB_{oi}\Delta_{j+1}\left(\frac{1}{B_g}\right)}{\left[\left(\frac{B_o}{B_g} - R_s\right)_{j+1} + \overline{R_p}\right]} \\
& + \frac{W_{ej}\Delta_{j+1}\left(\frac{B_w}{B_g}\right) - W_{pj}\Delta_{j+1}\left(\frac{B_w}{B_g}\right) + \Delta_{j+1}W_e\left(\frac{B_w}{B_g}\right)_{j+1} - \Delta_{j+1}W_p\left(\frac{B_w}{B_g}\right)_{j+1} + W_{Ij}\Delta_{j+1}\left(\frac{B_w}{B_g}\right) + \Delta_{j+1}W_I\left(\frac{B_w}{B_g}\right)_{j+1}}{\left[\left(\frac{B_o}{B_g} - R_s\right)_{j+1} + \overline{R_p}\right]} \\
& + \frac{\Delta_{j+1}G_I}{\left[\left(\frac{B_o}{B_g} - R_s\right)_{j+1} + \overline{R_p}\right]}
\end{aligned}
\tag{5.40}
$$

For the sake of easier explanations in the main part of this work **Equation 5.40** will be written for a unit initial oil volume. In this case the cumulative oil production N_p becomes the recovery factor E itself. The terms for the produced water (W_p), the water encroachment (W_e) and the injected cumulative amounts of water (W_I) and gas (G_I) have to be scaled to unit oil in place. In the applied notation those scaled amounts will be expressed by lower case symbols w for water and g for gas.

Finally the increase in recovery factor $\Delta_{j+1}E = E_{j+1} - E_j$ during a single time step $\Delta t = t_{j+1} - t_j$ is given by **Equation 5.41**.

$$\Delta_{j+1}E=\frac{(1-E)\Delta_{j+1}\left(\frac{B_o}{B_g}-R_s\right)+B_{oi}\Delta_{j+1}\left(\frac{1}{B_g}\right)\left(p_i c_{\phi a}-1\right)-B_{oi}c_{\phi a}\Delta_{j+1}\left(\frac{p}{B_g}\right)+mB_{oi}\Delta_{j+1}\left(\frac{1}{B_g}\right)}{\left[\left(\frac{B_o}{B_g}-R_s\right)_{j+1}+\overline{R_p}\right]}$$

$$+\frac{w_{ej}\Delta_{j+1}\left(\frac{B_w}{B_g}\right)-w_{pj}\Delta_{j+1}\left(\frac{B_w}{B_g}\right)+\Delta_{j+1}w_e\left(\frac{B_w}{B_g}\right)_{j+1}-\Delta_{j+1}w_p\left(\frac{B_w}{B_g}\right)_{j+1}+w_{Ij}\Delta_{j+1}\left(\frac{B_w}{B_g}\right)+\Delta_{j+1}w_I\left(\frac{B_w}{B_g}\right)_{j+1}}{\left[\left(\frac{B_o}{B_g}-R_s\right)_{j+1}+\overline{R_p}\right]}$$

$$+\frac{\Delta_{j+1}g_I}{\left[\left(\frac{B_o}{B_g}-R_s\right)_{j+1}+\overline{R_p}\right]}$$

(5.41)

Conversion Factors

acre	x	4.046873E+03	= m²	
bar	x	1.0*	E+05	= Pa
bbl	x	1.589 873E-01	= m³	
cp	x	1.0*	E-03	= Pa.s
ft	x	3.048*	E-01	= m
ft³	x	2.831685E-02	= m³	
lbm	x	4.535924E-01	= kg	
psi	x	6.894757E+00	= kPa	

*Conversion factor is exact.

Chapter 6

Nomenclature

Symbols

A - area, cross section, [m^2]
a - fracture spacing, [m]
b - fracture breadth, [m]
c_p - compressibility factor of phase *p* [1/bar]
c_t - total compressibility factor [1/bar]
c_ϕ - apparent pore compressibility factor [1/bar]
D_p - specific mole density, [kmol/m^3]
D_{pc} - diffusion coefficient, [m^2/s]
$\vec{g}$ - gravity acceleration vector, [m/s^2]
$\vec{J}_{pc}$ - molar flux of component *c* in phase *p*, [kmol/m^2 s]
$\bar{k}$ - permeability tensor
k - permeability, [m^2]
k_{rp} - relative permeability, [-]
M_c - molar mass of component *c*, [kg/mol]
$\vec{n}$ - normal unit vector
$P_{cpp'}$ - capillary pressure between phase *p* and *p'*, [bar]
p_e - net confining pressure, [bar]
p_h - healing pressure, [bar]
p_p - phase pressure, [bar]
q_p - flow rate of phase *p*, [m^3/s]
q_p - source/sink term for phase *p*, [kmol/day]
q_{cmf} - matrix-fracture transfer term, [kmol/day]
r_w - wellbore radius, [m]
S_p - phase saturation, [-]
T - temperature, [K]
$\vec{u}_p$ - filtration velocity, [m/day]
V_I - Volume of gridblock *I*, [m^2]
V_p - Pore volume, [m^3]
V_{p1} - Volume of phase *p* produced during phase *p'* imbibition, [m^3]
V_{p2} - Volume of phase *p* produced during phase *p'* flooding, [m^3]
V_T - Bulk volume, [m^3]
W - Effective fracture aperture (fracture width), [m]
WI - Wettability index (Amott-Harvey wettability index), [-]
x_{pc} - mole fraction of component *c* in phase *p*, [-]
z - depth, [m]

Greek Symbols

ϕ - porosity, [-]
Φ_p - phase potential, [bar]
λ_p - phase mobility, [1/cp]
μ_p - phase viscosity, [cp]
ρ_p - phase density, [kg/m³]
ρ_s - rock density, [kg/m³]
$\sigma_{pp'}$ - interfacial tension between phase *p* and *p’,* [N/m]
θ - contact angle, [°]
σ - shape factor, [m^{-2}]
$\bar{\sigma}$ - stress, [bar]
δ_p - displacement with phase *p* ratio (Amott wettability) [-]
ε - supplementary pressure drop function across an inner boundary [kg/m³]
τ_{IJ} - interblock transmissibility, [m³]
Δ_t - time difference operator, $\Delta_t\Gamma = \Gamma^{n+1} - \Gamma^n$
λ - interporosity flow coefficient, [-]
ω - storativity ratio [-]
Γ - boundary

Subscripts

a - apparent / average
c - component
e - effective
f - fracture
g - gas
i - initial conditions
i - point index
ir - irreducible
l - left
m - matrix
n - old time level
n+1 - new time level
o - oil
p - phase
r - relative
r - residual
r - right
w - water
x,y,z - coordinate directions

Superscripts

N_c - total number of components
N_p - total number of phases
ν - old iteration level
$\nu+1$ - new iteration level

Conversion Factors

bar = psia*0.06894757
m = ft*0.3048
kg = lb*0.453592
1000m^3 = MMSCF*26.795
kg/m^3 = lb/ft^3*16.01846
°F = °R - 459.67

$$°\mathrm{C} = \frac{(°\mathrm{F} - 32)}{1.8}$$

$$°\mathrm{API} = \frac{141.5}{\text{Spec. Gravity}-131.5}$$

Chapter 7

References

[1] Abushaikha,A.S.A. and Gosselin,O.R.: Matrix-Fracture Transfer in Dual-Medium Flow Simulation: Review, Comparison and Validation," paper SPE 113890 presented at the 2008 SPE/AEGE Annual Conference and Exhibition held in Rome, Italy, 9-12 June 2008.

[2] Ahmed,T. and McKinney, P.D.: "Advanced Reservoir Engineering", Elsevier, 2005.

[3] Amiry, M.T.: "Modeling Flow Behavior in Naturally-Fractured Reservoirs", PhD Dissertation, Montanuniversität Leoben, February 2014.

[4] Anderson, W., G.: "Wettability Literature Survey - Part 2: Wettability Measurement", *JPT* 1246-1262. (S), Nov. 1986.

[5] Aguilera, R.: "Naturally Fractured Reservoirs", Penn Well Books, Tulsa, Oklahoma, 1980, p.8.

[6] Aziz, K. and Settari A.: "Petroleum Reservoir Simulation", Elsevier, London and New York, 1979.

[7] Aziz, K.: "Reservoir Simulation", Lecture Notes, HOT Engineering, Leoben 1991.

[8] Barrenblatt, G. J., Zheltov, I. P., and Kochine, I. N.: "Basic Concepts in the Theory of Seepage of Homogeneous Liquids in Fissured Rocks*", J. Appl. Math. Mech.*, 1286-1303, 1960, p.24.

[9] Barker, J.A.: "Block-Geometry Functions Characterizing Transport in Densely Fissured Media", Journal of Hydrology, Vol. 77, 1985, pp.263-279.

[10] Blair, P.M. paper no. 1475G, *Trans. AIME* secondary Rec. Symp., Wichita Falls, Texas, U.S.A., May 1960.

[11] Bourdet, D. and. Gringarten, A.C.: "Determination of Fissure Volume and Block Size in Fractured Reservoirs by Type-Curve Analysis," paper SPE 9293 presented at the 55th Annual Fall Technical Conference and Exhibition, held in Dallas, TX., September 21-24, 1980.

[12] Bourdet,D, Alagoa,A., Ayoub,J.A. and Pirard, Y.M.: "New Type Curves aid Analysis of Fissured Zone Well Tests," Word Oil, Apr. 1984, pp.111-124.

[13] Bourdet,D., Whittle, T.M., Douglas, A.A. and Pirard, Y.M.: "A new set of type curves simplifies well test analysis," World Oil, May 1984. pp.111-124.

[14] Bratton, Tom et al.: "The Nature of Naturally Fractured Reservoirs", Schlumberger Oilfield Review, Summer 2006.

[15] Bremeier, M., Fink, G., and Heinemann, Z.E.: "Simulation of Dual Porous and Permeable

Hydrocarbon Reservoirs", Erdoel-Erdgas-Kohle, March, 1991, pp.110-117.

[16] Bremeier, M.: "Numerical Simulation of Fractured Petroleum Reservoirs with Interchangeable Matrix-Fracture Transfer Terms and Optional Subdivision of the Matrix Grid Cells". Ph.D. Dissertation, Mining University, Leoben, 1991.

[17] Buckley, S.E. and Leverett, M.C.: "Mechanism of Fluid Displacement in Sands", Trans AIME, Vol. 146, 1942, pp.107-116.

[18] Cardwell, W.T., Parsons, R.L., "Average permeabilities of heterogeneous oil sands", Trans. Am. Inst. Mining. Met. Pet. Eng., 1945, pp.34-42.

[19] Chen, J., Miller, M.A. and Sepehrnoori, K.: "Theoretical Investigation of Countercurrent Imbibition in Fractured Reservoir Matrix Blocks", paper SPE 29141 presented at the SPE Symposium of Reservoir Simulation, San Antonio, TX, USA, 12-15 February, 1995.

[20] Coats, K.H.: "Implicit Compositional Simulation of Single-Porosity and Dual-Porosity Reservoirs", Presented at the First International Forum on Reservoir Simulation, Alpbach, September 12-16, 1988 and SPE 18427.

[21] Coats, K.H., Nielsen, R.L., Terhune, M.H., and Weber, A.G.: "Simulation of Three-Dimensional, Two-Phase Flow in Oil and Gas Reservoirs". SPEJ, December, 1967, pp.377-88,.

[22] Comon, P., Sorensen, M., "Tensor Diagonalization By Orthogonal Transforms", Rapport de recherche, ISRN I3S/RR-2007-06-FR, 2007.

[23] Dagan, G., "Flow and Transport in Porous Formations", Springer-Verlag, New York, 1989.

[24] Da Silva, F.V., and Belery, P.: "Molecular Diffusion in Naturally Fractured Reservoirs: A Decisive Recovery Mechanism", SPE 19672, presented at the 64th Annual Technical Conference and Exhibition, San Antonio, Texas, October 8-11, 1989.

[25] Dean, R.H., and Lo, L.L.: "Simulations of Naturally Fractured Reservoirs", SPERE, May,1988, pp.638-648.

[26] Donaldson, E.C., Thomas, R.D., and Lorenz, P.B.: "Wettability Determination and Its Effect on Recovery Efficiency", *SPEJ*, March 1969, pp.13-20.

[27] Engelder, T.: "Loading Paths to Joint Propagation During a Tectonic Cycle: An Example from the Appalachian Plateau, USA", J. Struct. Geol., Vol. 7, 1987, pp. 450-476.

[28] Famy, C., Bourbiaux, B. and Quintard, M.: "Accurate Modeling of Matrix-Fracture Transfer in Dual Porosity Models: Optimal Subgridding of Matrix Blocks", paper SPE 93115 presented at the 2005 SPE Reservoir Simulation Symposium, Houston, TX, USA, 31 January-2 February 2005

[29] Fung, L.S.K.: "Simulation of Block-to-Block Processes in Naturally Fractured Reservoirs", SPE 20019, presented at the 60th California Regional Meeting, Ventura, California, April 4-6., 1990.

[30] Gerke, H.H. and van Genuchten, M.Th.: "Macroscopic Representation of Structural Geometry for Simulating Water and Solute Movement in Dual-Porosity Media ", Advances in Water Resources, Vol.19, No.6, 1996., pp.343-357

[31] Gilman, J.R., and Kazemi, H.: “Improved Calculation for Viscous Gravity Displacement in Matrix Blocks in Dual-Porosity Simulators”, SPE JPT, January, 60-70, 1988 and SPE 16010.

[32] Gilman, J.R. and Kazemi, H.: “Improvements in Simulation of Naturally Fractured Reservoirs”, Soc.Pet.Eng.J., August 1983, pp.695-707.

[33] Gilman, J.R.: “Practical Aspects of Simulation of Fractured Reservoirs,” paper presented at the Seventh International Forum on Reservoir Simulation, Baden-Baden, Germany, 2003.

[34] Graham, J.W. and Richardson, J.G: Note not published, Referenced in Collins,R.E.: “Flow of Fluids through porous materials”, Reinhold Publishing Corporation, New York, 1961, p.166.

[35] Gringarten A.C.: “Type Curve Analysis”, JPT Jan. 1987, p.11-13.

[36] Gurpinar, O. and Kossack, C.A.: “Realistic Numerical Models for Fractured Reservoirs”, paper SPE 59041 presented at the SPE International Petroleum Conference and Exhibition, Mexico, 1-3 February 2000.

[37] Harstad, H., Teufel, L.W. and Lorenz, J.C.: “Characterisation and Simulation of Naturally Fractured Tight Gas Sandstone”, paper SPE 30573 presented at the 70th Annual Fall Technical Conference and Exhibition, held in Dallas, TX, October 22-25, 1995.

[38] Heinemann, Z.E.: “Fluid Flow in Porous Media”, Textbook Montanuniversität Leoben, Austria, 2005, p.210.

[39] Heinemann, Z.E.: “Using Recovery Curves in Modeling Natural Fractured Hydrocarbon Reservoirs”, Proposal for a PhD Research Project at the Montanuniversität Leoben, Austria, March 2004.

[40] Heinemann Oil Technology: “***PRS*** Time-Dependent Data Manual, Version 2.1”, June 2012.

[41] Heinemann Oil Technology: “***PRS*** Technical Description, Version 2.1”, June 2012.

[42] Heinemann, G.F. and Heinemann, Z.E.: “Gridding Concept for Third Generation Reservoir Simulators”, paper presented at the Sixth Intl. Forum on Reservoir Simulation Fuschl, Hof-Salzburg. Austria., Sept. 3-7, 2001, p.110.

[43] Heinemann, Z.E., and Mittermeir, G.M.: “Derivation of the Kazemi-Gilman- Elsharkawy, Generalized Dual Porosity Shape Factor”, Transp. Porous Media, Sep. 2011.

[44] Jones, F.G.: “Laboratory study of the effects of confining pressure of fracture flow and storage capacity in carbonate rocks”, JPT Jan. 1975, p.21-29.

[45] Kazemi, H., Gilman,J.R. and El-Sharkawy, A.M.: “Analytical and Numerical Solution of Oil Recovery from Fractured Reservoirs Using Empirical Transfer Functions”, SPE Reservoir Engineering, May 1992, pp.219-227.

[46] Kazemi, H. and Gilman, J.R.: “Chapter 6, Multi-phase Flow in Fractured Petroleum Reservoirs”, in Flow and Contamination in Fractured Rock, Edited by J.Bear *et al.*, Academic Press, San Diego, CA, 1993, pp.267-323.

[47] Kazemi, H., Merril, L.S., Porterfield, K.L., and Zeman, P.R.: “Numerical Simulation of

Water-Oil Flow in Naturally Fractured Reservoirs", SPEJ December, pp.317-326 and SPE Paper 5719, 1976.

[48] Kazemi, H. and Shirta, A.A.: "Determining Orientation and Conductivity of High Permeability Channels in Naturally Fractured Reservoirs", Receiver Characterisation IV, Edited by Linville, Pennwell Books, 1993.

[49] Kazemi, H., Seth, J.S. and Thomas, G.W.: "The Interpretation of Interference Tests in Naturally Fractured Reservoirs with Uniform Fracture Distribution," SPE Journal, Dec. 1969, pp.463-472.

[50] Kossack, C.A.: "Simulation of Gas/Oil Displacements in Vuggy and Fractured Reservoirs", paper SPE 101674 presented at the 2006 SPE Annual Technical Conference and Exhibition, San Antonio, TX, USA, 24-27 September 2006.

[51] Lewandowska, J., Szymkiewicz, A., Burzynski, K. and Vauclin, M.: "Modeling of Unsaturated Water Flow in Double-Porosity Soil by the Homogenization Approach", Advances in Water Resources, Vol.27, 2004, pp.283-296.

[52] Lim, K.T, Aziz, K.: "Matrix-fracture transfer shape factors for dual-porosity simulators", Journal of Petroleum Science and Engineering 13, 1995.

[53] Litvak, B.L.: "Simulation and Characterization of Naturally Fractured Reservoirs", Reservoir Characterization Conference, Dallas, Academic Press, New York City, 1985, pp.561-583.

[54] Matherson, G., "Elements pour une Thèorie des Milieux Poreux", Masson, Paris, 1967.

[55] Mattax, C.C. and Kyte, J.R.: "Imbibition Oil Recovery from Fractured, Water-Drive Reservoirs," SPE Journal 177-84, June 1962, Trans. AIME, 225.

[56] McNaughton, D.a., Garb, F.A.: "Finding and Evaluating Petroleum Accumulations in Fractured Reservoir Rock," Exploration and Economics of the Petroleum Industry, Vol. 13 Matthew Bender & Company Inc., 1975.

[57] Muskat, M.: "Physical Principles of Oil Production", McGraw-Hill Book Company, New York, 1949.

[58] Muskat, M. and Taylor, M.O.: "Effect of Reservoir Fluid and Rock Characteristics on Production Histories of Gas-Drive Reservoirs", Trans., AIME 1946, 165, pp.78-93.

[59] Muskat, M.: "The Flow of Homogeneous Fluids Through Porous Media", 1937, reprinted 1982, IHRDC, Boston, Mass., pp.225-227.

[60] Narr, W., Schechter, D.W. and Thompson, L.B.: "Naturally Fractured Reservoir Characterization", ISBN 978-55563-112-3 Society of Petroleum Engineers, Richardson, TX, USA, 2006.

[61] Nelson, R.A.: "An Approach to Evaluating Fractured Reservoirs", SPE JPT, September 1992, pp.2167-2170.

[62] Oda,Mc.: "Permeability Tensor for Discontinuous Rock Masses", Geotechnique, 35, 1985, pp.483-495.

[63] Ouenes, A. and Feng Shen: "Fracture Characterisation", paper presented at the Sevent International Forum on Reservoir Simulation, Baden-Baden, 2003

[64] Quenes,A. and Hartley, L.J.: “Integrated Fracture Modeling Using Both Discrete and Continuum Approaches”, paper SPE 62939 presented at the 2000 SPE Annual Technical Conference and Exhibition in Dallas, Texas, 1-4 Oct.2000.

[65] Ouenes, A., Richardson, S., Weiss, W.: “Fractured reservoir characterization and performance forecasting using geomechanics and artificial intelligence,” paper SPE 30572 presented at the 1995 SPE Annual Technical Conference and Exhibition, 1995.

[66] Quandalle, P. and Sabathier, J.C.: “Typical Features of a Multipurpose Reservoir Simulator”, SPE Reservoir Engineering November 1989.

[67] Penuela, G., Civan, F., Hughes, R. G. and Wiggins, M.L.: “Time-Dependent Shape Factor for Interporosity Flow in Naturally Fractured Gas-Condensate Reservoirs,” paper SPE 75524 presented at the SPE Gas Technology Symposium held in Calgary, Alberta, Canada, 30 Apr. - 2 May 2002.

[68] Pirker, B., Mittermeir, G.M., Heinemann, Z.E.: “Numerically Derived Type Curves For Assessing Matrix Recovery Factors”, paper SPE 107074, prepared for presentation at the 2007 SPE EUROPEC/EAGE Annual Conference and Exhibition held in London, United Kingdom, 11 -14 June 2007.

[69] Pirker, B., Heinemann, Z.E.: “Method to Preliminary Estimation of the Reserves and Production Forecast for Dual Porosity Fractured Reservoirs”, paper SPE 113378, prepared for presentation at the 2008 SPE EUROPEC/EAGE Annual Conference and Exhibition held in Rome, Italy, 9 - 12 June 2008.

[70] Pirker B., Harrer, A.W., Heinemann, Z.E.: “Reserve Estimation for Naturally Fractured Reservoirs Using Numerically Derived Recovery Curves”, prepared for presentation at the 11th European Conference on the Mathematics of Oil Recovery (ECMOR XI) held in Bergen, Norway, 8 - 11 September 2008.

[71] Pirker, B.: “A New Approach for Modeling Dual Porosity Reservoirs Using Recovery Curves”, PhD theses, Montanuniversität Leoben, Nov.2008.

[72] Pirson,S.J.: “Oil Reservoir Engineering”, McGraw-Hill Book Company, New York, 1958.

[73] Powley, K.D., Peng, C.P. and Nazir, A.: “Simulation of North Sea Chalk Reservoir with Dynamic Rock and Natural Fracture Properties: Case Study of the Valhall Field”, paper SPE 24914 presented at the 67th Annual Fall Technical Conference and Exhibition, held in Washington, DC, October 4-7, 1992.

[74] Pruess, K. and Narasimhan, T.N.: “A Practical Method for Modeling Fluid and Heat Flow in Fractured Porous Medium”, SPEJ February, 14-26 and SPE Paper 10509, 1985.

[75] Pruess, K. and Karasaki, K.: “Proximity Functions for Modeling Fluid and Heat Flow in Reservoirs with Stochastic Fracture Distributions”, Proc., Eighth Workshop on Geothermal Reservoir Engineering, Stanford U., Palo Alto, CA (Dec. 1982) 219-24.

[76] Pruess, K.: “GMINC - A Mesh Generator for Flow Simulations in Fractured Reservoirs”, Lawrence Berkeley Laboratory, report LBL-15227, Berkeley, CA (March 1983).

[77] Rangel-German E.R. and Kovscek A.R.: “Time-Dependent Matrix-Fracture Shape Factors for Partially and Completely Immersed Fractures,” paper SPE 84411 presented at the SPE ATCE held in Denver, Colorado, USA, 5-8 Oct. 2003.

[78] Renard, Ph., de Marsily, G., “Calculating equivalent permeability: a review”, Advances in Water Resources 20, issues 5-6, 253-278, 1997

[79] Rosen, R,H. and Shen,E.L.: “Simulation of Gas/Oil Drainage and Water/Oil Imbibition in Naturally-Fractured Reservoirs”, paper SPE 16982 presented at the 1987 SPE Annual Technical Conference and Exhibition, Dallas, TX, Sept. 27-30,1987.

[80] Roxar training, “Naturally Fractured Reservoirs: An Introduction to their Appraisal and Management”, support.roxar.com.

[81] Ruddy, I., Andersen, M.A., Pattillo, P.D. and Bishlawi, M.: “Rock Compressibility, Compaction, and Subsidence in High-Porosity Chalk Reservoir: A Case Study of Valhall Field”, JPT, July 1989, pp.741-746.

[82] Sabet, M.: “Well Test Analysis”, Gulf Publishing, Dallas, TX, 1991.

[83] Saidi, A.M.: “Simulation of Naturally Fractured Reservoirs”, paper SPE 12270 presented at 7th SPE Symposium on Reservoir Simulation held inSan Francisco, CA., Nov. 15-18, 1983.

[84] Salathiel, R. A.: "Oil recovery by surface film drainage in mixed-wettability rocks," *J. Petrol. Technol.*, 25, 1216-1224, 1973.

[85] Schechter, D.S., Zhou, D. and Orr, F.M.: “Low IFT Drainage and Imbibition”, J. Pet. Sci. Eng. (1994) 11: pp.283-300.

[86] Schilthuis, R.J.: "Active Oil and Rerservoir Engergy", Trans., AIME, 118, (1936), 33-52.

[87] Schlumberger: “ECLIPSE Technical Description, 2004A_1”, 1982-2004.

[88] Sonier, F., Souillard, P., and Blaskovich, F.T.: “Numerical Simulation of Naturally Fractured Reservoirs”, SPERE 1988, November, 1114-1122.

[89] Thomas, L.K., Dixon, T.N., and Pierson, R.G.: “Fractured Reservoir Simulation”, SPE Journal, 638-648 (Feb. 1983) Trans. AIME, 243.

[90] Torsaeter, A., Abtahi, M: “Experimental Reservoir Engineering. Laboratory Handbook”, www.ipt.ntnk.no/~ oletor/labbook - 2003 pdf

[91] Treiber, L.E., Archer, D.L. and Owens, W.W.: “A Laboratory Evaluation of the Wettability of Fifty Oil Producing Reservoirs”, SPEJ (Dec. 1972) 531-40; *Trans AIME, **253***.

[92] Ueda, Y., Murata, S., Watanabe, Y. and Funatsu, K.: “Investigation of the Shape Factor Used in the Dual-Porosity Reservoir Simulator,” paper SPE 19469 presented at the SPE Asia-Pacific Conference held in Sydney, Australia, 13-15 Sept. 1989.

[93] Ulrich, D.O. and Ershagi,J.: “A Method for Estimating the Interporosity flow parameter in naturally fractured reservoirs”, SPEJ, Oct.1979. p.324-332.

[94] Van Golf-Racht, T.D. (1982): “Fundamentals of Fractured Reservoir Engineering”, Developments in Petroleum Science 12, Elsevier Scientific Publishing Company.

[95] Warren, J.E., and Root P.J.: “The Behavior of Naturally Fractured Reservoirs”, SPEJ, September, 245-255, 1963, Trans.AIME, 228.

Wuthichar, K. and Zimmerman, R.W.: Shape factors for Irregularly Shaped Matrix Blocks", paper SPE 148060 , presented at the SPE Reservoir Characterisation and Simulation Conference and Exhibition held in Abu Dhabi, UAE, 9-11 October 2011.International Petroleum Conference

[96] www.ngdir.ir/GeoportalInfo/SubjectInfoDetail.asp?PID=18

[97] www.netl.doe.gov/technologies/oil-gas/NaturalGas/Projects_n/EP/DCS/images/lpf31063 FracturedCore.jpg (August, 2008)

[98] http://en.wikipedia.org/wiki/Permeability_(earth_sciences)

[99] Zellou, A.M.: "Seismically Driven Improved Fractured Reservoir Characterization", paper SPE 92031, presented at the SPE International Petroleum Conference, Mexico, 2004.

[100] Zellou, A., Hartley, L.J., Hoogerduijn-Strating, E.H., Al Dhahab, S.H.H, Boom, W., Hadrami, F.: "Integrated Workflow Applied to the Characterization of a Carbonate Fractured Reservoir: Qarn Alam Field," paper SPE 81579 presented at SPE 13th Middle East Oil Show & Conference, Bahrain, 2003.